Curcumin-Loaded Block Copolymer Nanoparticles for Drug Delivery Using Microfluidics

by

Ruyao Chen
B.Eng., Donghua University, 2014

A Thesis Submitted in Partial Fulfillment
of the Requirements for the Degree of

MASTER OF SCIENCE

in the Department of Chemistry

Supervisory Committee

Curcumin-Loaded Block Copolymer Nanoparticles for Drug Delivery Using Microfluidics

by

Ruyao Chen
B.Eng., Donghua University, 2014

Supervisory Committee

Dr. Matthew G. Moffitt, Department of Chemistry
Supervisor

Dr. Jeremy E. Wulff, Department of Chemistry
Departmental Member

Abstract

This thesis includes three stages of experiments. The goal of the thesis was to prepare nanoparticle-encapsulated curcumin for the purpose of drug delivery. The first step was the nanoparticle preparation. The self-assembly of block copolymer (poly(ε-caprolactone)-*b*-poly(ethylene oxide)) and curcumin was conducted on a gas-liquid two phase microfluidic reactor. During preparation, various chemical parameters and flow rates were tested. The nanoparticles showed flow variability; the size decreased and the loading efficiency increased with increased flow rates. Increasing the water content and drug-to-polymer loading ratio also proved to increase loading efficiency and decrease the size of the nanoparticles. The release profiles, however, showed fast release rates under various preparation conditions, with a nearly complete release after ~5 h. In the next stage of the research, we considered release optimization in preparation for future pharmacokinetic studies. Increasing the flow rate had a greater influence on slowing down release rates than changing other parameters, such as decreasing the drug-to-polymer loading ratio or increasing the water content. A procedure to extract and quantify curcumin from mouse blood was also developed in this stage. In the final stage of the research, nanoparticle-encapsulated curcumin was tested on a human breast cancer cell line, MDA-MB-231. The result showed that the nanoparticle formulation had a growth inhibition effect on MDA-MB-231, although the cytotoxicity was compromised by encapsulation in the nanoparticles.

Table of Contents

List of Tables

List of Figures

List of Scheme

Acknowledgments

First, I would like to express my sincere gratitude to my supervisor Dr. Matthew Moffitt for the support, encouragement and patience in these two years. I have learned tremendously from you and the group.

I would also like to thank all group members, Zheqi Xu, Alex Leung, Yimeng Cao, Aman Bains, Sun Kly, Fraser Burns and Brian Colman. Thanks to Zheqi Xu who guided me through the training and research, Alex Leung who shared his experience and expertise in research and biology, Aman Bains who trained me on microfluidics and everyone in the group for the help whenever I had questions and met difficulties.

Finally, I would like to thank my family and friends. It would be impossible for me to get this far without your support and encouragement.

Chapter 1 General Introduction

1.1 General Backgrounds and Goal

A block copolymer consists of homopolymer subunits covalently bonded together. One interesting feature of block copolymers is their ability to self-assembly into nanoparticles in a selective solvent.[1-3] Polymeric nanoparticles have the potential in drug delivery with various chemical conjugations[4], responsive photonic crystal for sensing[5] and copolymer thin film with nanoscale pores. If block copolymers associate together to form micellar structures with the hydrophobic block in the core and the hydrophilic block in the shell in aqueous environments, this nanoparticle is called a regular micelle. On the other hand, if micelles have their hydrophilic part in the core and hydrophobic part in the corona contacting with organic media, these nanoparticles are reverse micelles. This leads to the use of block copolymer nanoparticles as containers for insoluble substances. For example, nanoparticles can solubilize hydrophobic drugs in their hydrophobic core and increase solubility of the drug in the blood. Poly(ε-caprolactone)-*block*-poly(ethylene oxide) (PCL-*b*-PEO) is widely studied as a drug delivery system because of its biocompatibility and biodegradability.[6-8]

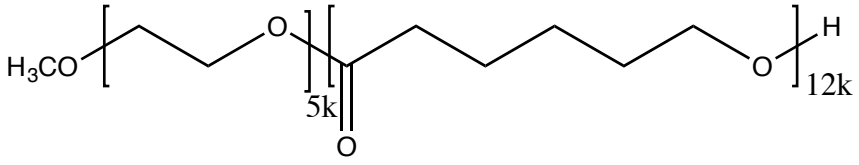

Figure 1-1 PCL-*b*-PEO structure formula

The PCL block was in solution state when it was dissolved in the organic solvent dimethylformamide (DMF). Then PCL block was considered to transfer to the melt state

upon mixing with water.[9] Medicinal drugs, such as paclitaxel and doxorubicin, can then solubilize in the hydrophobic block, PCL.[9, 10] The degradation of PCL block was concluded to be hydrolytic cleavage of the ester group.[11] The corona, PEO block, is hydrophilic and helps the nanoparticle to stabilize in aqueous environments.[12, 13] In a drug delivery application, nanoparticles could be injected into a blood vessel and released to the tumor with the help of the enhanced permeation and retention (EPR) effect.[14, 15] The EPR effect refers to higher permeation and retention of nanoparticle-encapsulated anticancer drugs due to defective and leaky blood vessel near the tumor site.[16] The EPR effect would strongly depend on the nanoparticle's structural properties such as size and morphology. Therefore, we are trying to tune nanoparticles' size and morphology for the purpose of improving its performance in drug delivery.[17-21]

There are two main approaches for preparing block copolymer nanoparticles. The conventional method to prepare nanoparticles is self-assembly *via* chemical forces only, for example when water is added dropwise to a polymer solution until a certain water content is achieved.[22, 23] The water content when block copolymers start to spontaneously form nanoparticles is defined as critical water content (cwc). Amphiphilic block copolymer self-assembly then leads to the formation of nanoparticles. This approach of preparing polymeric nanoparticles is defined as the bulk method. Nanoparticle properties depend on variations such as solvent, pH, block copolymer composition and polymer concentration. Variations in these chemical parameters will directly influence the interactions between polymer chains and control nanoparticle morphology.[22-26] Another method is to combine chemical forces and external forces such as shear force to produce the desired morphology. For example, our group developed a microfluidic approach to

prepare nanoparticles. A regular flow of argon gas bubbles divides a liquid stream into small segments and greatly enhances the mixing rate on the chip. The circulating flow inside liquid segments creates high shear rates in the corner of liquid segments, which is much higher than shear rates created by a bench top stir plate.[27] The high shear rate provides enough energy for newly formed nanoparticles to overcome the repulsion between nanoparticle corona and the viscosity in the core.[26] The aggregation number, the number of polymer chains in each single micelle, will increase because of the coalescence of nanoparticles in the high shear corner. The increasing aggregation number in nanoparticles will result in the chain stretching in the core-forming copolymer blocks. These high-energy state nanoparticles will then go through polymer chain rearrangement to relax. And therefore, morphologies with a lower curvature such as cylinder or lamellae were observed on the microfluidic chip. Previous group members have used PCL-*b*-PEO, poly(styrene)-block-poly(acrylic acid) (PS-*b*-PAA) as model block copolymer systems to control nanoparticles morphologies and other properties. Joe Wang prepared PS-*b*-PAA nanoparticles and observed vesicle morphology while no vesicle was formed using conventional bulk method.[26] Aman Bains encapsulated paclitaxel in PCL-*b*-PEO nanoparticles and observed increasing crystallinity with increasing flow rate.[9]

In this study, we aim to encapsulate curcumin by microfluidic methods. Curcumin is a hydrophobic polyphenol extracted from a plant of the ginger family, turmeric.[28] As a common food additive in southern Asia, curcumin was found to be reactive to various biological targets, including enzymes, transcription factors and growth factors. For example, curcumin can inhibit the proliferation of most cancer cell lines.[29-34] But the main limits of curcumin are its insolubility in water and fast degradation at neutral to

alkaline pH.[35, 36] The curcumin degradation *in vivo* is due to a continuous reduction of double bonds in the heptadienedione chain. Degradation products include di, tetra, hexahydrocurcumin.[37] Curcumin degradation in cell line experiment is considered to be slower in medium containing serum or human blood comparing to degradation in the serum-free medium.[37] However, considering the long incubation time in cell line experiments, degradation of curcumin is still a major problem because it is difficult to determine whether the observation is the result of curcumin or the degradation products.[38] As a result, there are researches focusing on improving curcumin efficacy. By encapsulating curcumin into nanoparticles, curcumin may be protected from degradation. Ma *et al.* successfully prepared PCL-*b*-PEO polymeric nanoparticles in bulk to encapsulate curcumin[24]. Grancharov *et al.* used PEO-*b*-PCL-*b*-PEO triblock to synthesis nanoparticles for drug delivery.[39] In these studies, there were a few problems. First of all, the low initial drug-to-polymer ratios resulted in low loading levels. For example, the highest loading level is only 6 wt % among all conditions in the result presented by Ma *et al.*[24] Considering drug-encapsulated nanoparticles acting as drug delivery vehicles, low loading level meant that most of the drug was wasted. Such drug-encapsulated nanoparticles with low loading levels may not be a successful delivery system in the further *in vivo* experiment. In the bulk method, the morphologies, crystallinity or other features of nanoparticle are influenced by variations in chemical conditions such as the choices of stirring speed, solvents and polymer compositions. Researchers need to screen various chemical conditions to see which set of conditions would be the best for a drug delivery system.

In this thesis, we intended to use our microfluidic reactor as a platform to prepare and tune nanoparticles' structural properties for drug delivery. By applying shear-induced control on nanoparticle-encapsulated curcumin, the nanoparticles showed pure spherical morphology, high loading level at 40 wt % and release profile up to 48 hours. These properties would be desirable characteristics of a drug delivery system for future *in vivo* studies. After successfully preparing nanoparticle-encapsulated curcumin, we present in this thesis the characterizations of nanoparticles' size, loading level and anti-cancer activity.

1.2 Polymer

1.2.1 The Concept of Polymer

A polymer is a macromolecule that has a high molar weight ranging from one thousand to millions of grams per mole.[40] A polymer is a macromolecule composed of many subunits that are connected by covalent bonds. For example, polyethylene, a common plastic, consists of many repeat units of $-CH_2-CH_2-$.

The microstructure of polymer chain has an influence on polymer physical properties. In general, there are three main polymer architectures (Figure 1-2): linear, branched and network structure. In branched polymers, branches sticking out from the main chain lead to less efficient chain packing than linear polymers. As a result, branched polymers have a lower crystallinity than linear polymer. If there are chemical bonds to connect branched polymer with its neighboring chains together, it will result in a large three-dimensional network structure called crosslinked polymer.

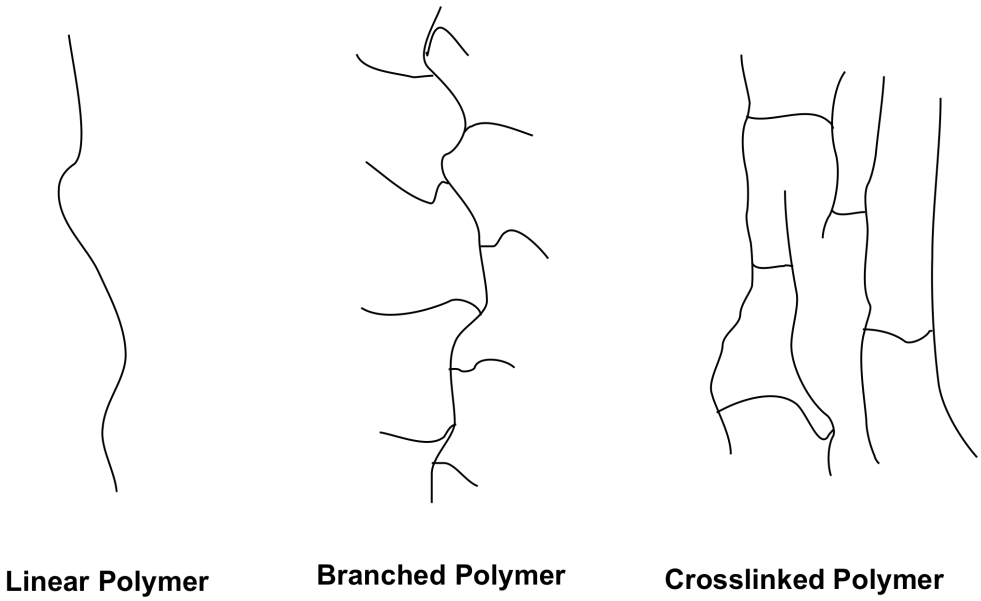

Figure 1-2 Three different polymer architectures.

If polymer chains derived from the same monomer, this polymer is called a homopolymer. But if there are two or more different types of monomers presenting in the polymer, such polymers can further be divided by the arrangement of monomers into four categories: statistical copolymer, block copolymer, alternating copolymer and graft copolymer. Statistical copolymers have two monomers randomly distributed in the chain. Block copolymers, as the name suggests, consist of two or more homopolymer subunits covalently bonded together. If two alternating monomers A and B are regularly arranged along the chain, this is called alternating copolymer. Finally, the structure composed of a chain of monomer A with blocks of monomer B grafting on it is a graft copolymer (Figure 1-3).

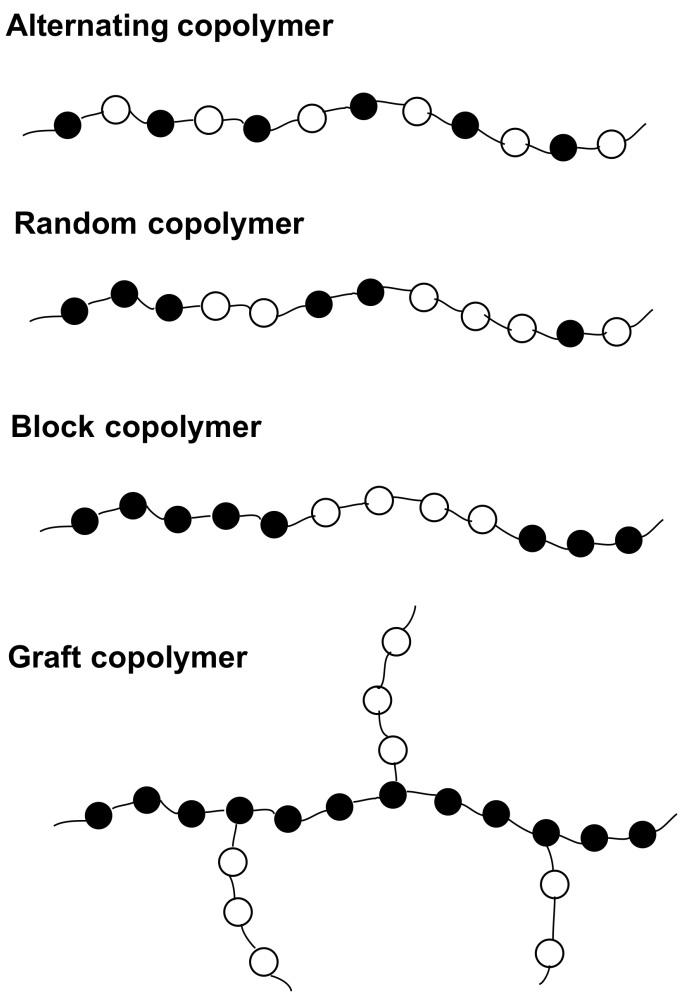

Figure 1-3 Four different arrangements of monomers.

Synthetic polymers cannot generally be assigned an exact molar mass but are instead described by a molar mass distribution. The reason is that a polymer sample usually consists of many polymer chains with different lengths. A typical molar mass distribution is shown in figure 1-4:

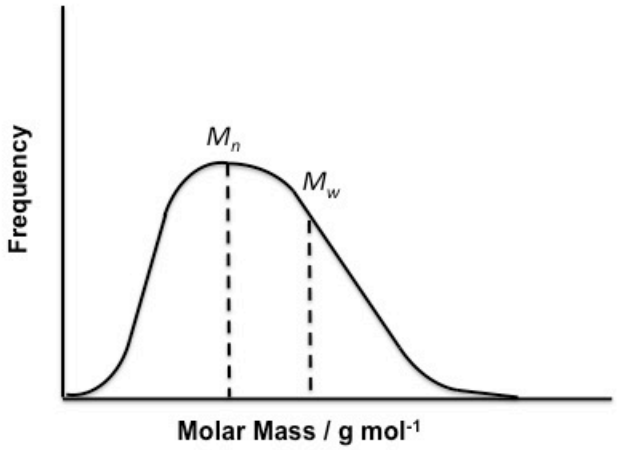

Figure 1-4 Polymer molar mass distribution.

Different types of average molar masses can be defined depending on whether the molar mass characterization method is sensitive to the number or the weight of polymer molecules. Gel permeation chromatography (GPC) is used to determine number average molar mass (M_n). M_n determines the average molar mass of individual polymer molecules. Small angle laser scattering and X-ray scattering were methods to determine weight average molar mass (M_w). In a small angle laser scattering experiment, large molecules have a larger contribution compared to small molecules. Therefore, this method is more sensitive to the weight of polymer molecules.[41] Molecular weights determined by such method are termed M_w. In the following equations, N_i represents the number of polymer molecules with the molar mass M_i. w_i represents the molar mass of species with the molar mass M_i.

Number-average molar mass: $M_n = \frac{\sum N_i \cdot M_i}{\sum N_i} = \frac{\sum w_i}{\sum (w_i / M_i)}$ (1-1)

Weight-average molar mass: $M_w = \frac{\sum N_i \cdot M_i^2}{\sum N_i M_i} = \frac{\sum w_i M_i}{\sum w_i}$ (1-2)

The ratio of M_n and M_w is defined as the polydispersity index (PDI) that is used to characterize the polydispersity of polymer samples.

$$PDI = \frac{M_w}{M_n} \quad (1\text{-}3)$$

1.2.2 The Crystalline State and the Glassy State

Crystallites are small, locally ordered arrangements of close-packed polymer chains. Below the melting point of a polymer, polymer chains first align at specific distances from each other to form nuclei (nucleation). These parallel arrays are then further packed to form a three-dimensional ordered structure (growth).[41] Crystallization is a temperature dependent process because of the competition between the kinetic effect and the thermodynamic effect. Thermodynamics describes how stable one state versus another state. A common thermodynamic quantity is free energy, ΔG. Due to the process of ordering, the entropy of crystallization is a negative number. At a high temperature, $-T\Delta S_{crystal}$ term becomes big enough so that $\Delta G_{crystal}$ becomes a positive number. In this situation, crystallization process would be thermodynamically unfavorable. If the temperature is lower than a certain level where $\Delta G_{crystal}$ is below 0, then crystallization process would be thermodynamically favorable. Even though the negative free energy, ΔG, can suggest that the products are more stable than the reactants, the reaction is still dictated by the kinetic effect. The kinetic effect determines how fast the species will be reacted. In crystallization process, the kinetic effect will dominate the process because chains may not have enough mobility to allow crystallite growth in the experimental time scale.[41, 42] Therefore, crystallization will only happen at a temperature below the melting

point where the negative enthalpy contribution to the free energy of crystallization is sufficiently large and above glass transition temperature (T_g) where polymer chains have sufficient mobility.

Non-crystalline (amorphous) state of polymers can be further divided into two different kinetic states, the rubbery/viscous state and the glassy state. Above the glass transition temperature (T_g), disordered polymer chains are highly dynamic such that the polymer material is rubbery or viscoelastic and can dissipate the stress applied on it by conformational changes of chains. Below the T_g (glassy state), on the other hand, disordered polymer chains are kinetically frozen and cannot change conformation under applied stress. Therefore, the material is often brittle in this state.

1.3 Block Copolymer and Micelle

1.3.1 Formation of Nanoparticle

Block copolymers have the ability to spontaneously self-assemble into nanoparticles in a selective solvent so that the free energy is minimized.[43-47] The free energy consists of two terms, entropy and enthalpy. Both terms may increase or decrease depending on parameters in the solution, such as the water content, polymer composition and solvent. Enthalpy may decrease because of decreasing unfavourable interactions between the hydrophobic blocks and water. On the other hand, enthalpy may also increase because of the repulsion between corona chains. In terms of entropy, it may decrease due to various reasons: repulsion between core-forming chains or increased stretching of corona-forming chains. Entropy may increase due to the hydrophobic effect: the hydrogen bonds formed by water molecules around hydrophobic blocks are broken upon micellization when hydrophobic chains are incorporated into the core of

nanoparticles. For example, for PCL-*b*-PEO, PEO is the hydrophilic block and can dissolve in the aqueous solution while PCL, the hydrophobic block, only dissolve in the organic solvent. When PEO-*b*-PCL is in a polar organic solvent, for example dimethylformamide (DMF), both blocks are able to dissolve such that single chains are dispersed in the solvent. The addition of water significantly changes the polarity of the polymer/DMF solution. As the percentage of water increases, the environment becomes more and more unfavourable for hydrophobic blocks. The block copolymers start to associate and form nanoparticles when the water content is above the critical water content (cwc). Under this situation, PCL will form the core to minimize the interaction with aqueous environments.

Just above the critical water content, nanoparticles and single chains are in dynamic equilibrium such that dissociation and association are happening at the same time. Therefore, the standard Gibbs free energy of micellization can be expressed as follows based on the relation between $\Delta G^{\circ}$and the equilibrium constant:

$$\Delta G^{\circ} = RTln(cmc) - RTm^{-1}\ln([C_m]) \quad (1\text{-}4)$$

In the equation, CMC represents critical micelle concentration that is equal to the molar concentration of single chains, while C_{m} represents the molar concentration of nanoparticles. And m is the association number, the number of single chains per nanoparticle. The above equation can be written as follows when m is sufficiently large:[42, 48, 49]

$$\Delta G^{\circ} = RTln(cmc) \quad (1\text{-}5)$$

$$\Delta H^{\circ} = R\frac{d\ln(cmc)}{d\frac{1}{T}} \quad (1\text{-}6)$$

$$\Delta S^{\circ} = (\Delta H^{\circ} - \Delta G^{\circ})/T \quad (1\text{-}7)$$

Therefore, one can estimate the contributions of enthalpy and entropy to the Gibbs free energy of micellization by the sign and magnitude of enthalpy and entropy. As the water content increases above cwc, the hydrophobic blocks will have very slow dynamics due to crystallization or vitrification. Therefore, in deionized water, nanoparticles are no longer in dynamic equilibrium anymore, which gives us the opportunity to characterize their properties such as the size and morphology. The critical water content can also be determined by static light intensity measurement. In this measurement, water is added to a polymer solution drop by drop. As the water content increases, polymer chains will not be able to form nanoparticles until the water content hits the cwc value. Therefore, at the point of cwc, there will be a significant change of the light intensity.

1.3.2 Morphologies

By minimizing the Gibbs free energy per block copolymer chain in nanoparticles, the association number and morphologies can be determined. For example, a small interfacial area per chain (denser chain packing at the interface) results in a lower interfacial energy per chain (decreasing the enthalpy) but stronger repulsive force between solubilized coronal blocks (increasing the enthalpy) and increased stretching of hydrophobic blocks in the core (decreasing the entropy). When the stretching of blocks in the core reaches a critical limit determined by the negative entropy contribution to the free energy, the nanoparticles will change morphology to decrease the concave curvature of the core/corona interface which increases the free volume between hydrophobic blocks and thus decreases the entropic penalty of stretching. Various morphologies under TEM are presented in Figure 1-5.

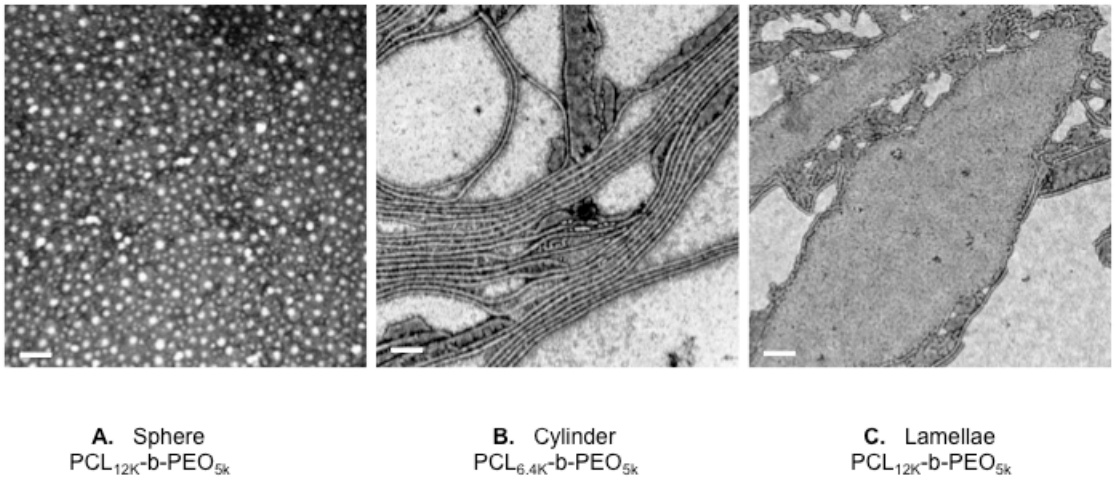

Figure 1-5 Various nanoparticle morphologies of PCL-*b*-PEO. A. sphere. B. cylinder. C. lamellae. Scale bar is 200 nm.

Two decades ago, Eisenberg reported the first example of multiple block copolymer nanoparticles morphologies in the system of polystyrene-*block*-poly(acrylic acid) (PS-*b*-PAA) in aqueous solutions. These morphologies included sphere, rods, lamellae, vesicles, reverse nanoparticles and a needle-like solid.[25] This group also investigated the effect of the relative hydrophilic and hydrophobic block lengths and the effect of adding homopolymers on the morphologies. As the length of the hydrophilic block (PAA) decreased, the morphology changed from sphere to cylinder and then to vesicle and lamellae structure. In contrast, adding hydrophobic homopolymers (PS) will increase the aggregation number of the core-forming blocks. The high entropic penalty will decrease by changing the morphologies in the direction from the bilayer aggregates (vesicles and lamellae) to spheres. Adding salt increased the electrostatic screening among PAA blocks (corona forming block). The decreased charge on PAA results in a

higher aggregation number and shifts nanoparticle morphologies from sphere to rod and bilayer. Finally, the water content was found to be able to change the boundary of these morphology transformations; higher water contents shift transition the boundaries to lower polymer concentrations.

1.4 Drug Delivery to Tumor Using Polymeric Nanoparticles

1.4.1 Passive Delivery and Active Delivery

Current anti-cancer drugs are developed based on their interactions with various biological pathways. Anticancer drugs' side effects are often attributed to their ability to kill cells indiscriminately.[50] Therefore, there is a need to develop drug delivery vehicles to target the drug more directly to the tumour cells. Moreover, some promising anticancer drugs failed to proceed to the formulation development because of their poor bioavailability or insolubility in the aqueous environment. As a result, to enhance drug efficacy, an increasing number of anti-cancer drug formulations employ targeted drug delivery.[17, 51-54] In this section, we will focus on drug delivery carriers composed of lipids or polymers. Encapsulation of drugs within such nanoparticles mitigates several undesirable properties of anticancer drugs, including low solubility in blood, cytotoxicity on normal cells, unfavourable pharmacokinetics and undesired biodistribution.[55] These nanoparticle-based drug delivery methods can be grouped into two categories: passive and active targeting.

Passive targeting is the result of the enhanced permeability and retention (EPR) effect (Figure 1-6).[16] As a tumour grows, it requires more nutrition and oxygen. As a result, tumor cells release signals to grow blood vessels near the tumour sites to transport nutrients and oxygen. Those newly grown blood vessels often have higher permeability

than blood vessels in healthy tissues and so allow nanoparticles of a certain size to permeate through the gaps between endothelial cells and localize in this affected area.[15] This EPR effect depends on the sizes of the nanocarriers and the gaps in blood vessels. As a result, drugs can passively accumulate in the affected area rather than distributing throughout the body.

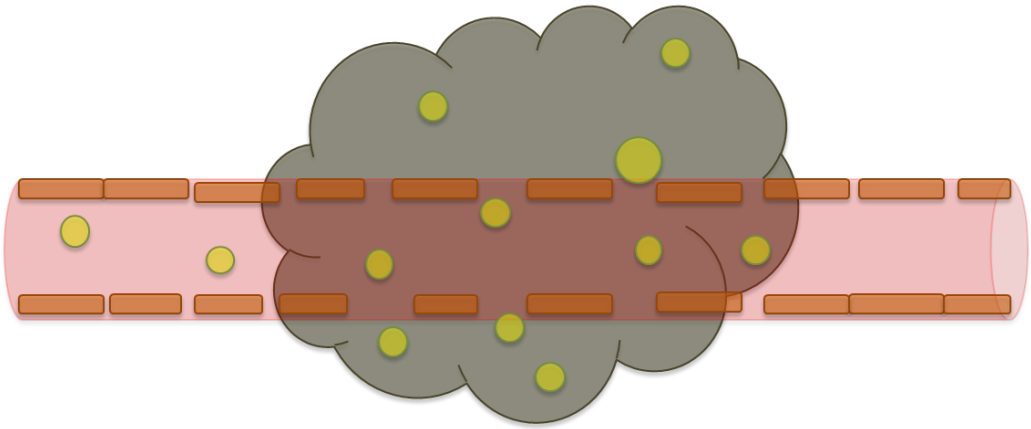

Figure 1-6 The EPR effect where vasculature is defective around tumor site.

Active targeting drug delivery systems often employ chemical conjugations or surface modification. Some nanocarriers achieved selective release by using pH- or temperature-sensitive polymers.[53, 56] Others used external heat, magnetic fields or ultrasound to guide nanocarriers to the tumour sites.[52, 54] Lee *et al*. developed a pH-sensitive polymeric carrier that degrades in slightly acidic environments, for example the usual environment around cancer cells, leading to the enhanced and faster accumulation of doxorubicin in the desired area.[53] Sershen *et al.* used poly(N-isopropylacrylamide) NIPAAM (which has a lower-critical solution temperature slightly above the body temperature), acrylamide, gold sulfide and gold shell to form a temperature-sensitive drug delivery system. The gold sulfide and gold form the shell of the nanoparticle and

respond to the irradiation by the light and transfer the heat to hydrogels made from NIPAAM-co-*N,N'*-methylenebisacrylamide copolymer. As a result, the temperature-sensitive hydrogel collapses and results in controlled release.[56]

1.4.2 Block Copolymer and Lipids in Drug Delivery

An important type of passive drug delivery nanocarriers is block copolymer nanoparticles containing a biocompatible hydrophilic corona-forming block. PEO is the most commonly used drug delivery carrier corona. It has been approved by the FDA to be used in the drug delivery for years[17, 18, 20, 57-60]. PEO corona was proved to prevent the opsonin absorption and macrophage clearance[12, 61]. Phagocytosis is an important mechanism by which the body protects itself. However, phagocytosis could clear pathogens as well as drug delivery vehicles or other therapeutic agents. And therefore it could be a barrier preventing drug delivery vehicles from accumulating in the human body.[6, 7] It turns out that the hydrophilic PEO corona can be used to avoid being phagocytized[13]. The PEO corona also helps to minimize undesirable interactions with products in the blood. Therefore, PEO successfully increases the circulation half-life of nanoparticle-encapsulated drugs in the body and, in combination with the EPR effect, increases the accumulation of drugs in the diseases area.[8] Kabanov AV *et al.* first reported using PEO block copolymers as the drug delivery carrier. They achieved a drastic increase in the drug effect.[62] G Kwon *et al.* encapsulated doxorubicin into PEO-*b*-PBLA nanoparticles. For the hydrophobic block, PCL and PS are widely studied for drug delivery carriers. The hydrophobic blocks generally form the nanoparticle core in aqueous environments and act as a reservoir for drugs suffering from poor solubility in the aqueous biological media.

Besides polymeric nanoparticles, lipids are also widely used as drug delivery nanocarrier materials. Liposome drug delivery systems include emulsions and solid lipid nanoparticles[63, 64,65]. Solid lipid nanoparticles contain drugs that are homogenously melted into lipid. Such nanoparticles have been used to encapsulate doxorubicin, timolol, idarubicin etc.[65]

Lipid-polymer hybrid nanoparticles have also been used as a drug delivery system.[21, 66, 67] The core consists of hydrophobic polymer chains, which is used as the reservoir for drugs. The hydrophilic polymer forms the shell and aims at increasing the nanoparticle circulation half-life. Lipids are placed at the interface of these two polymer chains and act as a barrier to the fast and immediate release of drugs inside the core. Using such a hybrid delivery system, the loading efficiency increased and the release rate slowed down compared to polymeric carriers that did not contain lipids.[66]

Although lipids are also popular in the drug encapsulation, the major disadvantage is the relatively high critical micelle concentration. The critical micelle concentration (cmc) of lipids was around 10^{-3} to 10^{-4}.[68] The cmc of lipids is much higher than the cmc of the amphiphilic copolymers (10^{-6} to 10^{-7}). Therefore, the low cmc makes polymeric nanoparticles more stable during the dilution and more robust as a drug delivery carrier.[69]

1.5 Characterization of Drug Delivery Nanoparticles

1.5.1 Dynamic Light Scattering (DLS)

DLS is used to characterize the hydrodynamic diameter of nanoparticles. This is a technique to determine the size distribution profile of a suspension. As nanoparticles move randomly in the solution, the distance among them and the intensity of the scattered light will also change. Big particles will have slower movement while small particles

move relatively faster. Therefore, the scattered light intensity is related to the size of particles. According to the Stokes-Einstein equation, we can then calculate the hydrodynamic diameter of nanoparticles by determining the diffusion coefficient (D_0) from the scattered light intensity.

$$r_h = \frac{\kappa_B T}{6\pi\eta D_0} \tag{1-8}$$

1.5.2 Transmission Electron Microscopy (TEM)

TEM is an application of electron diffraction. Current wave-particle duality states that matter, such as electrons, sometimes also behave like a wave. The wavelengths of electron waves are much smaller than visible light wavelengths. Visible light has wavelengths around 400 nm to 700 nm. But according to the de Broglie equation, the wavelength of electrons can be as small as picometer scale depending on the voltage applied to it.

$$\text{de Broglie equation}: \lambda = \frac{h}{p} = \frac{h}{mv} \tag{1-9}$$

Since the resolution of microscopy is determined by the wavelength of the emission source, TEM is able to work at a very high resolution.

The TEM image is generated when an accelerated electron beam passes through a thin film of the sample and scatters to different angles. When electrons hit the region with light atoms such as carbon, the scattering will be weak. On the other hand, heavy atoms will result in higher scattering. Therefore, the electrons that are not scattered then pass though the specimen and will be recorded by the camera. The bright area represents the higher transmission region while dark area means the lower transmission region.

In this study, PCL-*b*-PEO composed of mostly carbon atoms will have very high transmission and will not be able to provide enough contrast on TEM image. Therefore, we used uranyl acetate to stain our samples. Uranyl acetate, with a very heavy weight, binds to PEO blocks. As a result, the nanoparticles' core-forming blocks, PCL, had bright shapes under TEM.

1.5.3 Loading Efficiency and *In Vitro* Release Against PBS

High-performance liquid chromatography measures how many drugs were encapsulated inside the nanoparticles and how fast it will be released out in an environment similar to human. The definition of loading level, loading efficiency and initial loading ratio are listed as follows:

$$r(initial\ loading\ ratio) = \frac{mass\ of\ drug/g}{mass\ of\ polymer/g} \quad (1\text{-}10)$$

$$Loading\ efficiency = \frac{mass\ of\ encapsulated\ drug/g}{mass\ of\ total\ drug\ used/g} \times 100\% \quad (1\text{-}11)$$

$$Loading\ level = \frac{mass\ of\ encapsulated\ drug/g}{mass\ of\ polymer/g} = loading\ efficiency \times r \quad (1\text{-}12)$$

The HPLC system we used equipped with a hydrophobic C18 column. When the sample was injected into the HPLC carrying by the mobile phase, the molecules we are interested in will interact with the column while the hydrophilic part in the sample will be carried forward. Then the separated phases pass through the UV detector and the integrated area of its absorption at a certain wavelength is the indication of its concentration.

1.5.4 Cytotoxicity by Anti-proliferative Assay

A cell-based assay was used to investigate the cytotoxicity of the chosen agent, with and without nanoparticle encapsulation. The MDA-MB-231 cell line was chosen

because it is believed to provide more extensively vascularized tumours in animals. Since we planned to take this work forward to animal studies in the future, we decided to start with MDA-MB-231 cell line for the *in vitro* studies.[70] The key value generated by the cell line study is IC_{50}. IC_{50} is the drug concentration that can inhibit the growth of 50% cancer cells.

1.6 Therapeutic potential of Curcumin

1.6.1 Curcumin in General and Its Limitations

Curcumin is a hydrophobic polyphenol extracted from a plant of the ginger family, turmeric. It exists predominantly in its diketone form in water, but in its enol form in organic solvents.

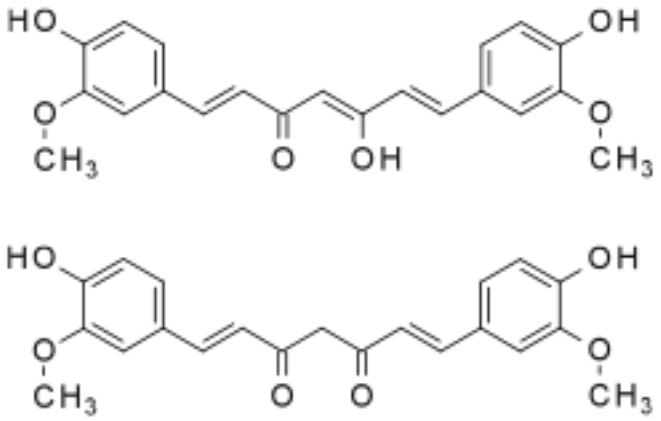

Figure 1-7 Keto (bottom) form and Enol (top) form of curcumin.

Curcumin received extensive researches at the early stage of drug formulation development because of its potential as anti-inflammatory, antiproliferative and antiangiogenic agent.[71-75] In terms of toxicity, no obvious side effect was noticed at a low dose. At a dose higher than 100 mg/day, curcumin may cause diarrhea, skin rash and other side effects.[76] Despite its attractive qualities in various biological activities such as

anti-oxidant, anti-carcinogenic and anti-bacterial, curcumin failed to progress to the formulation development because of its poor bioavailability, rapid degradation and being reactive to various targets. According to Wang *et al.,* curcumin blood circulation half-life was below 5 mins.[36] The rapid degradation led to the question whether the therapeutic effects were the results of curcumin or other reactive degradation products. Other drawbacks of curcumin reported in the reviewed literature are listed below. According to Y.J. Wang *et al.*, 90% curcumin decomposed in the PBS serum-free solution at 7.2 pH and 37°C. Further experiments also revealed that curcumin would be more stable in the environment containing fetal calf serum or human blood.[36] Moreover, curcumin also had low aqueous solubility. Kurien BT *et al.* reported that water solubility of curcumin is only 0.6 μg/mL.[77] The drug's serum concentrations, tissue distributions and half-life times are all indications of the bioavailability of a molecule[78]. The serum concentration is the concentration of the molecule in the blood plasma after administration. From several clinical trials and animal studies, even when administering several grams of curcumin, there was only a trace of curcumin presenting in the blood[73-75, 79, 80]. Another indication of the bioavailability is the drug's tissue distribution. Tissue distribution determines the amount of curcumin in each organ after administration. From the research by Pan *et al.* summarizing curcumin concentrations in each part of human and rodents, the result showed that the absorption in the body was also low (dose = 100 mg/Kg body weight)[81].

Table 1-1 Curcumin distribution in mice organs after 1h of intravenous injection

Sample or Tissue	Curcumin *μg/g*	Total Curcumin *μg/total organ*	Organ /g or Plasma/mL
Plasma	0.60 ± 0.03	0.52 ± 0.03	0.86 ± 0.01
Kidneys	7.51 ± 0.08	3.00 ± 0.03	0.40 ± 0.07
Spleen	26.06 ± 1.06	2.61 ± 0.11	0.10 ± 0.01
Liver	26.90 ± 2.58	33.09 ± 3.17	1.23 ± 0.08
Brain	0.41 ± 0.01	0.18 ± 0.01	0.43 ± 0.04
Intestine	117.04 ± 6.86	319.52 ± 18.73	2.73 ± 0.27

Curcumin is less potent compared to the typical anti-cancer drugs', such as paclitaxel[82, 83] or doxorubisin[84, 85]. In clinical trials or cell line experiments, only a very high therapeutic dose of curcumin was proved to be effective. Table 1-1 suggests that the poor absorption of curcumin in the intestine, the low plasma concentration and the fast exclusion and metabolism in bile and liver make it difficult for curcumin to reach its targets. Moreover, Nelson *et al.* reviewed several reported activities of curcumin such as inhibiting HAT p300[86] and tau fibril formation[87]. The author criticized that most papers he reviewed failed to consider the assay interference, curcumin instability and off-target effects. Therefore, curcumin was not considered as a promising therapeutic agent.[38]

Knowing the challenges of curcumin, there were several researches focusing on improving its instability. Banerjee *et al.* improved curcumin's hydrolytic instability by binding it to metal ions such as cobalt (III), zinc(II) and ruthenium(II).[76] The curcumin modified complexes showed an improved pharmacological effect. Therefore, a new direction for curcumin research is to improve its solubility, selectivity and stability first.

1.6.2 Free Curcumin in Clinical Trials

There were several reports about free curcumin phase one and phase two clinical trials. Both Phase 1 and Phase 2 clinical trials are designed to test new medicines on humans and to determine the safe dose and side effects. The difference is, in phase 1 clinical trials, the drug is tested on healthy volunteers. The goal is usually to investigate a range of dose. But in phase 2 clinical trials, the drug is tested on patients. In phase 2 clinical trials, the objective is to determine the drug's efficacy and side effects. Sharma *et al.* conducted a phase 1 clinical trial evaluating the efficacy of curcumin in treating colorectal cancer. Three biomarkers of activities of curcumin were monitored after one hour of oral administration for four months. The experiment did not conclude a definite optimum dose for treating gastrointestinal cancer due to low bioavailability of curcumin. Only one biomarker, prostaglandin E2 (PGE2), was affected by curcumin occasionally. Moreover, only the highest dose (3.6 g/day) was discussed in the paper, which indicated that low dose of curcumin might not be detectable or therapeutically effective in this study. Moreover, the researchers did not exclude the possibility that both curcumin and its degradation products might be bioactive in this experiment.[79]

Cheng *et al.* also conducted a phase 1 clinical trial for the purpose of evaluating curcumin's biologically effective dose. There were 25 participants with different kinds of cancer types. They took curcumin orally from a starting dose, 500 mg/day, to 8000 mg/day. And by monitoring biological components that worked as cell signaling or transcription of genetic information, they concluded that curcumin had a chemoprevention effect on bladder cancer and oral leukoplakia.[73, 79] However, there were several questions in their research. First, they did not use a placebo as the control. Second, they reported that there was no "treatment-related toxicity", which ignored life-

quality related problems such as nausea and diarrhea. Finally, although both Cheng *et al.* and Sharma *et al.* conducted the phase 1 clinical trial under similar conditions (bare curcumin, oral administration, similar dose per day), their results of the curcumin plasma concentration after one hour had a huge discrepancy. Cheng *et al.* reported a plasma concentration around 510 nM while Sharma *et al.* only detected 11 nM curcumin in a very similar experiment setting.

1.6.3 Curcumin in Drug Delivery Systems

Since the clinical trial results of bare curcumin described above were not promising, the research of curcumin has been shifting away from bare curcumin to developing drug delivery vehicles for this unstable drug. Encapsulation of curcumin in polymeric nanoparticles may mitigate many of the problems associated with curcumin. We would expect that encapsulation should improve overall bioavailability for curcumin or reduce the rate of decomposition. Ma Z *et al.* prepared PEO-*b*-PCL nanoparticle-encapsulated curcumin. They compared polymers with several different PCL block lengths and found out that PEO(5k)-*b*-PCL(13k) was the best carrier material due to its relatively high loading efficiency. Upon encapsulation, curcumin was dissolved in PCL blocks rather than aqueous environments. Therefore, the encapsulation not only increased the solubility and stability of free curcumin but also increased the possibility to achieve passive accumulation in the tumor due to the EPR effect. The cytotoxicity tests on four different cell lines, B16-F10, SP-53, Mino and JeKo-1, showed that cytotoxicity is concentration-dependant, suggesting that the cancer cells viability decreased with an increase of drug concentration. Moreover, after testing with different nanoparticle-encapsulated curcumin concentrations, the result showed that the cytotoxicity of

curcumin was not compromised even if it was encapsulated in the nanoparticles.[24] Raveendran *et al.* used solvent dialysis method to prepare pluronic/PCL nanoparticles. The loaded nanoparticles had sustained release over 100 hours. This drug delivery system was also proven to be compatible with blood by hemolysis study and stable in PBS. Besides the cytotoxicity test, fluorescence microscopy showed that colorectal adenocarcinoma cancer cells took up more encapsulated curcumin than taking up free curcumin. This research showed that the pluronic/PCL system improved curcumin's poor absorption and bioavailability.[88] Song *et al.* performed a pharmacokinetics and biodistribution study using tri-block copolymers as the carrier material. They successfully prepared nanoparticles with a small average hydrodiameter of 26 nm and a high loading efficiency of 70 wt %. After the nanoparticles were injected intravenously into mice, curcumin concentrations in plasma were similar between free drug and encapsulated drug from PK study. Both concentrations dropped quickly in the first hour after injection.[89] This study indicated promising results at the stage of nanoparticle structural properties control. However, due to the fast elimination of curcumin, this drug delivery system was not effective in terms of the controlled release and bioavailability.

In summary, encapsulated curcumin was reported to have higher solubility and increased stability and bioavailability than free curcumin. However, most papers reviewed in this section did not consider or check the effect of curcumin degradation products. Moreover, encapsulation in nanoparticle could use EPR effect to accumulate in tumor and partly solve the drawback that curcumin is non-selective. However, more problems need to be solved regarding the drug delivery system, such as improving loading efficiency, cytotoxicity and controlled release.

1.7 Microfluidics for Drug Delivery

1.7.1 Two-Phase Microfluidic Reactor

In the previous section, most of the polymeric nanoparticles were prepared using a conventional bulk method. Over the past few years, our group has developed a microfluidic reactor and studied its influence on polymeric nanoparticles. The microfluidic reactor has small size channels with diameters around 100 nm to several micrometers. It provides advantages such as a small reaction volume, fine tuning flow rate and a higher area-to-volume ratio. Reynolds number determines flow dynamics.[90]

$$Re = \frac{\rho v D}{\mu} \tag{1-13}$$

In the above equation, Re represents Reynolds number, which is used to describe the fluid flow situation. A large Reynolds number (over 2400) indicates the turbulent flow while small number represents the laminar flow. ρ is the density of the solution with a unit of kg/m^3. ν represents the velocity of the solution in the channel. μ is the dynamic viscosity. *D* is the diameter of channels. Therefore, for the microfluidic reactor with channels of a couple micrometers, the Reynolds number is so small that the flow is usually laminar flow. As the result, after injecting different chemicals into the channel, the liquid will flow as parallel layers with diffusion between different layers. This is the idea behind single-phase microfluidics where the main means of transportation between fluids is diffusion.

Julian Thiele *et al.* used single-phase microfluidic chip to prepare monodispersed P2VP-*b*-PEO vesicles.[91] Three different fluid streams were injected through perpendicular crossed inlets. After they joined together, it flew forward as laminar flow. The result showed that they were able to manipulate the size of vesicles from 40nm to

2μm. Rohit Karnik *et al.* also investigated the optimization of self-assembly nanoparticles by using single-phase microfluidics on PLGA-*b*-PEG block copolymer nanoparticles. By tuning the flow rate, polymer concentration and composition, they were managed to improve the polydispersity, control the size and release profile after encapsulation of drug.[92]

A major disadvantage of single-phase microfluidic reactor is its slow mixing. Since fast mixing is preferred in nanoparticle synthesis, there are several ways to increase mixing. One way to increase the mixing in the channel is to incorporate two immiscible solutions. In this situation, the liquid with higher surface tension forms drops of solution carried forward by the other liquid. Another method is to incorporate liquid and gas together on a microfluidic reactor.[27, 93] Our group started to investigate the gas liquid two-phase microfluidics so that the higher shear force can be used to prepare nanoparticles on the chip. See Figure.1-8. In the gas liquid two-phase microfluidics, different streams of fluids are injected into the channel. Another stream of argon gas is joined together with the fluid streams. The gas forms gas bubbles and compartmentalizes the liquid stream into small segments. As liquid and gas segments proceed into mixing and processing channels, the recirculating flow in the liquid segments significantly increases the shear force around the corner of the segments. The high shear created in the segments corners provides energy for nanoparticles coalescence and polymer chains rearrangement. After the collision of nanoparticles, newly formed nanoparticles with greater aggregation numbers are at a high unstable energy state. The high free energy particles will undergo on-chip relaxation until they reach equilibrium. This relaxation process is achieved *via* polymer chain rearrangement. As a result, we would be able to observe morphology

transition.[26] Nanoparticles either go through break-up process to form high curvature structure with small size and aggregation numbers or form low curvature structures such as cylinder and lamellae *via* shear-induced coalescence. In summary, there are three shear-induced mechanisms that result in morphology change. The first is break-up where big morphologies such as cylinder and bilayer break and form more thermodynamically stable morphologies such as small spheres. In this process, the chains are relaxed by reducing aggregation number. Another mechanism is coalescence where small spheres join together to form large morphologies. This mechanism reduces chains stretching by forming low curvature structures such as cylinder and lamellae. The third is crystallization where crystallinity inside the nanoparticle increases when shear force increase. Depending on the flow rate and other chemical parameters, coalescence and crystallization mechanisms may coexist or one of them will be dominant. Therefore, by controlling the flow rate of microfluidics, the morphology and also crystallinity can be manipulated.

1.7.2 Microfabrication of The Microfluidic Reactor Used in This Thesis

The two-phase microfluidic reactor used in this thesis has four inlets and one outlet. One of the four inlets is used to inject argon while the other three are used as the inlets for the polymer/drug solution, solvent DMF and solvent-water mixture solution. Then after the four streams join together, the regular gas stream mixes with the liquid stream and forms gas and liquid segments. Then the inlets are followed by a 100mm long mixing channel. The mixing channel has a sinusoidal shape and is 100μm wide, 100mm long and 150 μm deep. After that, a mixture of gas and liquid flows through the

processing channel which also has a sinusoidal shape. The processing channel is wider and longer than the mixing channel with a width of 200 μm and a length of 740 mm.

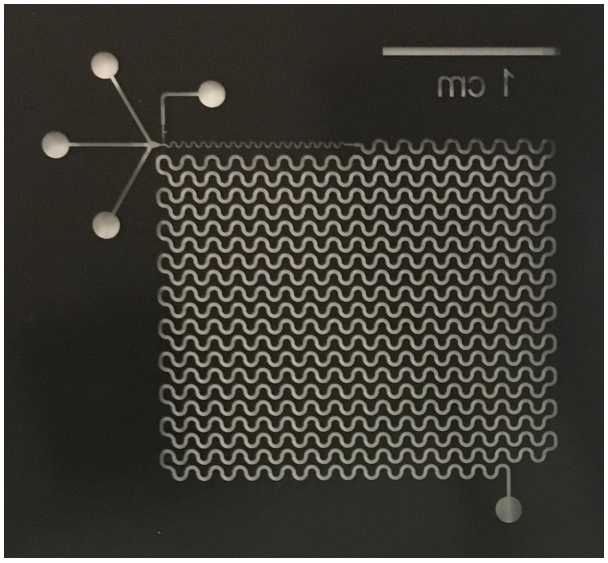

Figure 1-8 Photomask of the microfluidic chip.

There are two steps in making the microfluidic chip. The first step is making master chips. The specific process was described in Figure 1-9. First of all, SU-8, a photocurable material, is spin-coated on top of a clean silicon wafer. SU-8 would be cured on top of the silicon wafer after exposure to UV light. The depth of the spin-coated SU-8 layer on the wafer is 150 μm, which is controlled by the speed and time of spinning. Then the silicon wafer is transferred to a hot plate so that the solvent could evaporate and leave a hard coat on top of the wafer (Figure 1-9. step 2 pre-bake). Next, the photomask with the microfluidic reactor image is placed on the SU-8 layer and exposed to UV light. The features on the reactor image are transferred onto the SU-8 layer. The SU-8 part that is exposed to UV light would be cured while the other part that is hidden under the photomask would be washed away in the developing solution.

The next step is using the master chip to make a polydimethyl siloxane (PDMS) reactor. See Figure 1-10. This step uses the master chip as a negative model. PDMS and the curing agent are first measured to a specific weight ratio. Then PDMS and the curing agent are mixed up and degassed by a vacuum oven. Then the mixture is poured on master chip and forms a replica mold of the master chip. After the mold becomes hard, it would be peeled off the master chip gently. Then a PDMS covered glass slide is bonded to the PDMS chips by oxygen plasma treatment followed by heating on a hot plate. The methyl groups on the PDMS surface would be oxidized during the plasma treatment. After the oxygen plasma treatment, the PDMS mold is placed on the PDMS covered glass slide and sealed by heating.

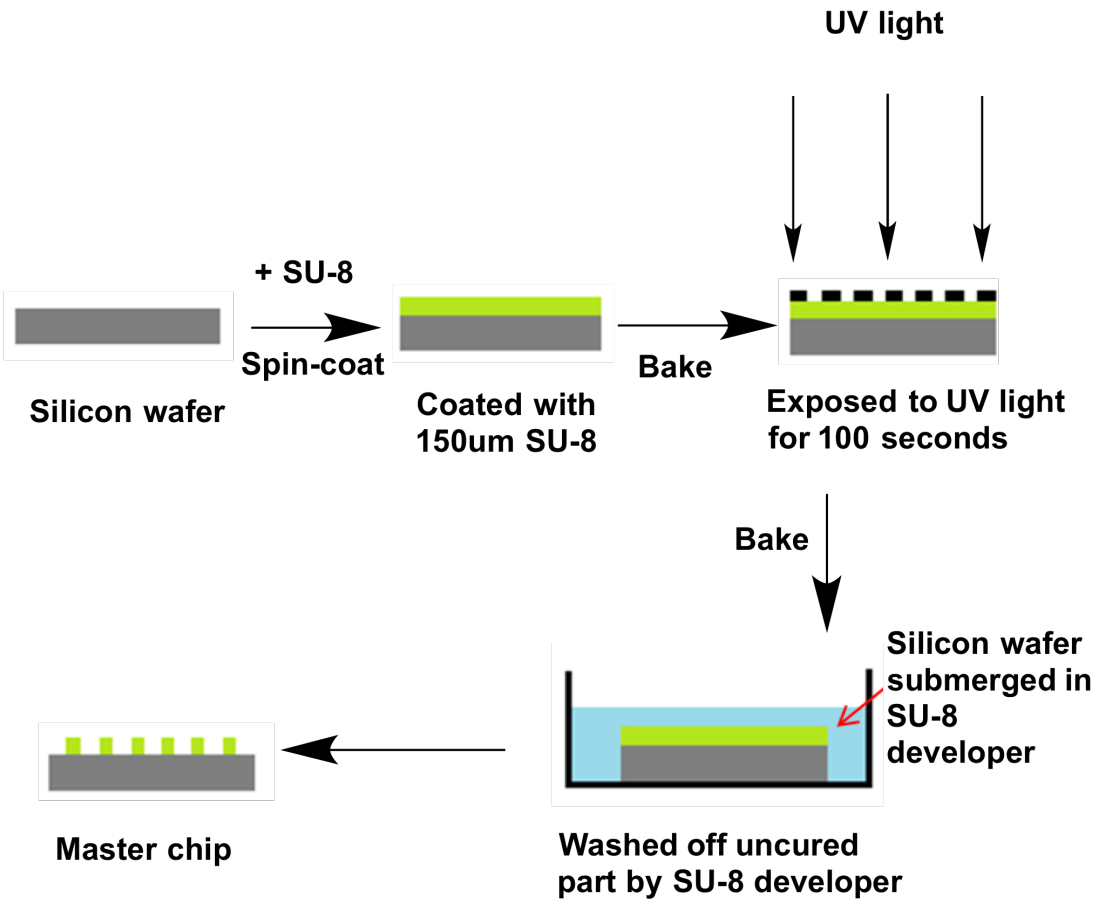

Figure 1-9 Procedure of making a master chip.

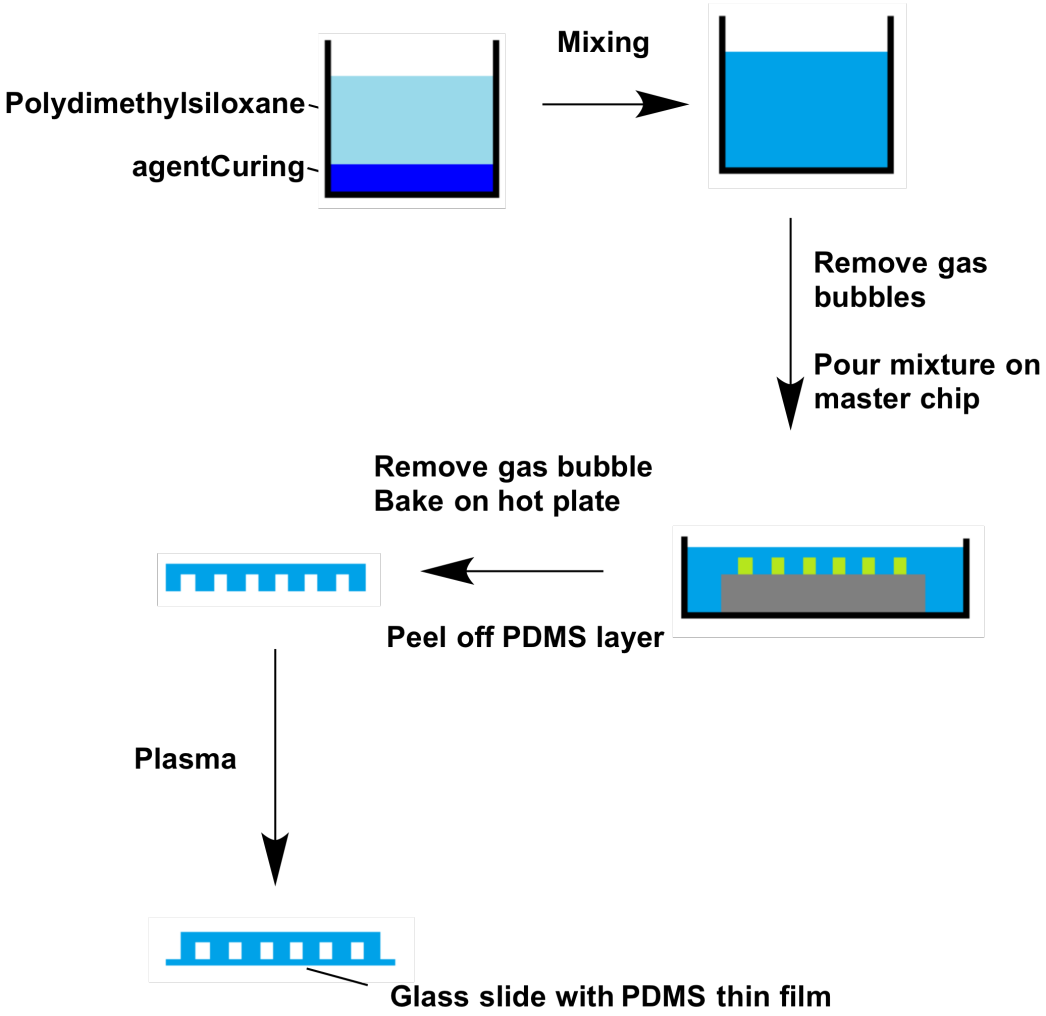

Figure 1-10 Procedure of producing PDMS chip.

1.8 Outline of Thesis: Description of Chapters

This thesis focuses on the application of microfluidic on curcumin drug delivery. The remaining chapters consist of three experimental chapters and a conclusion chapter. Experimental chapters discussed chemical parameters' influences on various properties of nanoparticles such as size, morphologies, loading efficiency, release rate and cytotoxicity.

Chapter 2 will describe microfluidics manufacturing and characterization of curcumin loaded PCL-*b*-PEO nanoparticles by TEM, DLS, loading efficiency and release

rate. It was shown that drug-loaded nanoparticles prepared by our microfluidic reactor had a more uniform distribution and better loading efficiency than the nanoparticles prepared using a more traditional bulk method. Both size and loading efficiency are controlled by flow rate and water content.

In Chapter 3, optimization experiments were done based on results from the previous chapter. It was concluded in Chapter 2 that the microfluidic reactor provided control over the size and loading efficiency. However, the release profiles we had from Chapter 2 were too fast for the possible *in vivo* pharmacokinetic experiment. In this chapter, we changed flow rate, drug-to-polymer ratio and water content, and investigated each parameter's influence on the sample's release rate. The result showed that increasing flow rate had the most significant effect on release rate. In this chapter, the procedure of extracting curcumin from plasma was developed. A calibration curve was obtained.

Chapter 4 describes the anticancer activity of curcumin loaded PCL-*b*-PEO nanoparticles on human breast cancer cell line MDA-MB-231. The group of samples with highest loading efficiency and smallest size were chosen. IC_{50} values, the concentration of a drug formulation when 50% cells growth is inhibited, were collected. The result showed that curcumin was able to inhibit the growth of breast cancer cells. However, the cytotoxicity was compromised after encapsulation in the nanoparticle.

Finally, Chapter 5 provides the general conclusion, outlook and future work.

1.9 Reference

1. Bhushan, B.; Schricker, S. R., A review of block copolymer-based biomaterials that control protein and cell interactions. *Journal of Biomedical Materials Research Part A* **2014,** *102* (7), 2467-2480.

2. Singh, A. N.; Thakre, R. D.; More, J. C.; Sharma, P. K.; Agrawal, Y. K., Block Copolymer Nanostructures and Their Applications: A Review. *Polymer-Plastics Technology and Engineering* **2015,** *54* (10), 1077-1095.

3. Hu, H. Q.; Gopinadhan, M.; Osuji, C. O., Directed self-assembly of block copolymers: a tutorial review of strategies for enabling nanotechnology with soft matter. *Soft Matter* **2014,** *10* (22), 3867-3889.

4. Robb, M. J.; Connal, L. A.; Lee, B. F.; Lynd, N. A.; Hawker, C. J., Functional block copolymer nanoparticles: toward the next generation of delivery vehicles. *Polymer Chemistry* **2012,** *3* (6), 1618-1628.

5. Kang, Y.; Walish, J. J.; Gorishnyy, T.; Thomas, E. L., Broad-wavelength-range chemically tunable block-copolymer photonic gels. *Nature Materials* **2007,** *6* (12), 957-960.

6. Seth, V.; Chandra, R. K., Opsonic activity, phagocytosis, and bactericidal capacity of polymorphs in undernutrition. *Arch Dis Child* **1972,** *47* (252), 282-4.

7. Tan, J. S.; Butterfield, D. E.; Voycheck, C. L.; Caldwell, K. D.; Li, J. T., Surface modification of nanoparticles by PEO/PPO block copolymers to minimize interactions with blood components and prolong blood circulation in rats. *Biomaterials* **1993,** *14* (11), 823-33.

8. Knop, K.; Hoogenboom, R.; Fischer, D.; Schubert, U. S., Poly(ethylene glycol) in drug delivery: pros and cons as well as potential alternatives. *Angew Chem Int Ed Engl* **2010,** *49* (36), 6288-308.

9. Bains, A.; Cao, Y.; Moffitt, M. G., Multiscale Control of Hierarchical Structure in Crystalline Block Copolymer Nanoparticles Using Microfluidics. *Macromol Rapid Commun* **2015,** *36* (22), 2000-5.

10. Malhotra, M.; Surnar, B.; Jayakannan, M., Polymer Topology Driven Enzymatic Biodegradation in Polycaprolactone Block and Random Copolymer Architectures for Drug Delivery to Cancer Cells. *Macromolecules* **2016,** *49* (21), 8098-8112.

11. Woodruff, M. A.; Hutmacher, D. W., The return of a forgotten polymer-Polycaprolactone in the 21st century. *Progress in Polymer Science* **2010,** *35* (10), 1217-1256.

12. Vittaz, M.; Bazile, D.; Spenlehauer, G.; Verrecchia, T.; Veillard, M.; Puisieux, F.; Labarre, D., Effect of PEO surface density on long-circulating PLA-PEO nanoparticles which are very low complement activators. *Biomaterials* **1996,** *17* (16), 1575-81.

13. Kwon, G. S.; Yokoyama, M.; Okano, T.; Sakurai, Y.; Kataoka, K., Biodistribution of micelle-forming polymer-drug conjugates. *Pharm Res* **1993,** *10* (7), 970-4.

14. Torchilin, V. P., Passive and active drug targeting: drug delivery to tumors as an example. *Handb Exp Pharmacol* **2010,** (197), 3-53.

15. Maeda, H.; Wu, J.; Sawa, T.; Matsumura, Y.; Hori, K., Tumor vascular permeability and the EPR effect in macromolecular therapeutics: a review. *Journal of Controlled Release* **2000,** *65* (1-2), 271-284.

16. Wong, A. D.; Ye, M.; Ulmschneider, M. B.; Searson, P. C., Quantitative Analysis of the Enhanced Permeation and Retention (EPR) Effect. *PLOS One* **2015,** *10* (5).

17. Ahmed, F.; Discher, D. E., Self-porating polymersomes of PEG-PLA and PEG-PCL: hydrolysis-triggered controlled release vesicles. *J Control Release* **2004,** *96* (1), 37-53.

18. Cai, S.; Vijayan, K.; Cheng, D.; Lima, E. M.; Discher, D. E., Micelles of different morphologies--advantages of worm-like filomicelles of PEO-PCL in paclitaxel delivery. *Pharm Res* **2007,** *24* (11), 2099-109.

19. Malik, N.; Evagorou, E. G.; Duncan, R., Dendrimer-platinate: a novel approach to cancer chemotherapy. *Anticancer Drugs* **1999,** *10* (8), 767-76.

20. Mikhail, A. S.; Allen, C., Block copolymer micelles for delivery of cancer therapy: transport at the whole body, tissue and cellular levels. *J Control Release* **2009,** *138* (3), 214-23.

21. Wong, H. L.; Bendayan, R.; Rauth, A. M.; Xue, H. Y.; Babakhanian, K.; Wu, X. Y., A mechanistic study of enhanced doxorubicin uptake and retention in multidrug resistant breast cancer cells using a polymer-lipid hybrid nanoparticle system. *J Pharmacol Exp Ther* **2006,** *317* (3), 1372-81.

22. Vyhnalkova, R.; Muller, A. H. E.; Eisenberg, A., Control of Corona Composition and Morphology in Aggregates of Mixtures of PS-b-PAA and PS-b-P4VP Diblock Copolymers: Effects of pH and Block Length. *Langmuir* **2014,** *30* (17), 5031-5040.

23. Vyhnalkova, R.; Muller, A. H. E.; Eisenberg, A., Control of Morphology and Corona Composition in Aggregates of Mixtures of PS-b-PAA and PS-b-P4VP Diblock Copolymers: Effects of Solvent, Water Content, and Mixture Composition. *Langmuir* **2014,** *30* (44), 13152-13163.

24. Ma, Z.; Haddadi, A.; Molavi, O.; Lavasanifar, A.; Lai, R.; Samuel, J., Micelles of poly(ethylene oxide)-b-poly(epsilon-caprolactone) as vehicles for the solubilization, stabilization, and controlled delivery of curcumin. *J Biomed Mater Res A* **2008,** *86* (2), 300-10.

25. Zhang, L.; Eisenberg, A., Multiple Morphologies of "Crew-Cut" Aggregates of Polystyrene-b-poly(acrylic acid) Block Copolymers. *Science* **1995,** *268* (5218), 1728-31.

26. Wang, C. W.; Sinton, D.; Moffitt, M. G., Flow-directed block copolymer micelle morphologies via microfluidic self-assembly. *J Am Chem Soc* **2011,** *133* (46), 18853-64.

27. Song, H.; Chen, D. L.; Ismagilov, R. F., Reactions in droplets in microflulidic channels. *Angewandte Chemie-International Edition* **2006,** *45* (44), 7336-7356.

28. Salem, M.; Rohani, S.; Gillies, E. R., Curcumin, a promising anti-cancer therapeutic: a review of its chemical properties, bioactivity and approaches to cancer cell delivery. *RSC Advances* **2014,** *4* (21), 10815-10829.

29. Bush, J. A.; Cheung, K. J.; Li, G., Curcumin induces apoptosis in human melanoma cells through a Fas receptor/caspase-8 pathway independent of p53. *Exp Cell Res* **2001,** *271* (2), 305-14.

30. Chen, H.; Zhang, Z. S.; Zhang, Y. L.; Zhou, D. Y., Curcumin inhibits cell proliferation by interfering with the cell cycle and inducing apoptosis in colon carcinoma cells. *Anticancer Res* **1999,** *19* (5A), 3675-80.

31. Hanif, R.; Qiao, L.; Shiff, S. J.; Rigas, B., Curcumin, a natural plant phenolic food additive, inhibits cell proliferation and induces cell cycle changes in colon adenocarcinoma cell lines by a prostaglandin-independent pathway. *J Lab Clin Med* **1997,** *130* (6), 576-84.

32. Kim, M. S.; Kang, H. J.; Moon, A., Inhibition of invasion and induction of apoptosis by curcumin in H-ras-transformed MCF10A human breast epithelial cells. *Arch Pharm Res* **2001,** *24* (4), 349-54.

33. Pan, M. H.; Chang, W. L.; Lin-Shiau, S. Y.; Ho, C. T.; Lin, J. K., Induction of apoptosis by garcinol and curcumin through cytochrome c release and activation of caspases in human leukemia HL-60 cells. *J Agric Food Chem* **2001,** *49* (3), 1464-74.

34. Yu, H.; Tran, T. T.; Teo, J.; Hadinoto, K., Dry powder aerosols of curcumin-chitosan nanoparticle complex prepared by spray freeze drying and their antimicrobial efficacy against common respiratory bacterial pathogens. *Colloids and Surfaces a-Physicochemical and Engineering Aspects* **2016,** *504*, 34-42.

35. Priyadarsini, K. I., The chemistry of curcumin: from extraction to therapeutic agent. *Molecules* **2014,** *19* (12), 20091-112.

36. Wang, Y. J.; Pan, M. H.; Cheng, A. L.; Lin, L. I.; Ho, Y. S.; Hsieh, C. Y.; Lin, J. K., Stability of curcumin in buffer solutions and characterization of its degradation products. *J Pharm Biomed Anal* **1997,** *15* (12), 1867-76.

37. Schneider, C.; Gordon, O. N.; Edwards, R. L.; Luis, P. B., Degradation of Curcumin: From Mechanism to Biological Implications. *Journal of Agricultural and Food Chemistry* **2015,** *63* (35), 7606-7614.

38. Nelson, K. M.; Dahlin, J. L.; Bisson, J.; Graham, J.; Pauli, G. F.; Walters, M. A., The Essential Medicinal Chemistry of Curcumin. *J Med Chem* **2017**.

39. Grancharov, G.; Gancheva, V.; Kyulavska, M.; Momekova, D.; Momekov, G.; Petrov, P., Functional multilayered polymeric nanocarriers for delivery of mitochondrial targeted anticancer drug curcumin. *Polymer* **2016,** *84*, 27-37.

40. Bohidar, H. B., Fundamentals of Polymer Physics and Molecular Biophysics. *Fundamentals of Polymer Physics and Molecular Biophysics* **2015**, 1-321.

41. Sperling, L. H., Introduction to Physical Polymer Science, 4th Edition. *Introduction to Physical Polymer Science, 4th Edition* **2006**, 1-845.

42. Rigby, M., Physical Chemistry, 3rd Edition Atkins, PW. *Nature* **1986,** *319* (6056), 820-820.

43. Rizis, G.; van de Ven, T. G.; Eisenberg, A., "Raft" formation by two-dimensional self-assembly of block copolymer rod micelles in aqueous solution. *Angew Chem Int Ed Engl* **2014,** *53* (34), 9000-3.

44. Sun, J.; Chen, X.; Lu, T.; Liu, S.; Tian, H.; Guo, Z.; Jing, X., Formation of reversible shell cross-linked micelles from the biodegradable amphiphilic diblock copolymer poly(L-cysteine)-block-poly(L-lactide). *Langmuir* **2008,** *24* (18), 10099-106.

45. Letchford, K.; Burt, H., A review of the formation and classification of amphiphilic block copolymer nanoparticulate structures: micelles, nanospheres, nanocapsules and polymersomes. *Eur J Pharm Biopharm* **2007,** *65* (3), 259-69.

46. Gaucher, G.; Dufresne, M. H.; Sant, V. P.; Kang, N.; Maysinger, D.; Leroux, J. C., Block copolymer micelles: preparation, characterization and application in drug delivery. *J Control Release* **2005,** *109* (1-3), 169-88.

47. Blanazs, A.; Armes, S. P.; Ryan, A. J., Self-Assembled Block Copolymer Aggregates: From Micelles to Vesicles and their Biological Applications. *Macromol Rapid Commun* **2009,** *30* (4-5), 267-77.

48. Ottewill, R. H., Surfactant Systems - Their Chemistry, Pharmacy and Biology - Atwood, D, Florence, AT. *Chemistry in Britain* **1984,** *20* (7), 634-634.

49. Alexandridis, P.; Holzwarth, J. F.; Hatton, T. A., Micellization of Poly(ethylene oxide)-Poly(propylene oxide)-Poly(ethylene oxide) Triblock Copolymers in Aqueous-Solutions - Thermodynamics of Copolymer Association. *Macromolecules* **1994,** *27* (9), 2414-2425.

50. Song, W. T.; Tang, Z. H.; Li, M. Q.; Lv, S. X.; Sun, H.; Deng, M. X.; Liu, H. Y.; Chen, X. S., Polypeptide-based combination of paclitaxel and cisplatin for enhanced chemotherapy efficacy and reduced side-effects. *Acta Biomaterialia* **2014,** *10* (3), 1392-1402.

51. Adinolfi, B.; Pellegrino, M.; Giannetti, A.; Tombelli, S.; Trono, C.; Sotgiu, G.; Varchi, G.; Ballestri, M.; Posati, T.; Carpi, S.; Nieri, P.; Baldini, F., Molecular beacon-decorated polymethylmethacrylate core-shell fluorescent nanoparticles for the detection of survivin mRNA in human cancer cells. *Biosensors & Bioelectronics* **2017,** *88*, 15-24.

52. Boissenot, T.; Bordat, A.; Fattal, E.; Tsapis, N., Ultrasound-triggered drug delivery for cancer treatment using drug delivery systems: From theoretical considerations to practical applications. *Journal of Controlled Release* **2016,** *241*, 144-163.

53. Lee, E. S.; Na, K.; Bae, Y. H., Super pH-sensitive multifunctional polymeric micelle. *Nano Lett* **2005,** *5* (2), 325-9.

54. Moreira, A. F.; Dias, D. R.; Correia, I. J., Stimuli-responsive mesoporous silica nanoparticles for cancer therapy: A review. *Microporous and Mesoporous Materials* **2016,** *236*, 141-157.

55. Allen, T. M.; Cullis, P. R., Drug delivery systems: entering the mainstream. *Science* **2004,** *303* (5665), 1818-22.

56. Sershen, S. R.; Westcott, S. L.; Halas, N. J.; West, J. L., Temperature-sensitive polymer-nanoshell composites for photothermally modulated drug delivery. *J Biomed Mater Res* **2000,** *51* (3), 293-8.

57. Shuai, X.; Ai, H.; Nasongkla, N.; Kim, S.; Gao, J., Micellar carriers based on block copolymers of poly(epsilon-caprolactone) and poly(ethylene glycol) for doxorubicin delivery. *J Control Release* **2004,** *98* (3), 415-26.

58. Yoo, H. S.; Park, T. G., Biodegradable polymeric micelles composed of doxorubicin conjugated PLGA-PEG block copolymer. *J Control Release* **2001,** *70* (1-2), 63-70.

59. Zhang, Q.; Ko, N. R.; Oh, J. K., Recent advances in stimuli-responsive degradable block copolymer micelles: synthesis and controlled drug delivery applications. *Chem Commun (Camb)* **2012,** *48* (61), 7542-52.

60. Zhang, Y.; Chan, H. F.; Leong, K. W., Advanced materials and processing for drug delivery: the past and the future. *Adv Drug Deliv Rev* **2013,** *65* (1), 104-20.

61. Mansour, H. M.; Sohn, M.; Al-Ghananeem, A.; Deluca, P. P., Materials for pharmaceutical dosage forms: molecular pharmaceutics and controlled release drug delivery aspects. *Int J Mol Sci* **2010,** *11* (9), 3298-322.

62. Kabanov, A. V.; Chekhonin, V. P.; Alakhov VYu; Batrakova, E. V.; Lebedev, A. S.; Melik-Nubarov, N. S.; Arzhakov, S. A.; Levashov, A. V.; Morozov, G. V.; Severin, E. S., The neuroleptic activity of haloperidol increases after its solubilization in surfactant micelles. Micelles as microcontainers for drug targeting. *FEBS Lett* **1989,** *258* (2), 343-5.

63. Wissing, S. A.; Kayser, O.; Müller, R. H., Solid lipid nanoparticles for parenteral drug delivery. *Adv Drug Deliv Rev* **2004,** *56* (9), 1257-72.

64. zur Mühlen, A.; Schwarz, C.; Mehnert, W., Solid lipid nanoparticles (SLN) for controlled drug delivery--drug release and release mechanism. *Eur J Pharm Biopharm* **1998,** *45* (2), 149-55.

65. Müller, R. H.; Mäder, K.; Gohla, S., Solid lipid nanoparticles (SLN) for controlled drug delivery - a review of the state of the art. *Eur J Pharm Biopharm* **2000,** *50* (1), 161-77.

66. Zhang, L.; Chan, J. M.; Gu, F. X.; Rhee, J. W.; Wang, A. Z.; Radovic-Moreno, A. F.; Alexis, F.; Langer, R.; Farokhzad, O. C., Self-assembled lipid--polymer hybrid nanoparticles: a robust drug delivery platform. *ACS Nano* **2008,** *2* (8), 1696-702.

67. Wong, H. L.; Rauth, A. M.; Bendayan, R.; Manias, J. L.; Ramaswamy, M.; Liu, Z.; Erhan, S. Z.; Wu, X. Y., A new polymer-lipid hybrid nanoparticle system increases

cytotoxicity of doxorubicin against multidrug-resistant human breast cancer cells. *Pharm Res* **2006,** *23* (7), 1574-85.

68. Oerlemans, C.; Bult, W.; Bos, M.; Storm, G.; Nijsen, J. F. W.; Hennink, W. E., Polymeric Micelles in Anticancer Therapy: Targeting, Imaging and Triggered Release. *Pharmaceutical Research* **2010,** *27* (12), 2569-2589.

69. Adams, M. L.; Lavasanifar, A.; Kwon, G. S., Amphiphilic block copolymers for drug delivery. *Journal of Pharmaceutical Sciences* **2003,** *92* (7), 1343-1355.

70. A, A. C., Personal communications. 2015. Oct 25.

71. Aggarwal, B. B.; Kumar, A.; Bharti, A. C., Anticancer potential of curcumin: preclinical and clinical studies. *Anticancer Res* **2003,** *23* (1A), 363-98.

72. Bansal, S. S.; Goel, M.; Aqil, F.; Vadhanam, M. V.; Gupta, R. C., Advanced drug delivery systems of curcumin for cancer chemoprevention. *Cancer Prev Res (Phila)* **2011,** *4* (8), 1158-71.

73. Cheng, A. L.; Hsu, C. H.; Lin, J. K.; Hsu, M. M.; Ho, Y. F.; Shen, T. S.; Ko, J. Y.; Lin, J. T.; Lin, B. R.; Ming-Shiang, W.; Yu, H. S.; Jee, S. H.; Chen, G. S.; Chen, T. M.; Chen, C. A.; Lai, M. K.; Pu, Y. S.; Pan, M. H.; Wang, Y. J.; Tsai, C. C.; Hsieh, C. Y., Phase I clinical trial of curcumin, a chemopreventive agent, in patients with high-risk or pre-malignant lesions. *Anticancer Res* **2001,** *21* (4B), 2895-900.

74. Dhillon, N.; Aggarwal, B. B.; Newman, R. A.; Wolff, R. A.; Kunnumakkara, A. B.; Abbruzzese, J. L.; Ng, C. S.; Badmaev, V.; Kurzrock, R., Phase II trial of curcumin in patients with advanced pancreatic cancer. *Clin Cancer Res* **2008,** *14* (14), 4491-9.

75. Perkins, S.; Verschoyle, R. D.; Hill, K.; Parveen, I.; Threadgill, M. D.; Sharma, R. A.; Williams, M. L.; Steward, W. P.; Gescher, A. J., Chemopreventive efficacy and pharmacokinetics of curcumin in the min/+ mouse, a model of familial adenomatous polyposis. *Cancer Epidemiol Biomarkers Prev* **2002,** *11* (6), 535-40.

76. Banerjee, S.; Chakravarty, A. R., Metal Complexes of Curcumin for Cellular Imaging, Targeting, and Photoinduced Anticancer Activity. *Accounts of Chemical Research* **2015,** *48* (7), 2075-2083.

77. Kurien, B. T.; Singh, A.; Matsumoto, H.; Scofield, R. H., Improving the solubility and pharmacological efficacy of curcumin by heat treatment. *Assay Drug Dev Technol* **2007,** *5* (4), 567-76.

78. Anand, P.; Kunnumakkara, A. B.; Newman, R. A.; Aggarwal, B. B., Bioavailability of curcumin: problems and promises. *Mol Pharm* **2007,** *4* (6), 807-18.

79. Sharma, R. A.; Euden, S. A.; Platton, S. L.; Cooke, D. N.; Shafayat, A.; Hewitt, H. R.; Marczylo, T. H.; Morgan, B.; Hemingway, D.; Plummer, S. M.; Pirmohamed, M.; Gescher, A. J.; Steward, W. P., Phase I clinical trial of oral curcumin: biomarkers of systemic activity and compliance. *Clin Cancer Res* **2004,** *10* (20), 6847-54.

80. Yang, K. Y.; Lin, L. C.; Tseng, T. Y.; Wang, S. C.; Tsai, T. H., Oral bioavailability of curcumin in rat and the herbal analysis from Curcuma longa by LC-MS/MS. *J Chromatogr B Analyt Technol Biomed Life Sci* **2007,** *853* (1-2), 183-9.

81. Pan, M. H.; Huang, T. M.; Lin, J. K., Biotransformation of curcumin through reduction and glucuronidation in mice. *Drug Metab Dispos* **1999,** *27* (4), 486-94.

82. Long, H. J., Paclitaxel (Taxol): a novel anticancer chemotherapeutic drug. *Mayo Clin Proc* **1994,** *69* (4), 341-5.

83. Rowinsky, E. K.; Donehower, R. C., Paclitaxel (taxol). *N Engl J Med* **1995,** *332* (15), 1004-14.

84. Murad, A. M.; Santiago, F. F.; Petroianu, A.; Rocha, P. R.; Rodrigues, M. A.; Rausch, M., Modified therapy with 5-fluorouracil, doxorubicin, and methotrexate in advanced gastric cancer. *Cancer* **1993,** *72* (1), 37-41.

85. Valdivieso, M.; Burgess, M. A.; Ewer, M. S.; Mackay, B.; Wallace, S.; Benjamin, R. S.; Ali, M. K.; Bodey, G. P.; Freireich, E. J., Increased therapeutic index of weekly doxorubicin in the therapy of non-small cell lung cancer: a prospective, randomized study. *J Clin Oncol* **1984,** *2* (3), 207-14.

86. Balasubramanyam, K.; Varier, R. A.; Altaf, M.; Swaminathan, V.; Siddappa, N. B.; Ranga, U.; Kundu, T. K., Curcumin, a novel p300/CREB-binding protein-specific inhibitor of acetyltransferase, represses the acetylation of histone/nonhistone proteins and

histone acetyltransferase-dependent chromatin transcription. *J Biol Chem* **2004,** *279* (49), 51163-71.

87. Dahlin, J. L.; Inglese, J.; Walters, M. A., Mitigating risk in academic preclinical drug discovery. *Nat Rev Drug Discov* **2015,** *14* (4), 279-94.

88. Raveendran, R.; Bhuvaneshwar, G.; Sharma, C. P., In vitro cytotoxicity and cellular uptake of curcumin-loaded Pluronic/Polycaprolactone micelles in colorectal adenocarcinoma cells. *J Biomater Appl* **2013,** *27* (7), 811-27.

89. Song, Z.; Feng, R.; Sun, M.; Guo, C.; Gao, Y.; Li, L.; Zhai, G., Curcumin-loaded PLGA-PEG-PLGA triblock copolymeric micelles: Preparation, pharmacokinetics and distribution in vivo. *J Colloid Interface Sci* **2011,** *354* (1), 116-23.

90. Squires, T. M.; Quake, S. R., Microfluidics: Fluid physics at the nanoliter scale. *Reviews of Modern Physics* **2005,** *77* (3), 977-1026.

91. Thiele, J.; Steinhauser, D.; Pfohl, T.; Förster, S., Preparation of monodisperse block copolymer vesicles via flow focusing in microfluidics. *Langmuir* **2010,** *26* (9), 6860-3.

92. Karnik, R.; Gu, F.; Basto, P.; Cannizzaro, C.; Dean, L.; Kyei-Manu, W.; Langer, R.; Farokhzad, O. C., Microfluidic platform for controlled synthesis of polymeric nanoparticles. *Nano Lett* **2008,** *8* (9), 2906-12.

93. Stone, H. A.; Stroock, A. D.; Ajdari, A., Engineering flows in small devices: Microfluidics toward a lab-on-a-chip. *Annual Review of Fluid Mechanics* **2004,** *36*, 381-411.

Chapter 2. Microfluidics Manufacturing and Characterization of Curcumin-Loaded PCL-*b*-PEO Nanoparticles

2.1 Introduction

Drug delivery is the method that can be used to modify drug release, distribution, and elimination for the improvement of its efficacy.[1-6] Cancer treatment is an example.[7-9] Distributing anticancer drug through blood stream may lead to side effects because of the un-desirable interactions in the body. Therefore, there has been great interest in using drug delivery system to target tumor cells and increase circulation time of drug in the blood. Encapsulation of anticancer drug in polymeric nanoparticles was one of these.[10-12] One explanation why drug delivery system could improve the anticancer drug efficacy and reduce its toxicity to healthy tissue was enhanced permeation and retention effect (EPR).[13, 14] As tumour growing, it requires more nutrition and oxygen. Therefore, tumour cells release signals to grow blood vessels to transport nutrition and oxygen. However, these newly formed blood vessels were different from the blood vessels in the healthy tissue. These blood vessels were more porous with defective structure. Nanoparticles with a certain size will not only control the release of the drug but also localize specifically in the tumour sites with such defective blood vessel structure. Once the nanoparticle locates in the tumour site, the porous structure of blood vessels results in a lower pressure in the tumour and makes it difficult for the nanoparticles to be removed from the tumour sites. Therefore, the EPR effect explained why nanoparticle formulations could be used to improve drug's efficacy.

The control over nanoparticles' structural properties is of great interest because it dictates nanoparticles' *in vivo* performance as drug delivery vehicles. For example, since

the EPR effect in the solid tumor was discovered, this characteristic of the tumor has been utilized in the antitumor drug delivery of the macromolecular drugs.[15] Depending on the type of the tumor, nanoparticles within hundreds of nanometers have a higher permeability and retention rate in the tumor. The localized nanoparticles then release payloads inside the tumor. Geng *et al.* reported that the cylindrical micelle had higher loading efficiency and longer circulation time up to one week. This circulation time was ten times longer than its spherical counterparts.[16] Moreover, the crystallinity of the core-forming copolymer block may influence the morphologies of nanoparticles because the low curvature morphology was preferred when the crystallinity increased.[17]

The anticancer drug we chose to be our model drug was curcumin. Curcumin is a polyphenol molecule extracted from Turmeric, a plant in the ginger family. There have been plenty of arguments about curcumin as anticancer drug.[18-21] In Chapter 1, we have reviewed researches about curcumin in the clinical trials, its therapeutic effects were questioned due to the poor stability and being non-selective. Although there has been a new direction for researches about encapsulating curcumin into nanoparticle for the drug delivery purpose[22, 23,24], there were still problems needed to be solved, such as curcumin degradation products, improving size control and loading efficiency of nanoparticles and release rate control. In this chapter, we explored a systematic control *via* the two-phase microfluidic platform over nanoparticle-encapsulated curcumin so that we can tune the structural properties of different drug delivery systems to achieve better efficacy.

Previous members of the Moffitt group have applied the gas-liquid segmented microfluidic reactor in the synthesis of block copolymer nanoparticles for drug delivery.[25-27] In these studies, Joe Wang prepared polystyrene-*b*-polyacrylic acid (PS-*b*-

PAA) nanoparticles using microfluidics. The morphologies of samples prepared on-chip were found to be different from conventional bulk experiments.[28] The "on-chip" method generated spheres, cylinders, Y-junction bilayers and network morphologies while there were only pure spheres from bulk experiments. He proposed that high shear on the microfluidic chip provided the energy for small spheres to overcome the repulsion between coronas and collide into the bigger spheres. Then due to the higher aggregation number, the polymer chains were rearranged to form low curvature morphologies so that the polymer chain stretching was decreased. Therefore, polymer chain rearrangement led to the change of morphologies on-chip. Furthermore, Aman Bains used PCL-*b*-PEO, a biodegradable block copolymer, to form nanoparticles also by gas-liquid two-phase microfluidic chips[29]. The experiment proved that the morphology changed significantly with the change of the water content and flow rate. Moreover, the internal crystallinity also increased with the increase of flow rate. These studies showed us that the microfluidic chip is a useful handle to control the morphology, size, crystallinity and some other properties of drug delivery vehicles. Therefore, we planned to apply this control on more drug delivery systems.

In this chapter, we prepared curcumin-loaded PCL-*b*-PEO nanoparticles using a conventional bulk method and in the gas-liquid segmented microfluidic reactor with different flow rates. We also explored the effects chemical variables of the nanoparticle preparation, including the flow rate, initial drug-to-polymer loading ratio and water content. We characterized the resulting nanoparticle sizes, morphologies, loading efficiencies / loading levels, and release rates of curcumin. The result showed that the high shear rate on the microfluidic reactor could be used to direct nanoparticles'

structural properties by tuning processing conditions. Drug-encapsulated nanoparticles prepared on-chip had flow-directed loading efficiencies and sizes. We proposed that shear-induced break-up at the high flow rate and other chemical parameters such as water content and initial drug ratio all played a role in the formation of nanoparticles.

2.2 Experimental

2.2.1 Materials

PCL(12k)-*b*-PEO(5k) was purchased from Advanced Polymer Materials Inc. Curcumin was purchased from Sigma Aldrich. NaCl (EMD Inc), KCl (Caledon), Na_2HPO_4 (BioBasic) and KH_2PO_4(Caledon) were used to prepare PBS solution. Dimethylformamide (DMF) and acetonitrile were purchased from Caledon. Dialysis tubing with molecular weight cut-off of 6.8 kD was purchased from SpectrumLabs.

2.2.2 Microfluidic Chip Fabrication

The master chip was made on a silicon wafer in the following manner. First, the photoresist material SU-8 100 was coated on the silicon wafer by spin coating at 2000 rpm. Then the wafer was baked on a hot plate at 65 °C for 12 minutes and 95 °C for 50 minutes. After that, the wafer was exposed to UV light for 100 seconds under the cover of the photomask. This was followed by baking at 65°C for 1 minute and 95°C for 20 minutes. Then the region covered by the photomask was washed off in the developing solution (Microchem) while the channel that was exposed to UV light remained after washing. Then the wafer was rinsed with isopropanol.

For poly(dimethyl siloxane) (PDMS) chips, an elastomer-to-curing agent weight ratio of 7:1 was used through this project. The kit containing elastomer and curing agent were purchased from DOW Corning as a SYLGARD elastomer kit. After vigorous

mixing, the mixture was placed in a vacuum oven to remove gas bubbles. Then the mixture of PDMS and curing agent was poured on the master chip and heated up on the hot plate at 85°C until it turned hard. After that, the chip was peeled off the master chip. Then the PDMS and curing agent with a ratio of 20:1 were mixed and degassed under the vacuum. It was followed by spin-coating on clean glass slides. After heating up, a thin film of PDMS was formed on the glass slide. The glass slide and the previously made chip were placed under the oxygen plasma for 30 seconds so that these two layers could be permanently bonded. The channels formed by this method had a width of 100 μm (mixing channel) and 200 μm (processing channel). The depth was 150 μm through the whole chip.

2.2.3 Microfluidic Preparation of PCL-*b*-PEO Nanoparticles

In this study, two different water contents relative to the critical water content (cwc) were applied to prepare the nanoparticles in the microfluidic reactor, cwc + 5 wt % and cwc + 10 wt %. For each water content, three different curcumin-to-polymer loading ratios (r = 0.25, 0.50, 0.75) were used. The definition of loading ratio, loading efficiency and loading level are listed in Chapter 1. For each of the resulting chemical compositions of the microfluidic reaction mixture, three flow rates were applied: Q = 50 μl/min, 100 μl/min, and 200 μl/min.

The solutions were injected using syringes (1mL, Hamilton, Reno, RV) with flow rates set by the syringe pump (Harvard Apparatus, Holliston, MA). From the syringe, a tube with a diameter of a $1/16^{th}$ inch (OD) Teflon (Scientific products and equipment, ON) was used to connect with the chip inlets. Besides inlets for solutions, there was also a gas regulator connected with chip via $1/16^{th}$ (OD) 100μm (ID) tubing (Upchurch

scientific, Oak Harbor, WA). The gas regulator could be fine-tuned so that the gas injected into the chip could be controlled. A camera was set above the chip so that pictures could be taken and used to determine the ratio between the gas segment and liquid segment on chip. The ratio of gas and liquid flow rates were set to be ~1. The total flow rate was set at 50 to 200 μL/min. However, during the experiment, the flow rate was a combination of the gas flow rate and liquid flow rate. The flow rate of gas was set at the level so that the lengths of the gas bubble and liquid plug are similar. Therefore, the actual flow rate may be different from the nominal flow rate we set at the beginning. The actual flow rate was calculated after taking photos of actual flow and measuring the relative length of liquid/gas segments. The full table with both actual flow and nominal flow was presented in the appendix.

$$Actual\ flow\ rate = liquid\ injection\ rate \times \frac{(gas+liquid)\ segment\ length}{liquid\ segment\ length} \quad (2\text{-}1)$$

Three solutions were injected individually and equally through the three inlets on the microfluidic reactor. When preparing nanoparticles on the chip, the following three liquid streams were combined at the same flow rate to form liquid flow on the chip. (1). 1.0 wt% PCL-*b*-PEO dissolved in DMF with different amount of curcumin. (2). DMF with either 31.5% or 46.5% deionized water. (3) Pure DMF. Due to three liquid streams combining at an equal flow rate, the on-chip concentrations were diluted by a factor of three. Therefore, the concentrations of polymer and water were 0.33 wt% and either 10.5 wt% (cwc + 5 wt%) and 15.5 wt% (cwc + 10 wt%). The concentration of polymer on-chip was 0.33 wt %, which was the same as the concentration in the bulk experiment. After collected from the outlet of the chip, the solution was collected in a vial with 10 times excess volume water so that the nanoparticle solution was immediately quenched.

After collecting samples from the reactor they were dialyzed against deionized water for 12 hours, changing the water every hour for the first four hours. The dialysis membrane was purchased from SpectrumLabs with a molecular weight cut-off of 6-8kD. After dialysis, the aqueous suspension was centrifuged at 14000 g for 5 minutes to remove the precipitate and unencapsulated drug. After centrifugation, the supernatant was collected in a clean vial while the solid pellet was left in centrifugation vials. The solid pellet in each vial was washed with deionized water for three times. After 30 seconds vortex and centrifugation, the supernatant from each wash was also collected in the vial.

2.2.4 Bulk Preparation of PCL-*b*-PEO Nanoparticles

0.33 wt % polymer and curcumin with different drug-to-polymer loading ratios were dissolved together in 5.0 g DMF. Then 1.0 mL of polymer/drug solution was put in the syringe and injected into 10 times diluted water with vigorous stirring by a magnetic stirring bar at 120 μl/min. Then the solution was transferred into a dialysis bag and dialyzed against deionized water for 12 hours. Deionized water was changed every hour for the first four hours. After dialysis, the sample was centrifuged at 14000 g for 5 minutes to remove any precipitates. Precipitates were also washed with deionized water three times.

2.2.5 Dynamic Light Scattering (DLS).

DLS was used to determine the hydrodynamic diameter distributions of prepared nanoparticles. The instrument used in this experiment is the Brookhaven BI200SM. The nanoparticle solution was transferred to a vial for DLS measurement. The goniometer arm angle was set at 90°, the detector filter was set at 633 nm. Detector filter turret with 200 micron pinhole was set for all DLS measurements.

2.2.6 Transmission Electron Microscopy (TEM).

The sample was prepared by depositing a drop of nanoparticle-encapsulated drug solution on copper TEM grid. Then the sample was stained with a drop of 1 wt % uranyl acetate aqueous solution. After removing excess liquid, the TEM grid with the sample on it was left to completely dry.

The instrument was JEOL JEM-1400 TEM. The accelerating voltage was set at 65k V. The backbone of our block polymer was mostly carbon. And it did not provide enough contrast for imaging the morphologies. Through this project, negative staining by uranyl acetate was used to get better contrast on TEM image.

2.2.7 Loading Efficiency

HPLC was used to measure how much curcumin was encapsulated inside the nanoparticles. A sample of ~1 g was used to measure loading efficiency. First, the water was removed from the sample by rotary evaporation at 25°C. Nanoparticles would be left in the vial as solid. Then ~0.5 g acetonitrile was added to dissolve the drug. This mixture was vortexed for 30 seconds to ensure complete dissolving of curcumin. All samples were analyzed by HPLC (Ultimate 3000, thermo scientific) with C18 column (Phenomenex Luna 5u). The composition of eluent was set at 35/65 water/acetonitrile. The acetonitrile was HPLC grade without further treatment while 0.3 v % acetic acid was added to deionized water to maintain an acidic environment. The wavelength of diode array detector was set at 420 nm. Then the acetonitrile solution with the drug in it was injected with a flow rate of 1 ml/min. The calibration curve was generated by measuring 6 stock solutions containing known and different amount of curcumin in acetonitrile.

According to the peak areas and the calibration curve, the amount of drug and loading efficiency were determined.

2.2.8 *In Vitro* Release Rate Measurements.

It was important to determine how fast curcumin will be released from nanoparticles in an aqueous environment under physiological conditions. For release determination, the sample from microfluidic chip was collected in a vial containing 20 times excess volume water. Other sample preparation procedures were kept the same as the method described before in Chapter 2.2.3. The sample was collected in a more diluted environment for the purpose of long-time storage. Diluted samples were easier to store without observation of colloidal instability. Drug encapsulated nanoparticle solution was divided into 10 parts and put into 2 mL Float-A-Lyzer tubes (SpectrumLabs, MWCO 100 kDa) respectively. Then 2L PBS solution was made and maintained at 37°C ± 0.1°C. Then release tubes were placed in the PBS environment. During the release experiment, a stir bar was placed in the media to keep a homogeneous environment. At each time point, one release tube was taken out. The drug solution was transferred to a vial and dried by rotary evaporation. Then, a known amount of acetonitrile was added to each vial so that the dried drug was quickly dissolved in the solvent while the block copolymer and salt were not dissolved in acetonitrile. Then the concentration of curcumin was measured by HPLC (Ultimate 3000, thermo scientific) with C18 column (Phenomenex Luna 5u). The composition of eluent was set at 35:65 0.3v% acetic acid aqueous solution:acetonitrile. The wavelength of diode array was set at 420 nm. The flow rate was set at 1 ml/min. According to the peak areas and the calibration curve, the amount of drug at each time point was determined.

2.3 Results and Discussion

2.3.1 Bulk Experiment Results

We first determined the size, morphology and loading efficiency of bulk samples. Bulk samples were prepared by injecting the organic solvent containing the polymer and the drug into the water under fast stirring. Nanoparticles were formed spontaneously by self-assembly. The properties of the bulk sample such morphologies and sizes are the result of three factors: core-forming block copolymer chain stretching, repulsion between corona-forming block, and interfacial tension between solvent and core-forming block. Therefore, changing chemical conditions in the preparation process would have significant effects on nanoparticle's properties. Under this conditions and preparation procedure we set, the bulk experiment results were presented (size distribution, morphology and loading efficiency) in Figure 2-1 and Figure 2-3 as the baseline for on-chip samples prepared when the water content equals to cwc + 10 wt %. From the bulk experiment, one thing we noticed was its loading efficiency. It decreased when the initial drug-to-polymer ratio increased. The photo (Figure 2-2) taken after dialysis against deionized water showed that there were precipitates indicating the un-encapsulated curcumin.

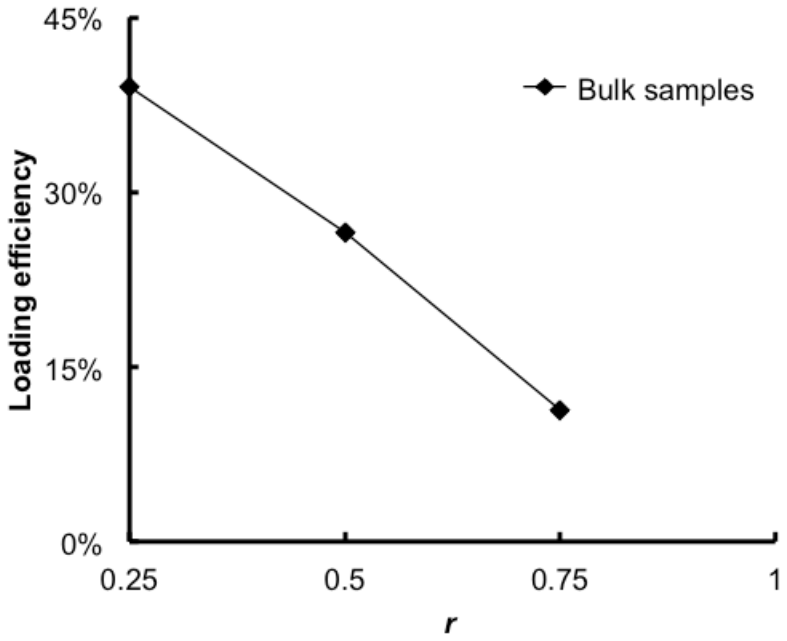

Figure 2-1 Loading efficiency of nanoparticles prepared by bulk mothod (r = 0.25, 0.50, 0.75).

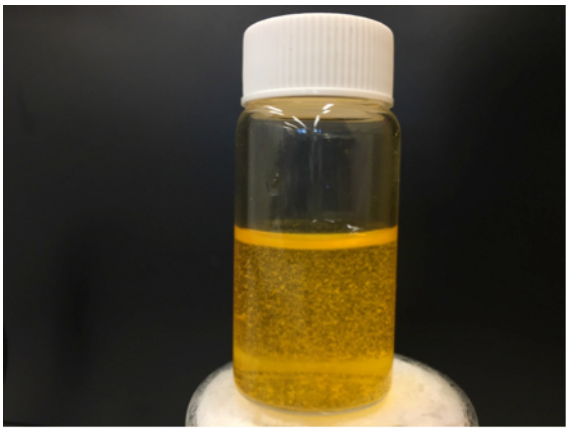

Figure 2-2 The bulk sample (r = 0.75) after dialysis. The precipitate was observed.

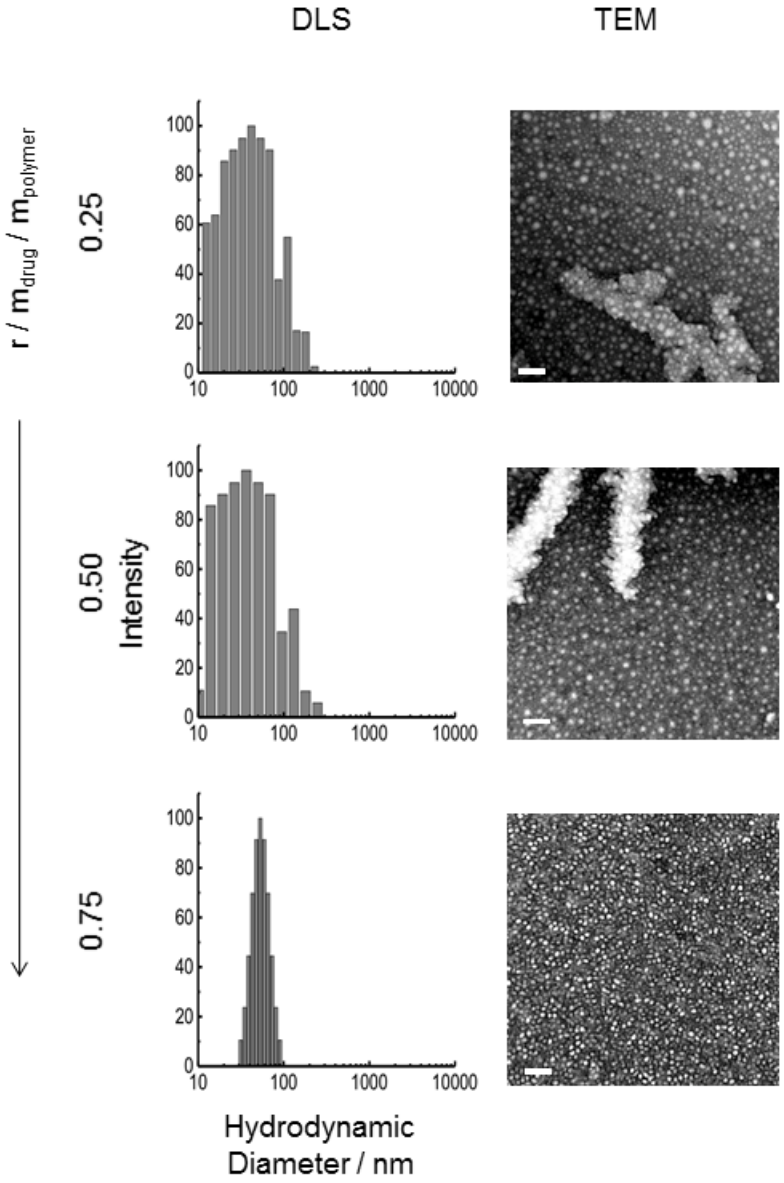

Figure 2-3 Results of nanoparticles prepared by the bulk method with different initial drug ratios. The left column is the size distribution characterized by dynamic light scattering. The right column is TEM images for morphology characterization. The scale bar is 200 nm.

The hydrodynamic sizes did not change significantly in the bulk experiment when the drug-to-polymer ratio increased from 0.25 to 0.75. However, there were still

morphologies and the size distribution changes. At a low drug-to-polymer ratio, there were big morphologies such as lamellae exist. When the drug-to-polymer ratio increased, big morphologies disappeared and the size distribution became narrow.

2.3.2 Effects of Flow Rate and Loading Level on Nanoparticle Morphologies and Size Distributions.

Both DLS and TEM results were used to characterize nanoparticles morphologies and sizes. The TEM results are presented in Figure 2-4. In Figure 2-4, there were 9 conditions. All experiments were conducted at cwc + 10 wt % that was 15.5 wt % water content on-chip. Each row represents one drug-to-polymer ratio. And from left to right, flow rate increases from 50 to 200 μl/min. From A to C, nanoparticles were prepared at r = 0.25. From D to F, nanoparticles were prepared when r = 0.50. From G to I, nanoparticles are prepared when r = 0.75. Water content is cwc + 10 wt %. From Figure 2-4, it was clearly shown large lamellar aggregates were broken down with the increase of flow rate. At high flow rate (200 μl/min), both conditions where drug-to-polymer ratios = 0.50 and 0.75 were having pure sphere morphology. Figure 2-4 also showed that large aggregates also gradually disappeared from on-chip method prepared sample when drug-to-polymer ratio increased.

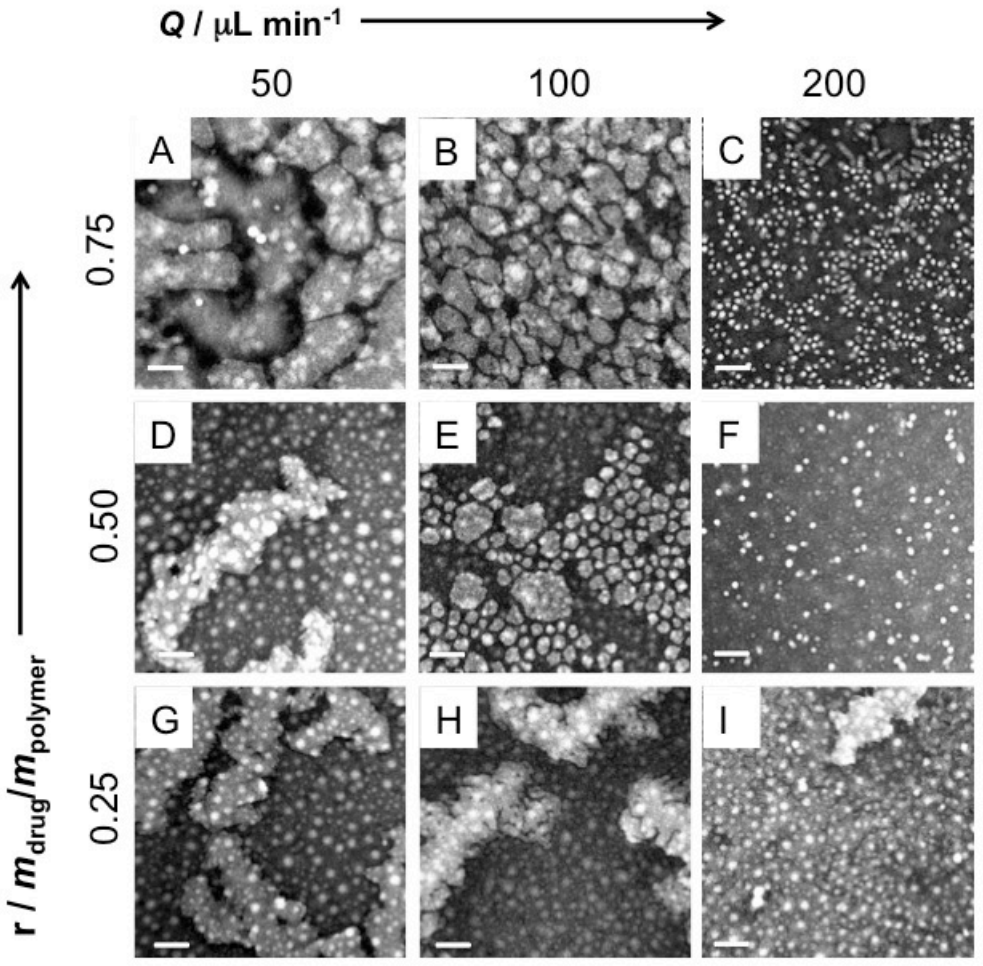

Figure 2-4 A-I are TEM images of nanoparticles prepared from different drug ratio and flow rate. Scale bars are 200 nm.

Furthermore, the dynamic light scattering results agreed with the TEM results and showed a more general size distribution in the sample. The Figure 2-5 represents nanoparticles prepared from cwc + 10 wt % with different initial drug-to-polymer ratios. Each row represents one drug-to-polymer with flow rates increasing from left to right. In each column, drug-to-polymer ratios increase from bottom to top. In the DLS size distribution image, the *x*-axis is hydrodynamic diameter while the *y*-axis represents the

intensity-weighted population distribution. DLS results showed big morphologies with a diameter larger than 1000 nm presented under low flow rate conditions. The hydrodynamic diameter was 328 ± 72 nm for samples prepared at the low flow rate condition (r = 0.25, Q = 50 μL/min and cwc + 10 wt %). Increasing flow rates to 100 μl/min or 200 μl/min resulted in disappear of big morphologies from the samples. At the highest flow rate, 200 μl/min, small spheres became the dominant morphology. The hydrodynamic diameter was only 76 nm for the high flow rate sample (r = 0.25, Q = 200 μL/min, cwc + 10 wt %). The result of TEM and DLS results showed a clear trend of decreasing size under the influence of increasing flow rate. The result showed the control over the size and the morphology via flow rates under constant chemical conditions.

Moreover, the size and morphology were also influenced by initial drug-to-polymer ratio. The big morphologies with hydrodynamic diameter around 10000 nm were presented in low drug-to-polymer ratio samples. They disappeared gradually when drug-to-polymer ratio increased. In the highest initial drug-to-polymer ratio (0.75) samples, small nanoparticles with diameters smaller than 100 nm were dominant. One explanation is that curcumin may inhibit the crystallinity of PCL blocks. And as a result, nanoparticles with low crystallinity formed small size structure.

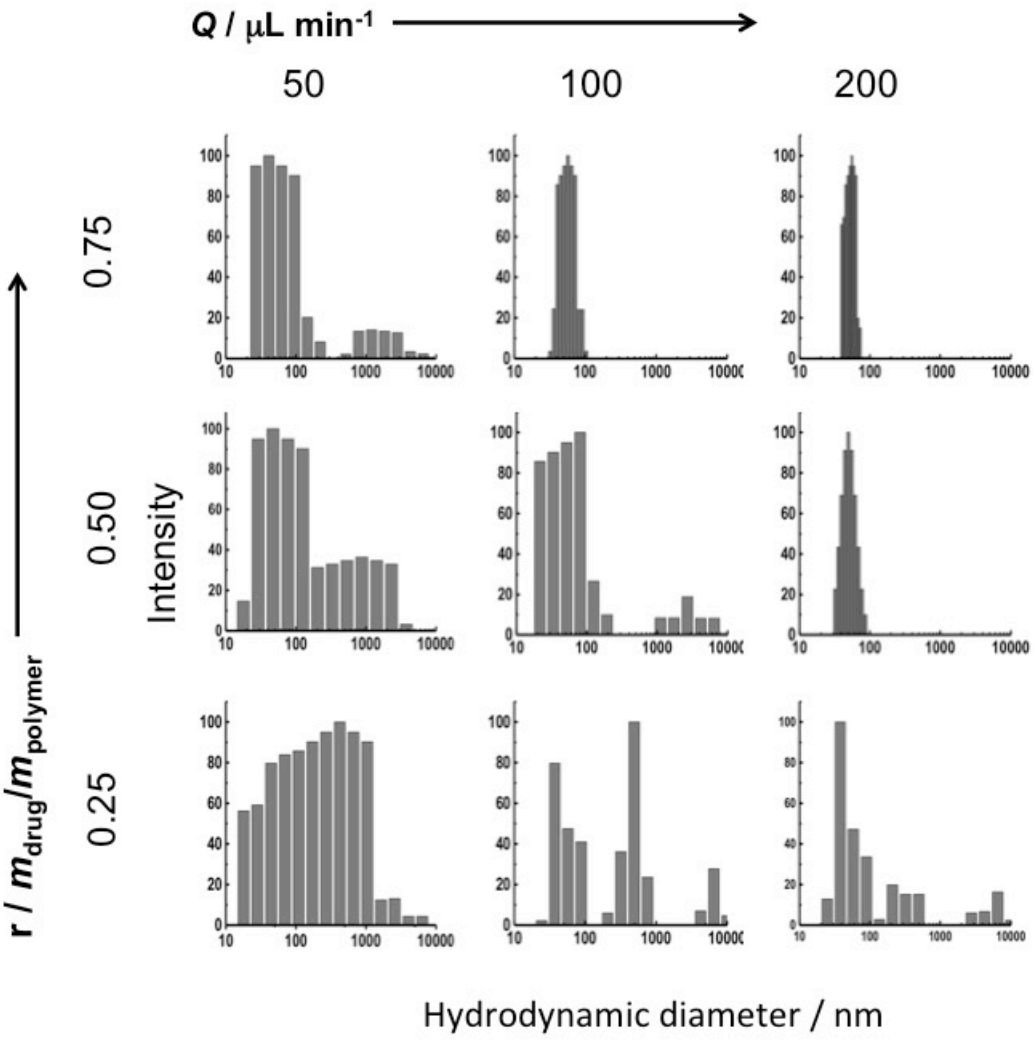

Figure 2-5 DLS size distribution of nanoparticles prepared on chip with different drug ratio and flow rate. All samples were prepared at cwc + 10 wt % water content.

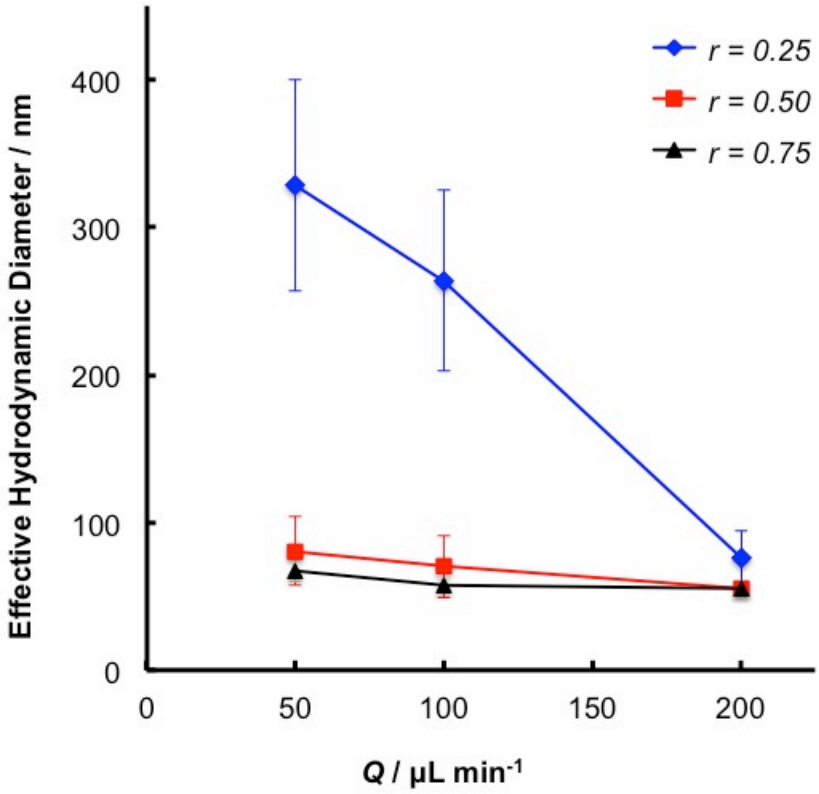

Figure 2-6 Effective hydrodynamic diameter of samples prepared on chip cwc + 10 wt %.

In Figure 2-6, we presented the summary of nanoparticle-encapsulated curcumin size result. This result showed top-down control of nanoparticle self-assembly when other chemical conditions were kept the same. The changes of size and morphologies when we tuned the flow rate and the drug-to-polymer ratio could be explained by the shear-induced break-up mechanism. On microfluidic chips, three mechanisms may influence the morphologies – coalescence, break-up and crystallinity of nanoparticle. As nanoparticles moved through the "hot spot" with high shear rates, the high shear rates greatly increased the rate of coalescence and resulted in the formation of non-equilibrium

nanoparticles. Then various morphologies were formed via intramicellar chain rearrangement. From the result where the size decreased with increasing flow rate and drug-to-polymer ratio, we proposed that under this condition, shear-induced break-up had the dominant impact.

2.3.3 Effects of Flow Rate on Curcumin Loading Efficiency.

Next, we demonstrated the effect of flow rate on curcumin's loading efficiency in PCL-*b*-PEO nanoparticles. In Figure 2-7, the x-axis represented increasing flow rates from 50 to 200 μL/min. It showed an overall increase of loading efficiency with the increase of flow rate. Previous group member, Aman Bains, have shown that increasing flow rate resulted in increased crystallinity in the core of paclitaxel-encapsulated PCL-*b*-PEO nanoparticles[30]. And since high crystallinity decreased the space in the core for the payloads, Aman observed decreasing loading efficiency of paclitaxel-encapsulated PCL-*b*-PEO nanoparticles with increasing flow rate. One possibility was curcumin might be located at the interface of the core. When the flow rate and the drug-to-polymer ratio increased, we observed big nanoparticles changed to small spheres, which had a higher surface area-to-volume ratio. Therefore, the increase of flow rate and drug-to-polymer ratio led to the increase of relative surface area for curcumin to locate. This may explain why a high drug ratio and flow rate resulted in a higher loading efficiency in this drug delivery system. However, the hypothesis that curcumin located at the interface of PCL and PEO block needs further experiment to prove.

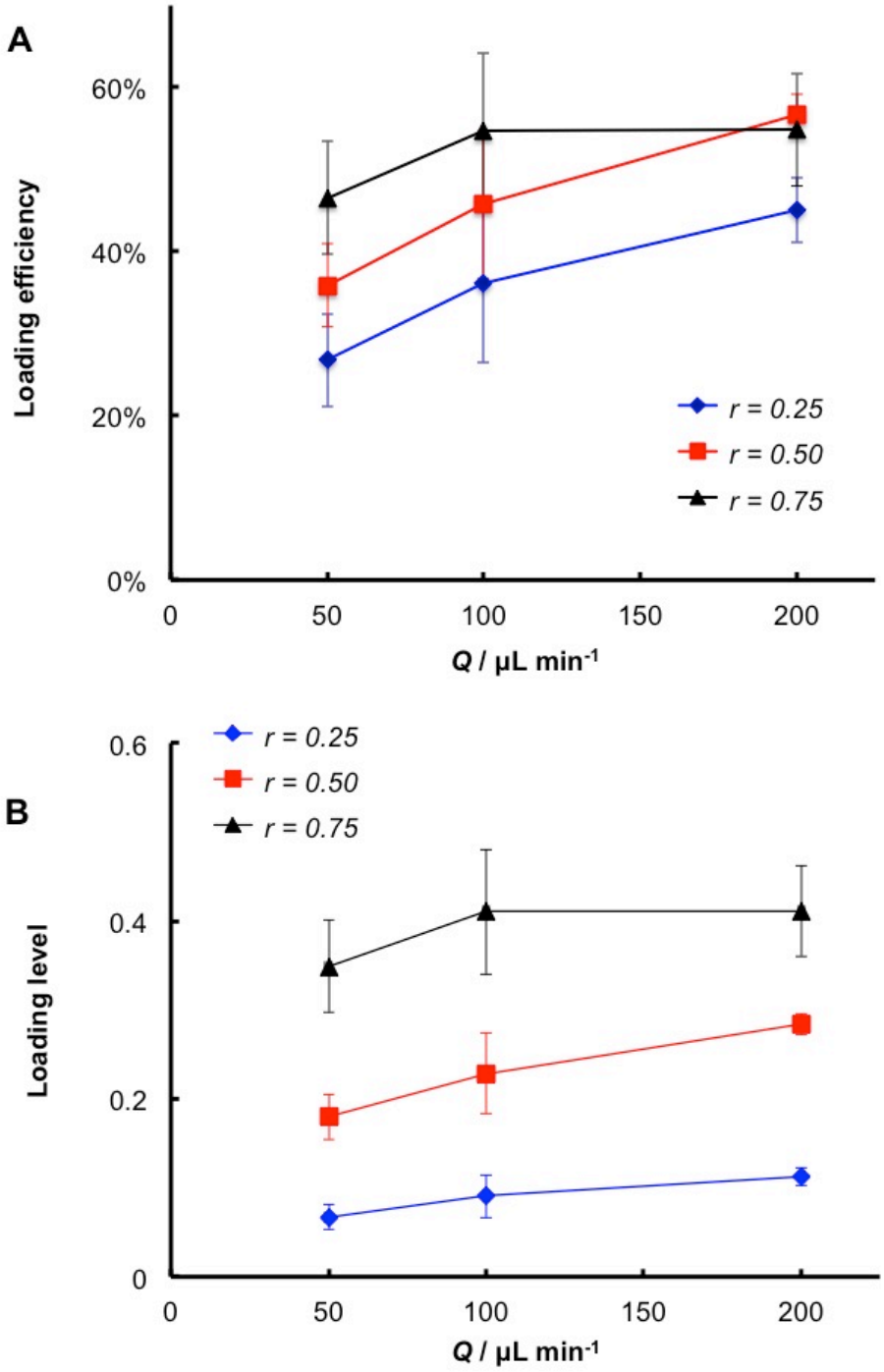

Figure 2-7 At cwc + 10 wt %, loading efficiency (A) and loading level (B) of curcumin increased with the increase of flow rate.

2.3.4 Effect of Water Content on Size and Loading Efficiency

In bulk experiment, when the polymer/drug solution was added to water, nanoparticles were formed to minimize the interaction between hydrophobic blocks and aqueous environment. The nanoparticles were formed depending on how unfavorable the aqueous environment was. Therefore, the water content when block copolymer started to form nanoparticle was defined as critical water content (cwc). We then used the same method and parameters to prepare nanoparticles when the water content is cwc + 5 wt %. The trend of size change with the increasing flow rates is the same as the trend we observed on nanoparticles prepared using cwc + 10 wt % water content. In Table 2-1, as the flow rate increases from Q = 50 μl/min to Q = 200 μl/min, the size of nanoparticles decreased.

Table 2-1 Hydrodynamic size of nanoparticles (cwc + 10 wt % on chip)

Water content	Drug:Polymer Loading Ratio(w/w)	Flow rate /μL min^{-1}	Hydrodynamic diameter / nm
cwc+5%	0.25	50	942±256
		100	533±55
		200	243±97
	0.50	50	208±177
		100	127±34
		200	95±5
	0.75	50	103±10
		100	83±13
		200	157±109
cwc+10%	0.25	50	328±72
		100	264±61
		200	76±18
	0.50	50	81±24
		100	70±21
		200	55±3
	0.75	50	67±7
		100	57±4
		200	55±2

We further compared the loading efficiencies of samples prepared between the water content of cwc + 5 wt % and cwc + 10 wt %. The result is showed in Table 2-1. Unlike the cwc + 10 wt % case, for the condition cwc + 5 wt %, r = 0.75, the loading efficiency actually decreases when the flow rate increases. Overall, the loading efficiencies at cwc + 5 wt % were lower at a given flow rate than loading efficiencies at cwc + 10 wt %.

By comparing the hydrodynamic sizes from both water contents, we noticed that the sizes of nanoparticles from cwc + 5 wt % were bigger than the sizes of nanoparticles from cwc + 10 wt % at a given flow rate. However, the loading efficiency increased with the increase of water content. See Figure 2-8. The reason that higher water content led to higher loading efficiency was probably a thermodynamic effect. As water content increased, curcumin, as a hydrophobic molecule, would then have higher tendency to move into PCL core and resulted in higher loading efficiency.

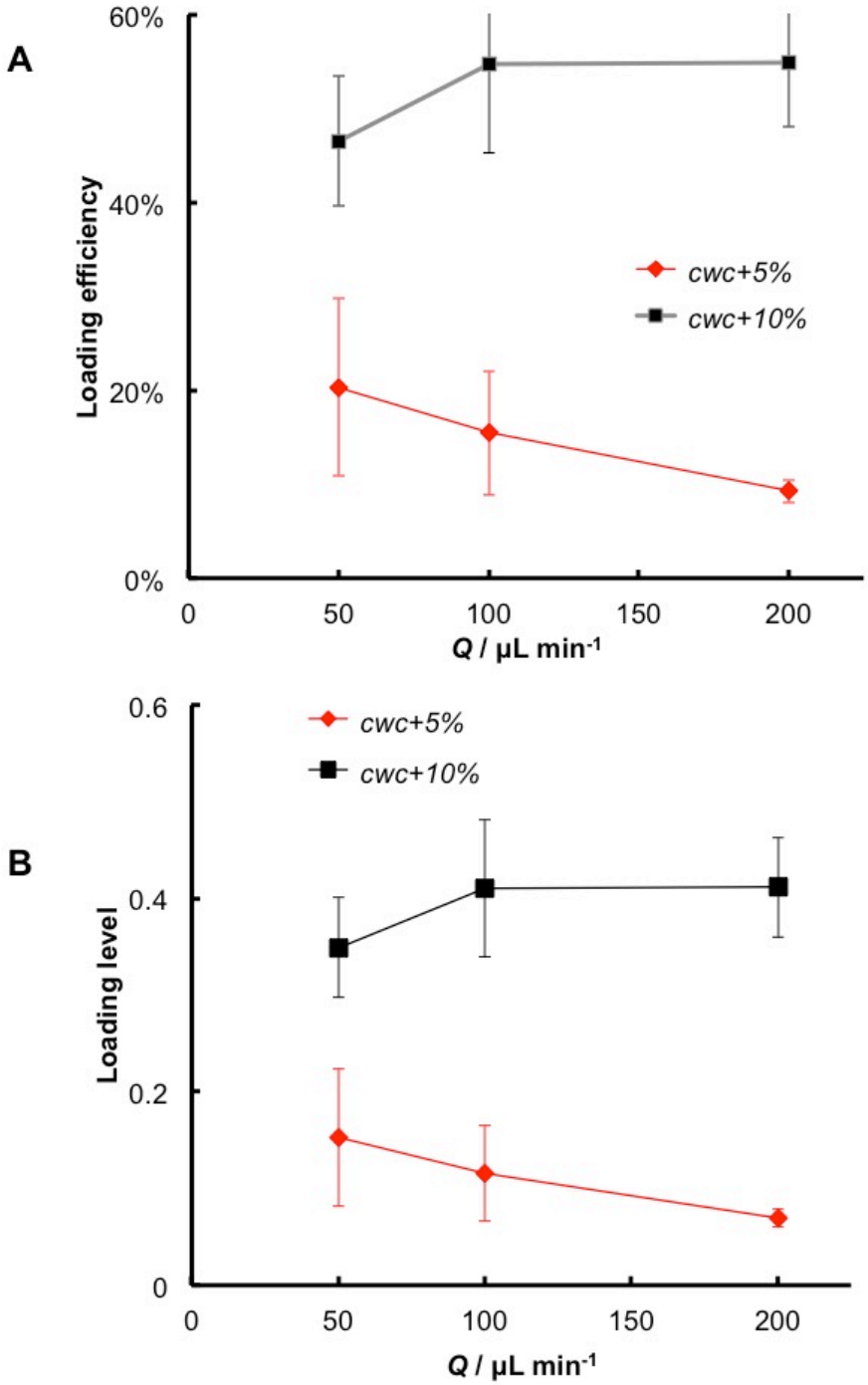

Figure 2-8 Comparison of loading efficiency (A) and loading level (B) of nanoparticles prepared with different water contents.

2.3.5 Effect of Flow Rate on *In Vitro* Release

The *in vitro* release was done in the PBS solution. The results with two different water contents are shown in Figure 2-9. A is the sample prepared at initial drug-to-polymer ratio 0.50. B is the sample prepared at drug-to-polymer ratio 0.75. Comparing the results of two different drug-to-polymer ratios, the results showed that the release of curcumin was still fast at the beginning of release. For both conditions, 50% drug was released within the first 30 minutes. And there was no significant effect of flow rate or drug-to-polymer ratio because all release profiles were pretty much the same. The reason of fast release may be because curcumin mostly localized at the interface of the core and the corona. Considering the diffusion distance, it was easier and fast for curcumin to diffuse from the interface to the medium than from the core to the medium. And that might be why we observed the fast release for both conditions.

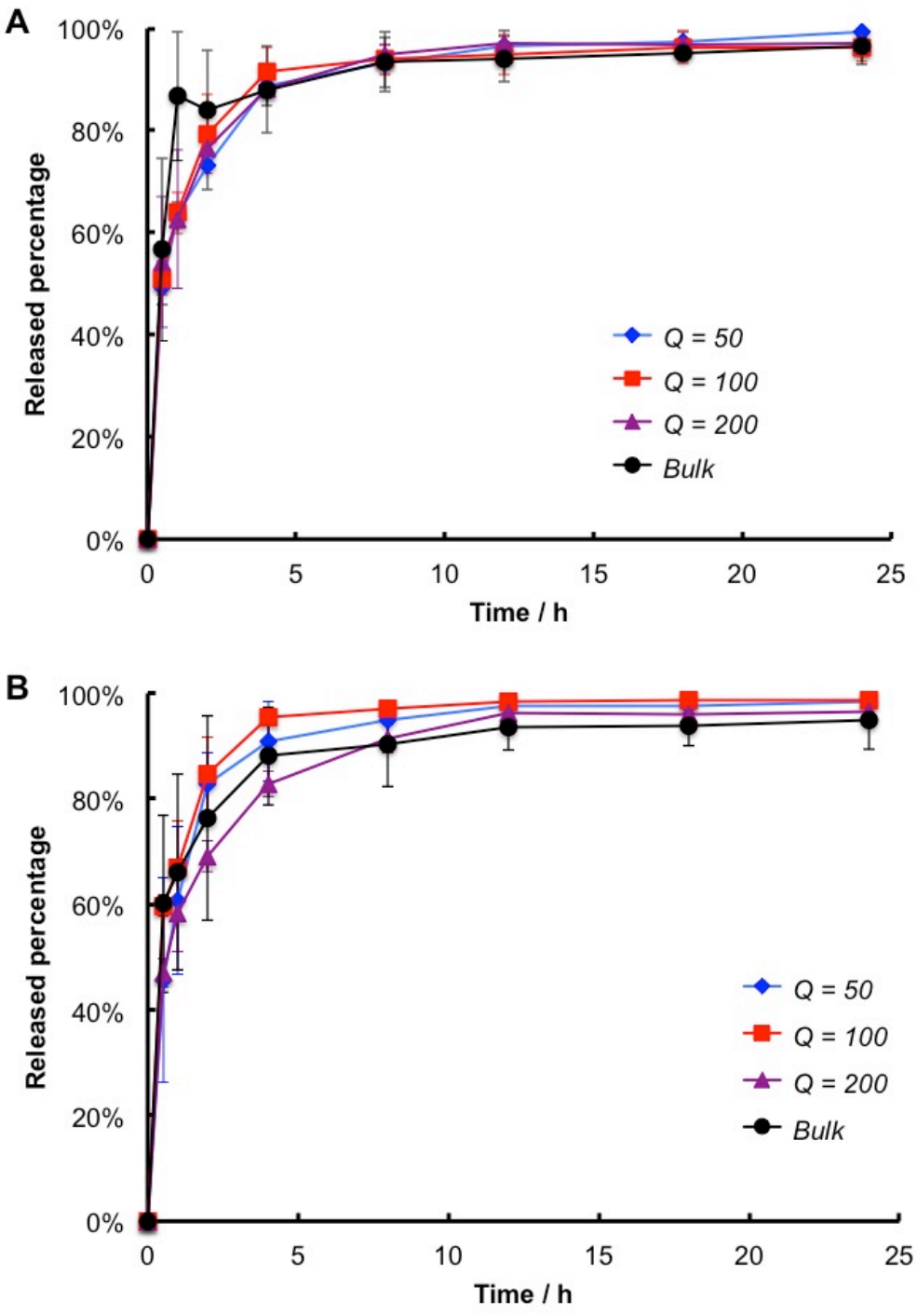

Figure 2-9 Release profile of nanoparticle-encapsulated curcumin: A. nanoparticle prepared at r = 0.50; B. nanoparticle prepared at r = 0.75; the water content for all microfluidic preparations was cwc + 10 wt %.

2.4 Conclusion

In this chapter, we successfully prepared PCL(12k)-*b*-PEO(5k) nanoparticle-encapsulated curcumin. We explored different flow rates, water contents and initial drug-to-polymer ratios on the microfluidic chip. Encapsulating in the nanoparticles improved the solubility of curcumin in the aqueous environment. Moreover, the microfluidic chip showed the control on the nanoparticle size, morphologies and loading efficiency. By tuning flow rates on microfluidic chips, we were able to achieve smaller and homogeneous sizes and higher loading efficiency. The effect of flow rate was considered as a result from the shear-induced break-up. Increasing the drug-to-polymer ratios led to smaller sizes and higher loading efficiency. With higher water contents, nanoparticles had higher loading efficiencies and smaller sizes.

2.5 Reference

1. Saffari, M.; Moghimi, H. R.; Dass, C. R., Barriers to Liposomal Gene Delivery: from Application Site to the Target. *Iranian Journal of Pharmaceutical Research* **2016,** *15*, 3-17.

2. Ingato, D.; Lee, J. U.; Sim, S. J.; Kwon, Y. J., Good things come in small packages: Overcoming challenges to harness extracellular vesicles for therapeutic delivery. *Journal of Controlled Release* **2016,** *241*, 174-185.

3. Farjami, T.; Madadlou, A., Fabrication methods of biopolymeric microgels and microgel-based hydrogels. *Food Hydrocolloids* **2017,** *62*, 262-272.

4. Fong, W. K.; Negrini, R.; Vallooran, J. J.; Mezzenga, R.; Boyd, B. J., Responsive self-assembled nanostructured lipid systems for drug delivery and diagnostics. *Journal of Colloid and Interface Science* **2016,** *484*, 320-339.

5. Shahabipour, F.; Banach, M.; Sahebkar, A., Exosomes as nanocarriers for siRNA delivery: paradigms and challenges. *Archives of Medical Science* **2016,** *12* (6), 1324-1326.

6. Zhang, Y.; Cui, L. L.; Li, F.; Shi, N. Q.; Li, C. L.; Yu, X. H.; Chen, Y.; Kong, W., Design, fabrication and biomedical applications of zein-based nano/micro-carrier systems. *International Journal of Pharmaceutics* **2016,** *513* (1-2), 191-210.

7. Moreira, A. F.; Dias, D. R.; Correia, I. J., Stimuli-responsive mesoporous silica nanoparticles for cancer therapy: A review. *Microporous and Mesoporous Materials* **2016,** *236*, 141-157.

8. Guo, X.; Wang, L.; Wei, X.; Zhou, S. B., Polymer-Based Drug Delivery Systems for Cancer Treatment. *Journal of Polymer Science Part a-Polymer Chemistry* **2016,** *54* (22), 3525-3550.

9. Boissenot, T.; Bordat, A.; Fattal, E.; Tsapis, N., Ultrasound-triggered drug delivery for cancer treatment using drug delivery systems: From theoretical considerations to practical applications. *Journal of Controlled Release* **2016,** *241*, 144-163.

10. Barud, H. G. D.; da Silva, R. R.; Barud, H. D.; Tercjak, A.; Gutierrez, J.; Lustri, W. R.; de Oliveira, O. B.; Ribeiro, S. J. L., A multipurpose natural and renewable polymer in medical applications: Bacterial cellulose. *Carbohydrate Polymers* **2016,** *153*, 406-420.

11. Cho, K.; Wang, X.; Nie, S.; Chen, Z. G.; Shin, D. M., Therapeutic nanoparticles for drug delivery in cancer. *Clin Cancer Res* **2008,** *14* (5), 1310-6.

12. Knop, K.; Hoogenboom, R.; Fischer, D.; Schubert, U. S., Poly(ethylene glycol) in drug delivery: pros and cons as well as potential alternatives. *Angew Chem Int Ed Engl* **2010,** *49* (36), 6288-308.

13. Wong, A. D.; Ye, M.; Ulmschneider, M. B.; Searson, P. C., Quantitative Analysis of the Enhanced Permeation and Retention (EPR) Effect. *PLOS One* **2015,** *10* (5).

14. Baek, S.; Taylor, R. A.; Barber, T. J.; Asme, *DEVELOPMENT OF A DYNAMIC TESTING DEVICE FOR PREDICTING THE ENHANCED PERMEATION AND*

RETENTION (EPR) EFFECT OF DIFFERENT NANOPARTICLES IN TUMOR VESSELS. 2013; p 65-69.

15. Maeda, H.; Wu, J.; Sawa, T.; Matsumura, Y.; Hori, K., Tumor vascular permeability and the EPR effect in macromolecular therapeutics: a review. *Journal of Controlled Release* **2000,** *65* (1-2), 271-284.

16. Geng, Y.; Dalhaimer, P.; Cai, S. S.; Tsai, R.; Tewari, M.; Minko, T.; Discher, D. E., Shape effects of filaments versus spherical particles in flow and drug delivery. *Nature Nanotechnology* **2007,** *2* (4), 249-255.

17. Massey, J. A.; Temple, K.; Cao, L.; Rharbi, Y.; Raez, J.; Winnik, M. A.; Manners, I., Self-assembly of organometallic block copolymers: The role of crystallinity of the core-forming polyferrocene block in the micellar morphologies formed by poly(ferrocenylsilane-b-dimethylsiloxane) in n-alkane solvents. *Journal of the American Chemical Society* **2000,** *122* (47), 11577-11584.

18. Pradhan, D.; Tripathy, G.; Pradhan, R. K.; Dasmohapatra, T.; Pradhan, S. P., A Review on Cuminosides Nanomedicine-: Pharmacognostic approach to Cancer therapeutics. *Journal of Young Pharmacists* **2016,** *8* (2), 61-71.

19. Wang, Y. T.; Wang, C. Y.; Zhao, J.; Ding, Y. F.; Li, L., A cost-effective method to prepare curcumin nanosuspensions with enhanced oral bioavailability. *Journal of Colloid and Interface Science* **2017,** *485*, 91-98.

20. Wang, X.; Wang, Z. N.; Zhao, X.; Zhang, L.; Fan, J., Rheological properties of lyotropic liquid crystals encapsulating curcumin. *Journal of Dispersion Science and Technology* **2017,** *38* (1), 132-138.

21. Pham, X. N.; Nguyen, T. P.; Pham, T. N.; Tran, T. T. N.; Tran, T. V. T., Synthesis and characterization of chitosan-coated magnetite nanoparticles and their application in curcumin drug delivery. *Advances in Natural Sciences-Nanoscience and Nanotechnology* **2016,** *7* (4).

22. Rejinold, N. S.; Sreerekha, P. R.; Chennazhi, K. P.; Nair, S. V.; Jayakumar, R., Biocompatible, biodegradable and thermo-sensitive chitosan-g-poly (N-

isopropylacrylamide) nanocarrier for curcumin drug delivery. *Int J Biol Macromol* **2011,** *49* (2), 161-72.

23. Bansal, S. S.; Goel, M.; Aqil, F.; Vadhanam, M. V.; Gupta, R. C., Advanced drug delivery systems of curcumin for cancer chemoprevention. *Cancer Prev Res (Phila)* **2011,** *4* (8), 1158-71.

24. Ma, Z.; Haddadi, A.; Molavi, O.; Lavasanifar, A.; Lai, R.; Samuel, J., Micelles of poly(ethylene oxide)-b-poly(epsilon-caprolactone) as vehicles for the solubilization, stabilization, and controlled delivery of curcumin. *J Biomed Mater Res A* **2008,** *86* (2), 300-10.

25. Wang, C. W.; Bains, A.; Sinton, D.; Moffitt, M. G., Flow-Directed Loading of Block Copolymer Micelles with Hydrophobic Probes in a Gas-Liquid Microreactor. *Langmuir* **2013,** *29* (26), 8385-8394.

26. Wang, C. W.; Sinton, D.; Moffitt, M. G., Morphological Control via Chemical and Shear Forces in Block Copolymer Self-Assembly in the Lab-on-Chip. *Acs Nano* **2013,** *7* (2), 1424-1436.

27. Wang, C. W.; Bains, A.; Sinton, D.; Moffitt, M. G., Flow-Directed Assembly of Block Copolymer Vesicles in the Lab-on-a-Chip. *Langmuir* **2012,** *28* (45), 15756-15761.

28. Wang, C. W.; Sinton, D.; Moffitt, M. G., Flow-directed block copolymer micelle morphologies via microfluidic self-assembly. *J Am Chem Soc* **2011,** *133* (46), 18853-64.

29. Bains, A.; Wulff, J. E.; Moffitt, M. G., Microfluidic synthesis of dye-loaded polycaprolactone-block-poly(ethylene oxide) nanoparticles: Insights into flow-directed loading and in vitro release for drug delivery. *J Colloid Interface Sci* **2016,** *475*, 136-48.

30. Bains, A.; Wulff, J. E.; Moffitt, M. G., Microfluidic synthesis of dye-loaded polycaprolactone-block-poly (ethylene oxide) nanoparticles: Insights into flow-directed loading and in vitro release for drug delivery. *J Colloid Interf Sci* **2016,** *475*, 136-148.

Chapter 3 Release Rate Optimization and Curcumin Extraction from Mouse Plasma: Towards *In Vivo* Pharmacokinetic Studies

3.1 Introduction

Although curcumin has promising therapeutic effects, its current application is limited by drawbacks such as the low solubility and poor bioavailability.[1-5] Therefore, there are numerous studies developing nanoparticles to encapsulate curcumin in aqueous media and protect it from undesirable degradation.[6-8] For such nanoparticle delivery systems, *in vivo* pharmacokinetic (PK) experiments can provide insights into drug bioavailability (concentration of drug reaching the circulation) and how fast the drug will be eliminated from the body, with longer circulation times providing more exposure time for therapeutic effect.[9-12] In a typical PK study of a pharmaceutical drug, the whole process from the moment that it is administered to the moment of it is eliminated from the body was tracked. Analytical determination of the fate of drug was performed.[13-15] There are several PK parameters in such experiments to describe the influence of living organism on the pharmaceutical drug such as C_{max} (the peak plasma concentration), t_{max} (the time to reach C_{max}), and elimination half-time (the time used to reach the half original concentration). A typical graph of PK study is presented in Figure 3-1. Such experiments require extraction of blood from the experiment animal at certain time point followed by quantitative measurement of the concentration of drug in that given volume. In order to measure these parameters in PK study, one prerequisite is to develop a procedure for extraction drug from blood and a calibration curve.

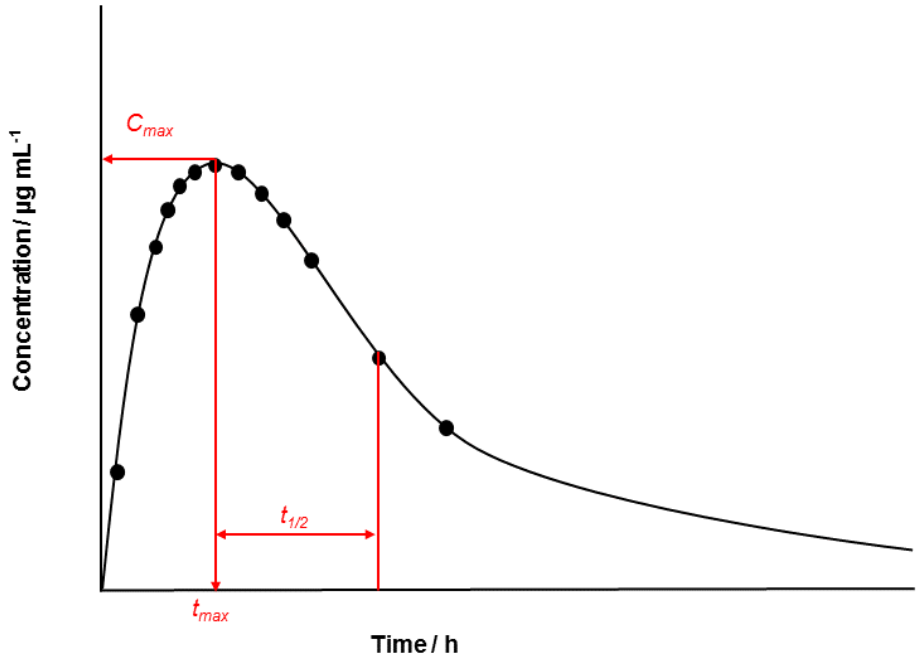

Figure 3-1 A typical graph of drug PK study. The key parameters (C_{max}, t_{max}, $t_{1/2}$) of the PK study are labeled on the graph.

In general, nanoparticle formulations selected for PK studies should exhibit relatively slow release in *in vitro* release experiments such as those described in the previous chapter. Researchers focusing on nanoparticle-encapsulated drugs, including curcumin, have found that *in vitro* release rates were significantly slower than *in vivo* elimination times. For example, Khalil *et al.* encapsulated curcumin in PLGA-PEG nanoparticles and found *in vitro* release times up to 10 days with only half of the curcumin being released; however, the *in vivo* elimination half time for the same formulations was only ~6 h.[16] Zou *et al.* conducted PK experiments of polymeric nanoparticle-encapsulated curcumin and obtained elimination half times of ~3 h. [17] Prof.

Christine Allen, the collaborator for proposed PK studies of our nanoparticles, advised us that *in vitro* release times over 4-7 days, with less than ~40% release in 24 h, should be achieved before embarking on a PK study.[18]

In the previous chapter, we produced various samples of curcumin encapsulated PCL-*b*-PEO nanoparticles using the two-phase microfluidics, and demonstrated variability in nanoparticle size, morphology, and curcumin encapsulation efficiency. However, the measured *in vitro* curcumin release rates were fast, with 50% release in 30 minutes and complete curcumin release in 12 hours. Therefore the first goal of this chapter was to explore some new microfluidic chemical and flow conditions for nanoparticle preparation in an attempt to produce formulations with slower *in vitro* release rates. We selected conditions expected to give higher PCL crystallinities (higher water content, lower loading levels, and higher flow rates), hoping that increased core crystallinities would lead to higher core viscosities and slower release, as demonstrated previously by our group.[19] In preparation for future PK studies, the second goal of this chapter was to develop extraction procedure, HPLC measurement, and calibration methods for determination of curcumin concentrations in the blood plasma.

3.2 Experimental

3.2.1 Materials

All materials used to prepare curcumin-encapsulated nanoparticles were the same as described in the previous chapter. Dialysis bags used for preparation and release experiments were purchased from SpectrumLabs (MWCO: 6-8kD).

3.2.2 Microfluidic Preparation of Curcumin-Loaded PCL-*b*-PEO Nanoparticles

The method used to prepare the nanoparticles in the two-phase microfluidic mixer was identical to the one described in the previous chapter. The conditions in this study were chosen based on the result from the previous experiment. We concluded that increasing flow rate, decreasing drug ratio and increasing water content might all increase crystallinity and slowed down release. Therefore, we changed these three parameters for the improvement of release rate. The condition with cwc + 10 wt %, 0.75 initial drug ratio and 200 µL/min flow rate was chosen to be the baseline. For the first part of optimization, we changed flow rate, drug ratio and water content individually. The result showed sample prepared by higher flow rate had a slower release. Based on this result, in the second part of optimization study, the flow rate and water content were set at 400 µL/min and cwc + 10 wt % while three different drug ratios were chosen. A scheme of how conditions were chosen was presented in Scheme 3-1.

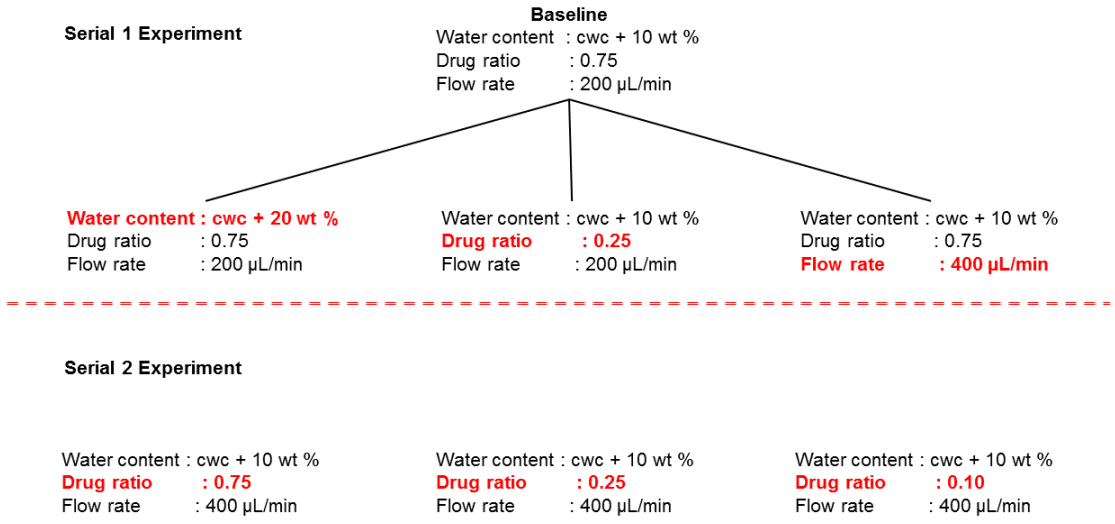

Scheme 3-1 Optimization experiment conditions.

3.2.3 Transmission Electron Microscopy

Transmission electron microscopy (TEM) was used to characterize nanoparticle-encapsulated curcumin morphologies. The instrument was JEOL JEM-1400 TEM. The accelerating voltage is 65 kV. The TEM sample was prepared by the same method described in the previous chapter.

3.2.4 Dynamic Light Scattering

The effective hydrodynamic diameter was determined by dynamic light scattering. The instrument was Brookhaven Instruments photon correlation spectrometer with a BI-9000AT digital autocorrelator, a BI-200SM goniometer, and a He-Ne laser (633 nm). The solvent was deionized water. The measurement temperature was set at 23°C. The scattering angle was set at 90°.

3.2.5 Loading Efficiency Determination by HPLC

The sample preparation method was exactly the same as what was described in the previous chapter. The HPLC system we used is Agilent 1100 with Agilent Zorbax SB-C18 5 μm column. The composition of mobile phase was set at 31:20:49 0.3 v% acetic acid:methanol:acetonitrile. The flow rate was set at 1 mL/min. The detector was diode array detector. We used absorbance at 420 nm to measure the concentration of our samples and determine a calibration curve.

3.2.6 *In Vitro* Release Rate

The sample preparation procedure was the same as the previous description in Chapter 2. Release tubing had a different molecular weight cut off (6-8kD) than the release tubing used in Chapter 2, which had a MWCO of 100 kD. In this chapter, except

the condition with 0.75 drug ratio and 400 μL/min, all conditions only conducted once. Therefore, in the result, some release curves do not show error bars, The HPLC system was also exactly the same as the one used for loading efficiency determination.

3.2.6 Extraction, HPLC Measurement, and Calibration of Curcumin from Mouse Plasma

The procedure for extracting curcumin from plasma was modified from a procedure developed by Schiborr.[14] During extraction, 2.0 mg of curcumin was dissolved in 5.0 mL methanol to make a stock solution of concentration 400 μg/mL. Working solutions were prepared by diluting stock solution to different concentrations (400 μg/mL, 200 μg/mL, 100 μg/mL, 20 μg/mL). Then 20 μL of each curcumin working solution was added to 200 mL mouse plasma followed by 30 seconds vortex. The spiked plasma was combined with 400 mL ethyl acetate (Sigma Aldrich) for the purpose of extracting curcumin. In this liquid-liquid extraction, curcumin will then transfer from the blood plasma to the organic solvent. 12000g centrifugation speed was applied to assist with layer separation. After centrifugation, the upper organic layer was moved to a clean vial and dried under ambient conditions overnight. Then 0.2 grams of acetonitrile was added to each sample to dissolve the dried residue. The acetonitrile solution was then vortex-mixed and transferred to a HPLC sample vial for the determination of concentration by HPLC. The HPLC system was exactly the same as the one we used for loading efficiency determination. The calibration curve was plotted by UV light absorbance area integration at 420nm against the known concentration of curcumin.

3.3 Results

3.3.1 Characterization of Nanoparticle-Encapsulated Curcumin

We first characterized the size and morphologies of these optimization samples. The results are presented in Figure 3-2.

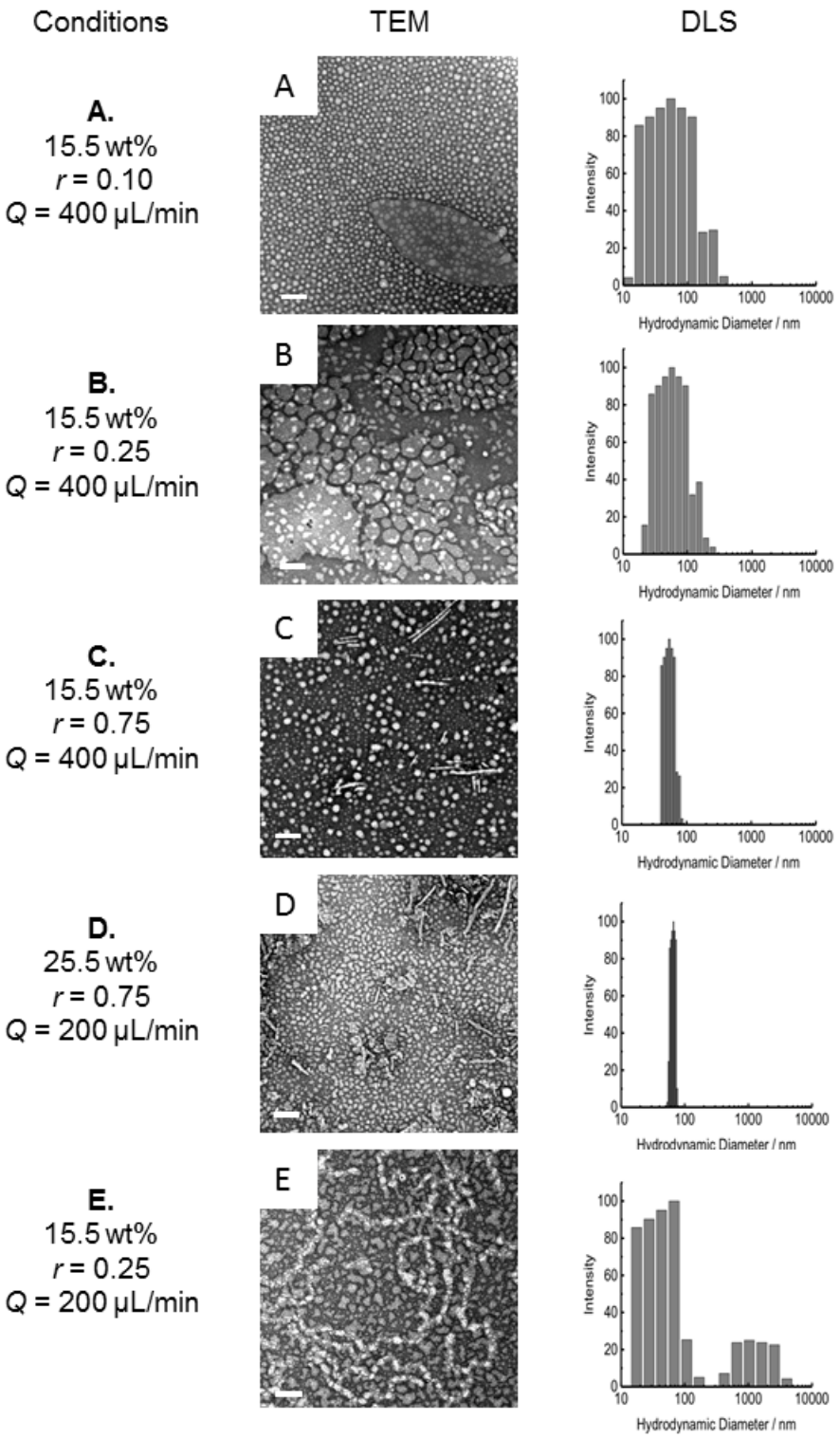

Figure 3-2 The summary of size distribution and morphology of optimization experiment samples.

Table 3-1 Size and loading efficiency of optimization experiment samples

Condition	Hydrodynamic diameter /nm	Loading efficiency / %
A. 15.5 wt % r = 0.10 Q = 400 μL/min	53.9 ± 1.7	9.6
B. 15.5 wt % r = 0.25 Q = 400 μL/min	57.2 ± 2.7	11.5
C. 15.5 wt % r = 0.75 Q = 400 μL/min	59.7 ± 1.0	58.0
D. 25.5 wt % r = 0.75 Q = 200 μL/min	62.1 ± 2.7	40.6
E. 15.5 wt % r = 0.25 Q = 200 μL/min	75.3 ± 17.8	29.6

The samples prepared at the higher flow rate (400 μL/min) had slightly greater sizes and wider size distribution comparing to the sample prepared at 200 μL/min. For example, in Chapter 2, we presented samples when r equals 0.75 and the flow rate set at 200 μL/min had pure sphere morphology. However, when we increased the flow rate to 400 μL/min, there was short cylinder structure presented in TEM images. The average hydrodynamic size also increased from 55.2nm (0.75, 200 μL/min) to 59.7 nm (0.75, 400

μL/min). Increasing water content resulted in a narrower size distribution. However, there were still small platelets and short cylinders presented. The condition (r = 0.25 and Q = 200 μL/min) resulted in the formation of bigger morphologies such as long cylinders. Since each condition had various morphologies. It was difficult to find a direct relationship between the release rate and morphologies/size.

3.3.2 Release Rate Optimization Result

In this optimization experiment, we were trying to decrease the release rate by increasing core crystallinity. The optimization process could be divided into two parts. The first part of optimization was to explore the influence of three variables: flow rate, drug-to-polymer ratio and water content. The result was shown in Figure 3-3 "Release profile of optimization part 1". The result showed that the highest flow rate (400 μL/min) sample had relatively slower release rate comparing to the other conditions (Q = 25-200 μL/min, cwc + 20 wt %). It might indicate higher flow rate had better control on release rates. Therefore, we designed the second part optimization experiment where all flow rates were set at 400 μL/min. The result of second part of optimization experiment was summarized in Figure 3-4.

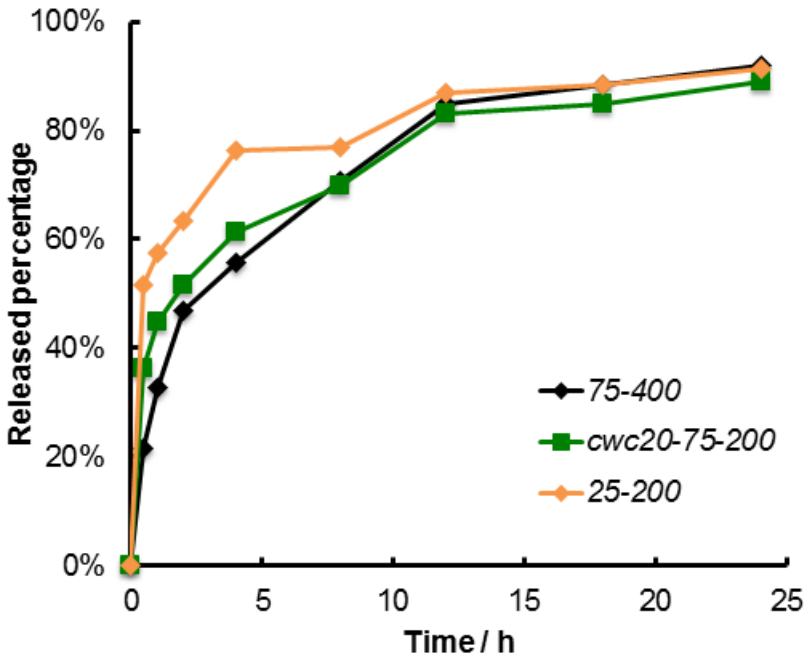

Figure 3-3 The release profile of optimization part 1.

The result from Figure 3-4 showed relatively long release time up to 48 hours for all conditions. The condition labeled as "75-200" was the condition where the drug-to-polymer ratio was 0.75 and the flow rate was 200 µL/min. This condition was presented here as a baseline of conditions with a higher flow rate (400 µL/min). This optimization experiment showed that all conditions with a higher flow rate (400 µL/min) slowed down the release rate at the beginning comparing to the baseline condition (75-200). Figure 3-4 (B) showed a zoomed-in picture of release profile. In the first 30 minutes, 40 % curcumin was released from the nanoparticles while only 20% curcumin released from samples prepared at 400 µL/min. However, the release rates between different drug-to-polymer ratios were very similar. The samples prepared at 400 µL/min flow rate and three

different drug ratios (0.75, 0.25, 0.10) did not show a significant difference in both Figure 3-5 A and B.

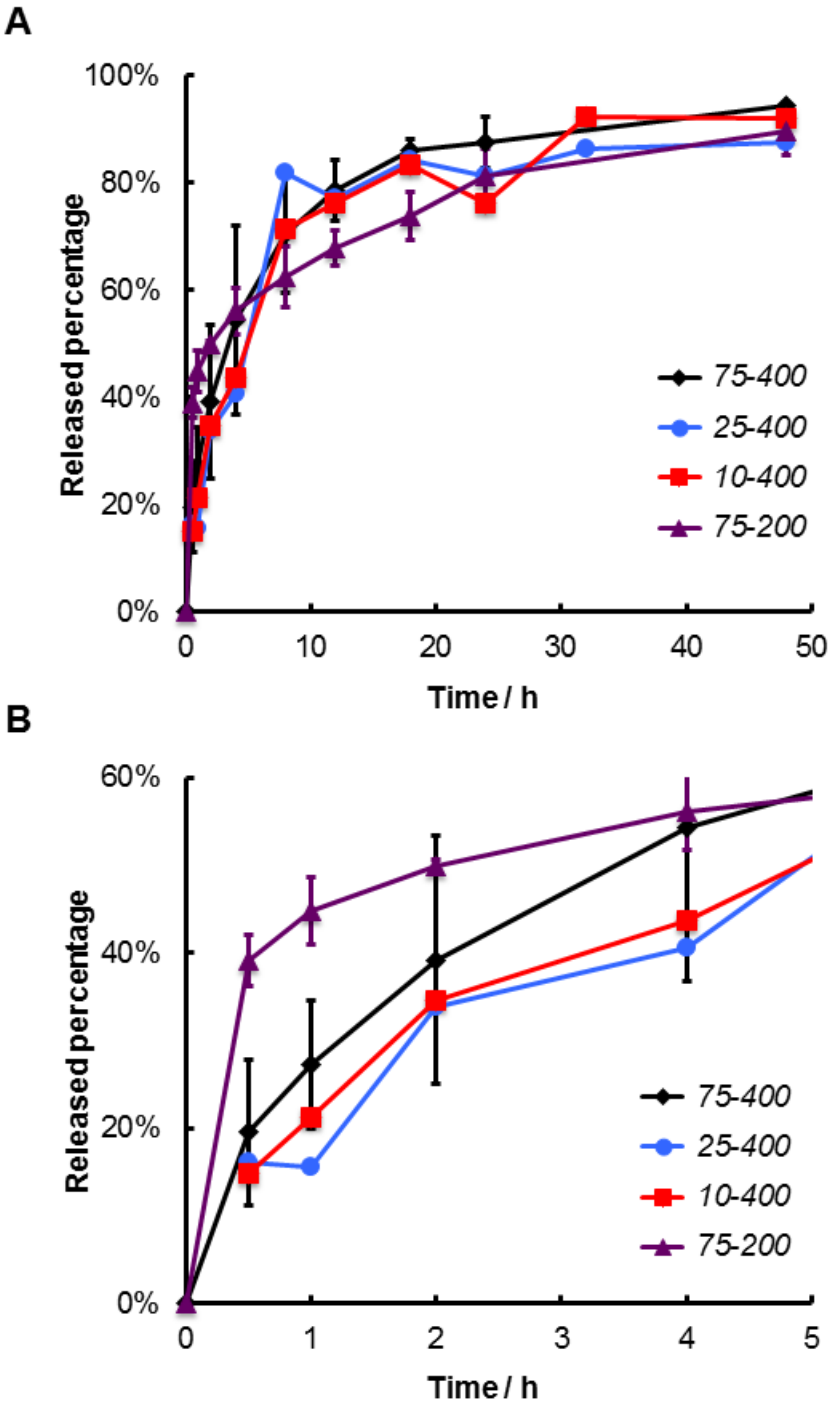

Figure 3-4 Release serial 2. A is the summary of all conditions. B is zoomed image to present release profile in the first 5h.

In general, higher flow rate produced the slower release rate, especially at the beginning of the release. We measured released percentages after 72 hours but found out the release rates does not go up anymore to 100%. It may be attributed to the fact that some drug molecules were trapped in the crystalline area and never been able to get out of it. The release experiment in this chapter used a different type of release tubing with smaller MWCO. Therefore, the results between release rate in Chapter 2 and Chapter 3 cannot be compared.

3.3.3 Extraction of Curcumin from Mouse Plasma

After release optimization studies, we developed a protocol for extracting curcumin from the mouse plasma for future *in vivo* studies. The procedure of extraction has been described in experimental work in this chapter. The calibration curves from three repeat preparations were showed in Figure 3-5.

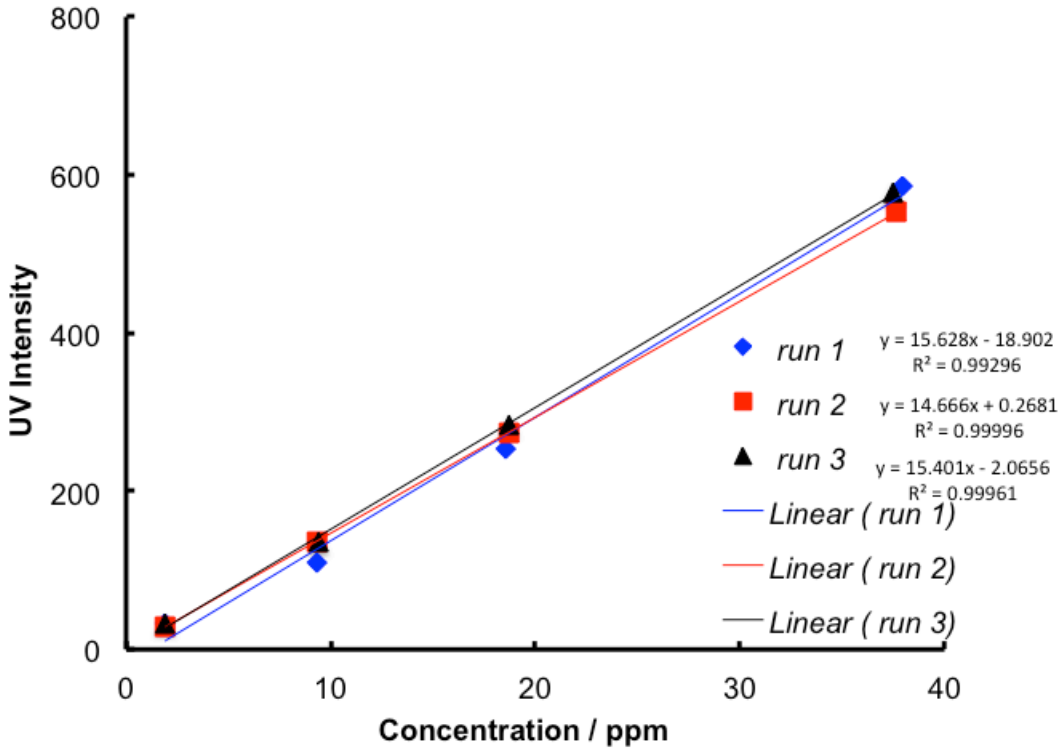

Figure 3-5 Calibration curve of curcumin extracting from plasma.

A representative HPLC curve of curcumin extracted from plasma was presented in Figure 3-6. The curcumin and its derivatives (demethoxycurcumin and bisdemethoxycurcumin) were eluted after 5 minutes. The assignment of these three HPLC peaks was based on the information from the literature.[20] From the right to the left, the peaks are curcumin, demethoxycurcumin and bisdemethoxycurcumin. At 2 minutes, there was a very small peak. This might be other components extracted from plasma.

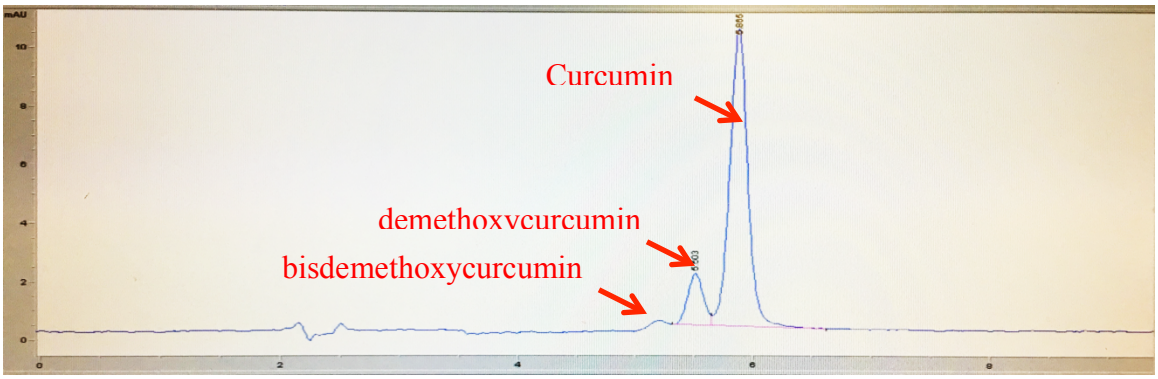

Figure 3-6 A representative HPLC curve of curcumin extracted from mouse plasma.

The recovery of curcumin from the plasma sample was compared with that obtained from direct injection of a known amount of curcumin in the acetonitrile. The extraction recovery percentages were calculated by the following equation:

$$Recovery = \frac{UV\ detector\ response\ of\ curcumin\ extracted\ from\ plasma}{UV\ detector\ response\ of\ the\ same\ amount\ curcuin\ dissolved\ directly}$$

Table 3-2 Recovery rate of curcumin extracted from mouse plasma

Concentration/ppm	Recovery rate	Standard Deviation
438	27%	0.008
219	26%	0.014
110	25%	0.028
22	30%	0.018

Ethyl acetate was used as an extraction solvent for spiked plasma. It was a well-established method in extracting curcumin from the blood plasma.[21-23] The recovery rates listed in the literature were about 60 - 90%. The recovery rate in this experiment was only 25-30 %. The extraction procedure was similar to the procedure from Schoborr *et al.* where the recovery rate was not reported.[14] The experiments with relatively high reported

recovery rates usually added some other steps during extraction. For example, the HCl solution was added into the plasma sample before curcumin extraction. Or after extracting curcumin from the plasma to ethyl acetate, some researchers dried the organic layer under nitrogen rather than in the air.[21-23] The preliminary experiment where curcumin was extracted from deionized water showed that the recovery rate of curcumin from water (60 – 80%) was much higher than the recovery rate of curcumin from the plasma (25 – 30%). The hypothesis was adding acid might be helpful to break interaction between proteins and curcumin. And therefore, adding acid might be the future work to improve the recovery rate. Although, it would be better if future work could improve recovery rate for the purpose of reducing curcumin loss in the extraction process, the low recovery rate would still allow the actual amount of curcumin in the plasma to be determined as long as the extraction rate for the calibration and for the unknown sample are the same.

3.4 Conclusion

In chapter 3, we varied several chemical parameters related to on-chip encapsulation for the purpose of slowing down nanoparticle-encapsulated curcumin release rate. We found out that increasing flow rate had the most significant effect on the release rate at the beginning of release. Other variables such as drug-to-polymer ratio and water content had a weaker effect. We also successfully developed the procedure of extracting curcumin from the plasma. The calibration curve showed a good linearity, but a low recovery rate.

3.5 Reference

1. Aggarwal, B. B.; Kumar, A.; Bharti, A. C., Anticancer potential of curcumin: preclinical and clinical studies. *Anticancer Res* **2003,** *23* (1A), 363-98.

2. Priyadarsini, K. I., The chemistry of curcumin: from extraction to therapeutic agent. *Molecules* **2014,** *19* (12), 20091-112.

3. Yang, K. Y.; Lin, L. C.; Tseng, T. Y.; Wang, S. C.; Tsai, T. H., Oral bioavailability of curcumin in rat and the herbal analysis from Curcuma longa by LC-MS/MS. *J Chromatogr B Analyt Technol Biomed Life Sci* **2007,** *853* (1-2), 183-9.

4. Anand, P.; Kunnumakkara, A. B.; Newman, R. A.; Aggarwal, B. B., Bioavailability of curcumin: problems and promises. *Mol Pharm* **2007,** *4* (6), 807-18.

5. Wang, Y. J.; Pan, M. H.; Cheng, A. L.; Lin, L. I.; Ho, Y. S.; Hsieh, C. Y.; Lin, J. K., Stability of curcumin in buffer solutions and characterization of its degradation products. *J Pharm Biomed Anal* **1997,** *15* (12), 1867-76.

6. Yang, X.; Li, Z.; Wang, N.; Li, L.; Song, L.; He, T.; Sun, L.; Wang, Z.; Wu, Q.; Luo, N.; Yi, C.; Gong, C., Curcumin-encapsulated polymeric micelles suppress the development of colon cancer in vitro and in vivo. *Sci Rep* **2015,** *5*, 10322.

7. Song, Z.; Feng, R.; Sun, M.; Guo, C.; Gao, Y.; Li, L.; Zhai, G., Curcumin-loaded PLGA-PEG-PLGA triblock copolymeric micelles: Preparation, pharmacokinetics and distribution in vivo. *J Colloid Interface Sci* **2011,** *354* (1), 116-23.

8. Rejinold, N. S.; Sreerekha, P. R.; Chennazhi, K. P.; Nair, S. V.; Jayakumar, R., Biocompatible, biodegradable and thermo-sensitive chitosan-g-poly (N-isopropylacrylamide) nanocarrier for curcumin drug delivery. *Int J Biol Macromol* **2011,** *49* (2), 161-72.

9. Chaurasia, S.; Chaubey, P.; Patel, R. R.; Kumar, N.; Mishra, B., Curcumin-polymeric nanoparticles against colon-26 tumor-bearing mice: cytotoxicity, pharmacokinetic and anticancer efficacy studies. *Drug Development and Industrial Pharmacy* **2016,** *42* (5), 694-700.

10. Gaur, P. K.; Mishra, S.; Verma, A.; Verma, N., Ceramide-palmitic acid complex based Curcumin solid lipid nanoparticles for transdermal delivery: pharmacokinetic and pharmacodynamic study. *Journal of Experimental Nanoscience* **2016,** *11* (1), 38-53.

11. Li, S. L.; Fang, C. S.; Zhang, J. Q.; Liu, B. L.; Wei, Z. Q.; Fan, X. Q.; Sui, Z.; Tan, Q. Y., Catanionic lipid nanosystems improve pharmacokinetics and anti-lung cancer activity of curcumin. *Nanomedicine-Nanotechnology Biology and Medicine* **2016,** *12* (6), 1567-1579.

12. Liu, R.; Sun, L.; Fang, S. M.; Wang, S. T.; Chen, J. J.; Xiao, X. F.; Liu, C. X., Thermosensitive in situ nanogel as ophthalmic delivery system of curcumin: development, characterization, in vitro permeation and in vivo pharmacokinetic studies. *Pharmaceutical Development and Technology* **2016,** *21* (5), 576-582.

13. Ma, Z.; Shayeganpour, A.; Brocks, D. R.; Lavasanifar, A.; Samuel, J., High-performance liquid chromatography analysis of curcumin in rat plasma: application to pharmacokinetics of polymeric micellar formulation of curcumin. *Biomed Chromatogr* **2007,** *21* (5), 546-52.

14. Schiborr, C.; Eckert, G. P.; Rimbach, G.; Frank, J., A validated method for the quantification of curcumin in plasma and brain tissue by fast narrow-bore high-performance liquid chromatography with fluorescence detection. *Anal Bioanal Chem* **2010,** *397* (5), 1917-25.

15. Ramalingam, P.; Ko, Y. T., A validated LC-MS/MS method for quantitative analysis of curcumin in mouse plasma and brain tissue and its application in pharmacokinetic and brain distribution studies. *Journal of Chromatography B-Analytical Technologies in the Biomedical and Life Sciences* **2014,** *969*, 101-108.

16. Khalil, N. M.; do Nascimento, T. C.; Casa, D. M.; Dalmolin, L. F.; de Mattos, A. C.; Hoss, I.; Romano, M. A.; Mainardes, R. M., Pharmacokinetics of curcumin-loaded PLGA and PLGA-PEG blend nanoparticles after oral administration in rats. *Colloids Surf B Biointerfaces* **2013,** *101*, 353-60.

17. Zou, P.; Helson, L.; Maitra, A.; Stern, S. T.; McNeil, S. E., Polymeric curcumin nanoparticle pharmacokinetics and metabolism in bile duct cannulated rats. *Mol Pharm* **2013,** *10* (5), 1977-87.

18. Allen, C. A., Personal communication. July 2016.

19. Bains, A.; Cao, Y.; Moffitt, M. G., Multiscale Control of Hierarchical Structure in Crystalline Block Copolymer Nanoparticles Using Microfluidics. *Macromol Rapid Commun* **2015,** *36* (22), 2000-5.

20. Jayaprakasha, G. K.; Rao, L. J. M.; Sakariah, K. K., Improved HPLC method for the determination of curcumin, demethoxycurcumin, and bisdemethoxycurcumin. *Journal of Agricultural and Food Chemistry* **2002,** *50* (13), 3668-3672.

21. Yang, X. Z.; Ma, J. S.; Ye, Y.; Zhang, Y. A.; Lin, G. Y.; Zheng, Y. C.; Li, X.; Wang, X. Q., LC-APCI-MS Quantitative Analysis of Curcumin in Rabbit Plasma. *Chromatographia* **2011,** *73* (5-6), 605-608.

22. Hao, K.; Zhao, X. P.; Liu, X. Q.; Wang, G. J., LC determination of curcumin in dog plasma for a pharmacokinetic study. *Chromatographia* **2006,** *64* (9-10), 531-535.

23. Liu, A. C.; Lou, H. X.; Zhao, L. X.; Fan, P. H., Validated LC/MS/MS assay for curcumin and tetrahydrocurcumin in rat plasma and application to pharmacokinetic study of phospholipid complex of curcumin. *Journal of Pharmaceutical and Biomedical Analysis* **2006,** *40* (3), 720-727.

Chapter 4 Anticancer Activity of Curcumin Loaded PCL-*b*-PEO Nanoparticles

4.1 Introduction

In Chapter 2, we successfully prepared and characterized nanoparticles for delivering curcumin. In this chapter, we present nanoparticle-encapsulated curcumin's performance on a cancer cell line. Curcumin has been shown to induce apoptosis in various cancer cell lines, for example, breast cancer[1-5], colon cancer[6-10], melanoma cells[11], hepatocellular carcinoma[12], leukemia cell[13]. However, free curcumin was not successful in the clinical trials due to its insolubility and poor bioavailability. Therefore, developing a drug for drug delivery system for curcumin is necessary. Several drug delivery formulations of curcumin have been tested in cell viability assays, leading to a variety of results dependent on the specific delivery systems. Khosropanah *et al.* employed an acid-chitosan nano-gel as a drug delivery system for curcumin; the nanoparticle formulation was tested on the breast adenocarcinoma cancer cell line MDA-MB-231 for cytotoxicity. The curcumin encapsulated in chitosan nano-gel was found to be at least twice as potent (IC_{50} values twice as small) compared to free curcumin, possibly due to enhanced uptake of the nanoparticles.[14] However, another system of encapsulated curcumin was shown to be less cytotoxic than the free drug; this delivery system, consisting of pluronic, chitosan and alginate did not increase the drug efficacy on the human cervical cancer cell (HeLa), with an IC_{50} value of the nanoformulation being slightly higher than free curcumin.[15] There were several similar studies about IC_{50} values of nanoparticle-encapsulated curcumin. Bisht *et al.* synthesized polymeric nanoparticles using *N*-isopropylacrylamide (NIPAAM), N-vinyl-2-pyrrolidone and poly(ethyleneglycol) monoacrylate. Curcumin was encapsulated in nanoparticles with

the average size less than 50 nm. And viability assays were carried out on the human pancreatic cancer cell line. The IC_{50} values were determined to be similar for free curcumin and nanoparticle-encapsulated curcumin in the range of 15 to 20 μM. The IC_{50} values were very similar to the results of this study (Figure 4-1).[16] Yallapu *et al*. encapsulated curcumin into PLGA nanoparticles and tested on the same human breast cancer cell line applied in this work, MDA-MB-231; in that work the determined IC_{50} for the nanoformulation was 9.1 μM while IC_{50} for the bare drug is 16.4 μM. An experiment evaluating apoptosis associated protein (PARP) was performed to show the mechanism of the higher cytotoxicity of nanoformulation. PARP cleavage was a marker of cell apoptosis. The results showed a higher PARP cleavage when cancer cells were treated with nanoparticle-encapsulated curcumin. Therefore, the proposed reason behind improved therapeutic effect of nanoparticle-encapsulated curcumin was that nanoparticle-encapsulated curcumin had higher efficacy in inhibition of cell growth by influencing its apoptotic pathways.[17] In summary, the reported IC_{50} value of nanoparticle-encapsulated curcumin could be either higher or lower than the IC_{50} value of free curcumin.

In this chapter, we selected the samples prepared under following conditions: r = 0.75, water content = cwc + 10 wt % and Q = 50 ~ 200 μL/min for cell viability assays. Samples prepared under these conditions were found to have optimum properties including low-polydispersity small sizes and high loading efficiencies. The result was compared with the bare curcumin.

In this chapter, all cytotoxicity experiments of microfluidic prepared nanoparticles were carried out on the breast cancer cell line MDA-MB-231. This MDA-MB-231 tumor model has been shown to be well vascularized and should be more suitable for a drug

delivery system taking advantage of the EPR effect.[18, 19] IC_{50} values were determined from the antiproliferative assays to investigate the differences in cytotoxicity between the bare curcumin and nanoparticle formulations prepared at different microfluidic flow rates.

4.2 Experimental

4.2.1 Materials.

The synthesis and characterization (morphology, size, loading efficiency and release rates) of various samples of curcumin-loaded PCL-*b*-PEO nanoparticles were described in Chapters 2 and 3. The MDA-MB-231 human breast adenocarcinoma cell line was generously provided by Dr. Christine Allen (University of Toronto, Toronto, Canada). Fetal Bovine Serum (FBS) and Dulbecco's Modified Eagle's Medium Nutrient Mixture F-12 HAM with 15 mM HEPES, $NaHCO_3$, pyridoxine and L-glutamine (DMEM) was purchased from Sigma Aldrich life science. The CellTiter-Blue cell viability assay kit was purchased from Promega. Cells were grown in a sterile tissue culture flask with a surface area of 75 cm^2. Sterile, 96-well flat-bottomed plates were purchased from Becton Dickinson Labware.

4.2.2 Antiproliferation Assay and Cell Culture

MDA-MB-231 cells were grown in DMEM F12-HAM with 10% fetal bovine serum. The cells were placed and grew in the 75 cm^2 tissue culture flask at 37°C in a 5% CO_2 incubator. Trypsin was used to dissociate adherent cells from the flask surface when cells were grown to 80% confluence. Then the cells were collected and pelleted down by centrifugation at 4°C and 1200 rpm for 5 minutes. The cell pellet was re-suspended in media (DMEM F12-HAM with 10% fetal bovine serum) and a hemocytometer was used

to determine the concentration of cells. After the concentration has been determined, cells were diluted by media so that the concentration was 1.0×10^5 cells / mL. This diluted cell suspension was transferred to 96-well plate with 100 μL in each well. The plate was placed in 5% CO_2 at 37°C for 24 hours. After that, 65 μL curcumin formulation of known polymer/drug content was added to 585 μL media to make a total volume of 650 μL. A multichannel pipet was used to dilute this working dispersion to achieve a series of curcumin concentrations. 100 μL of dispersions with various curcumin concentrations were then added to corresponding wells in the 96-well plates. The 96-well plates were then put back to 5% CO_2 incubator at 37°C and incubated for 48, 72, 96 hours. The plate was taken out and 20 μL CellTiter Blue was added to each well. After incubation (5% CO_2, 37°C) for another 4 hours, the plate was taken for the fluorescence measurement (λ_{ex} = 560 nm, λ_{em} = 590 nm).The IC_{50} was measured based on the following equation:

$$Cell\ death = 1 - \frac{S - B_0}{B_t - B_0} \times 100\% \quad (4\text{-}1)$$

S is the fluorescence reading from wells dosed with drug formulation; B_0 is the average fluorescence reading from wells containing pure media; and B_t is the average fluorescence reading from wells containing cells only. Mean IC_{50} values and standard deviations were determined from three repeated preparations of curcumin-encapsulated nanoparticles. The cell death was plotted against corresponding drug concentration. The scatter plots were then fitted using the XLfit software on Microsoft Excel. Each repeated preparation was able to generate a set of data with cell viability and corresponding concentration. Results from three repeated runs were combined together and fitted in XLfit to generate an average IC_{50} for each condition. This analysis method was chosen so that there were enough data points at high formulation concentration for the fitting.

4.3 Results

Figure 3-1 summarizes IC_{50} values determined for three different incubation times (48, 72, and 96 h) of bare curcumin and various microfluidic-prepared curcumin nanoparticle formulations. These results showed that free curcumin had slightly lower IC_{50} values than the various nanoparticle formulations, and that these differences are more accentuated for the 72 h and 96 h incubation times. It meant that the nanoparticle curcumin formulations had marginally lower cytotoxicity. In literature, there were similar results where nanoparticle-encapsulated curcumin had higher IC_{50} than the free curcumin indicating a low toxicity. In the literature where encapsulated curcumin showed to be more potent in cell line studies, one explanation was that nanoparticle was easier to accumulate in tumor than free curcumin.[17] However, this hypothesis that nanoparticle formulations accumulated more effectively in cancer cells was not observed in this experiment.

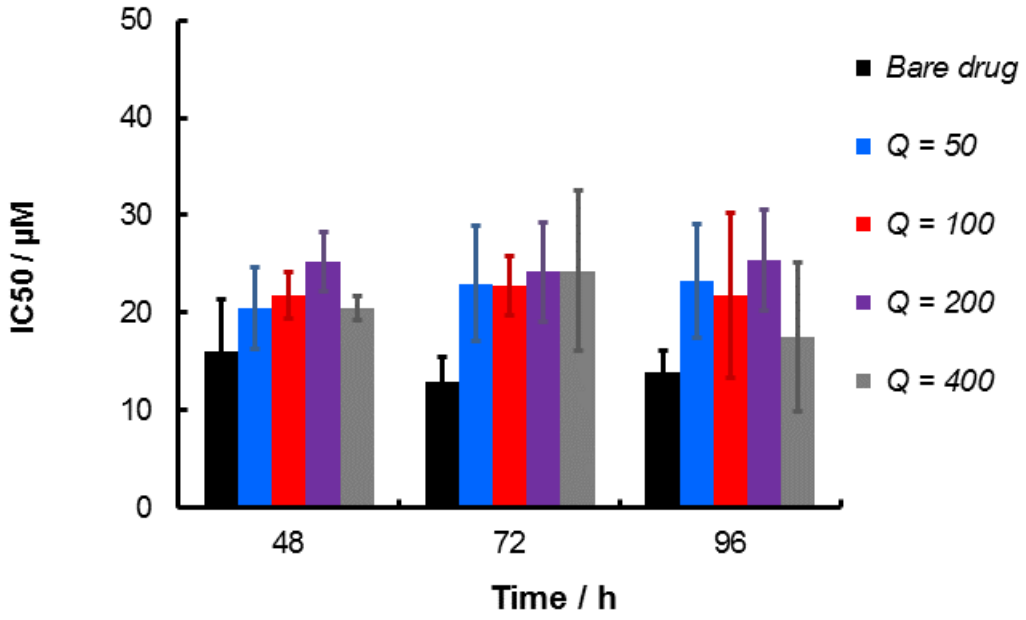

Figure 4-1 IC_{50} values of samples prepared on the chip with different flow rates and bare curcumin (r = 0.75)**.**

The experiment used bare curcumin as the baseline for samples prepared on the microfluidic chip. The reason was that samples prepared by the bulk experiment had a low loading efficiency that was not able to concentrate to a therapeutic dose. The comparison of loading efficiency of bulk samples and on-chip samples were presented in Figure 4-2. The plotted data of bulk sample loading efficiency is the same one presented in Chapter 2 Figure 2-1. The on-chip loading efficiency data presented in Figure 4-2 was also the same data presented in Chapter 2 Figure 2-7 (A). In the cell line experiment, all samples were prepared at the following conditions: r = 0.75, water content = cwc + 10 wt %. Therefore, under the same condition (r = 0.75), the bulk sample had significantly lower loading efficiency. For the bulk sample, nanoparticles would precipitate before its concentration achieved the desired level for the cell line experiment. As a result, the bulk

sample was not used in the cell line study. In contrast, samples prepared on the microfluidic chip had better loading efficiency and better stability.

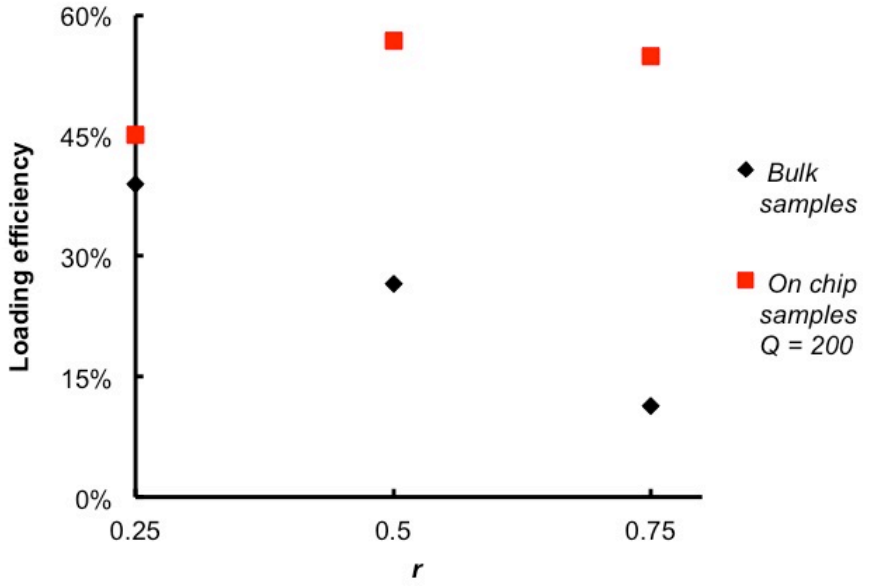

Figure 4-2 Comparing loading efficiency of bulk samples and on-chip samples prepared at $r = 0.75$ (cwc + 10 wt %).

4.4 Conclusion

This chapter showed the cytotoxicity of nanoparticle-encapsulated curcumin on the human breast cancer cell line MDA-MB-231. It proved the antiproliferation effect of curcumin. However, encapsulation of curcumin resulted in a compromised toxicity. No statistical strong influence of flow rate was observed. Samples prepared on the microfluidic chip had higher loading efficiency and better colloidal stability comparing to the bulk sample. And these features made on-chip sample suitable for the further *in vitro* and *in vivo* studies.

4.5 Reference

1. Mehta, K.; Pantazis, P.; McQueen, T.; Aggarwal, B. B., Antiproliferative effect of curcumin (diferuloylmethane) against human breast tumor cell lines. *Anticancer Drugs* **1997,** *8* (5), 470-81.

2. Verma, S. P.; Salamone, E.; Goldin, B., Curcumin and genistein, plant natural products, show synergistic inhibitory effects on the growth of human breast cancer MCF-7 cells induced by estrogenic pesticides. *Biochem Biophys Res Commun* **1997,** *233* (3), 692-6.

3. Simon, A.; Allais, D. P.; Duroux, J. L.; Basly, J. P.; Durand-Fontanier, S.; Delage, C., Inhibitory effect of curcuminoids on MCF-7 cell proliferation and structure-activity relationships. *Cancer Lett* **1998,** *129* (1), 111-6.

4. Ramachandran, C.; You, W., Differential sensitivity of human mammary epithelial and breast carcinoma cell lines to curcumin. *Breast Cancer Res Treat* **1999,** *54* (3), 269-78.

5. Kim, M. S.; Kang, H. J.; Moon, A., Inhibition of invasion and induction of apoptosis by curcumin in H-ras-transformed MCF10A human breast epithelial cells. *Arch Pharm Res* **2001,** *24* (4), 349-54.

6. Hanif, R.; Qiao, L.; Shiff, S. J.; Rigas, B., Curcumin, a natural plant phenolic food additive, inhibits cell proliferation and induces cell cycle changes in colon adenocarcinoma cell lines by a prostaglandin-independent pathway. *J Lab Clin Med* **1997,** *130* (6), 576-84.

7. Samaha, H. S.; Kelloff, G. J.; Steele, V.; Rao, C. V.; Reddy, B. S., Modulation of apoptosis by sulindac, curcumin, phenylethyl-3-methylcaffeate, and 6-phenylhexyl isothiocyanate: apoptotic index as a biomarker in colon cancer chemoprevention and promotion. *Cancer Res* **1997,** *57* (7), 1301-5.

8. Yang, X.; Li, Z.; Wang, N.; Li, L.; Song, L.; He, T.; Sun, L.; Wang, Z.; Wu, Q.; Luo, N.; Yi, C.; Gong, C., Curcumin-encapsulated polymeric micelles suppress the development of colon cancer in vitro and in vivo. *Sci Rep* **2015,** *5*, 10322.

9. Chen, H.; Zhang, Z. S.; Zhang, Y. L.; Zhou, D. Y., Curcumin inhibits cell proliferation by interfering with the cell cycle and inducing apoptosis in colon carcinoma cells. *Anticancer Res* **1999,** *19* (5A), 3675-80.

10. Moragoda, L.; Jaszewski, R.; Majumdar, A. P., Curcumin induced modulation of cell cycle and apoptosis in gastric and colon cancer cells. *Anticancer Res* **2001,** *21* (2A), 873-8.

11. Bush, J. A.; Cheung, K. J.; Li, G., Curcumin induces apoptosis in human melanoma cells through a Fas receptor/caspase-8 pathway independent of p53. *Exp Cell Res* **2001,** *271* (2), 305-14.

12. Pan, M. H.; Chang, W. L.; Lin-Shiau, S. Y.; Ho, C. T.; Lin, J. K., Induction of apoptosis by garcinol and curcumin through cytochrome c release and activation of caspases in human leukemia HL-60 cells. *J Agric Food Chem* **2001,** *49* (3), 1464-74.

13. Kuo, M. L.; Huang, T. S.; Lin, J. K., Curcumin, an antioxidant and anti-tumor promoter, induces apoptosis in human leukemia cells. *Biochim Biophys Acta* **1996,** *1317* (2), 95-100.

14. Khosropanah, M. H.; Dinarvand, A.; Nezhadhosseini, A.; Haghighi, A.; Hashemi, S.; Nirouzad, F.; Khatamsaz, S.; Entezari, M.; Hashemi, M.; Dehghani, H., Analysis of the Antiproliferative Effects of Curcumin and Nanocurcumin in MDA-MB231 as a Breast Cancer Cell Line. *Iranian Journal of Pharmaceutical Research* **2016,** *15* (1), 231-239.

15. Das, R. K.; Kasoju, N.; Bora, U., Encapsulation of curcumin in alginate-chitosan-pluronic composite nanoparticles for delivery to cancer cells. *Nanomedicine* **2010,** *6* (1), 153-60.

16. Bisht, S.; Feldmann, G.; Soni, S.; Ravi, R.; Karikar, C.; Maitra, A., Polymeric nanoparticle-encapsulated curcumin ("nanocurcumin"): a novel strategy for human cancer therapy. *J Nanobiotechnology* **2007,** *5*, 3.

17. Yallapu, M. M.; Gupta, B. K.; Jaggi, M.; Chauhan, S. C., Fabrication of curcumin encapsulated PLGA nanoparticles for improved therapeutic effects in metastatic cancer cells. *J Colloid Interface Sci* **2010,** *351* (1), 19-29.

18. Jiang, H. C.; Chen, C. S.; Sun, Q. M.; Wu, J.; Qiu, L. J.; Gao, C. G.; Liu, W. Q.; Yang, J.; Jun, N.; Dong, J., The role of semaphorin 4D in tumor development and angiogenesis in human breast cancer. *Oncotargets and Therapy* **2016,** *9*, 5737-5750.

19. Bajou, K.; Lewalle, J. M.; Martinez, C. R.; Soria, C.; Lu, H.; Noel, A.; Foidart, J. M., Human breast adenocarcinoma cell lines promote angiogenesis by providing cells with uPA-PAI-1 and by enhancing their expression. *International Journal of Cancer* **2002,** *100* (5), 501-506.

Chapter 5. Conclusion and Future Work

5.1 General Conclusion

In this thesis, we applied "on-chip" control on a new drug delivery system, PCL-*b*-PEO/curcumin. The experiment was based on the previous work in this group that the high shear rates created by the vortex flow within the gas and liquid segments introduce flow-directed effects on various properties of the nanoparticle-encapsulated drug. We examined different chemical parameters' influence on the size, morphology, loading efficiency, release and cancer cell line. Under the optimum condition, we were able to prepare nanoparticles with high loading efficiency and small size.

Previous group members investigated the PS-*b*-PAA and PCL-*b*-PEO drug delivery system. The results showed that the microfluidics was a useful handle to control and create various morphologies[1, 2]. Zheqi Xu observed PNBA-*b*-PDMA spooled cylinder on the microfluidic chip with medium flow rate, which was a new morphology to us[3]. Besides the new morphology, various other morphologies and different crystallinities could also be achieved by tuning other parameters. Comparing to the conventional bulk method, the high shear rates on the chip provided us the control and possibility to tune different drug delivery systems to achieve better efficacy. The photodissociation kinetics of P(MCL-*co*-CL)-*b*-PEO, PNBA-*b*-PDMA was also studied by Zheqi Xu. All these previous studies on microfluidic chips enhanced our understandings and provided us the next step for utilizing microfluidic chips in the anticancer drug delivery. Therefore, in this thesis, we applied microfluidics to synthesize PCL-*b*-PEO encapsulated curcumin and systematically control its structural properties.

Structural control of nanoparticle-encapsulated curcumin from the gas-liquid microfluidic chip was proven to be effective. The polymer we used was PCL-*b*-PEO, a well-established drug delivery vehicle material[4-9]. It was well studied by previous group members and proved to be easy to tune on the microfluidic chip.[10] Curcumin, a polyphenol extracted from the plant, was chosen for this study. Curcumin suffers from low solubility and poor bioavailability, which makes a drug delivery vehicle to be necessary for curcumin. In the thesis, we successfully encapsulated curcumin in the PCL-*b*-PEO nanoparticles. The size distribution, morphology and loading efficiency were all controlled by the flow rate, drug-to-polymer ratio and water content. In general, the flow rate introduced shear-induced break-up and led to smaller sizes. There were both lamellae and spheres in the bulk and low flow rate samples. Then the lamellae disappeared in the high flow rate samples. High flow rates also led to a higher loading efficiency. The drug-to-polymer ratio was used to quantitatively represent the initial amount of drug added in nanoparticles. In Chapter 2, we proposed that curcumin assisted the movement of PCL blocks. Therefore, at a high drug-to-polymer ratio, polymer chains may be easier to be closely packed and form smaller size nanoparticles. Moreover, this higher loading efficiency at the high drug-to-polymer ratio could be explained by curcumin localization. Since spheres had the highest surface area, curcumin might be localized at the interface of the core so that it had more space to stay. The water content was also found to influence nanoparticle size and loading efficiency. We were able to achieve a higher loading efficiency at higher water content. The explanation might be curcumin, as a hydrophobic molecule, moved to the core of nanoparticles when the aqueous environment became more unfavourable.

After the preparation and characterization of nanoparticle-encapsulated curcumin, we tested samples *in vitro* release rates and tried to slow down the release rate for future *in vivo* pharmacokinetic study. The original release rate was fast and did not show significant effects of flow rates. The optimization process consisted of tuning flow rate, water content, drug-to-polymer ratio individually. The result showed that tuning flow rate had the most significant effect on the release rate. And at the same flow rate, drug-to-polymer ratio did not show significant effects on the release rate. The reason may be, at such a high flow rate, the dominant effect of high flow rate overcame the effect of drug ratio.

Finally, we tested the nanoparticle-encapsulated drug on the human breast cancer cell line MDA-MB-231. The drug concentration when the growth of 50% cells was inhibited was defined as IC_{50}. Nanoparticle-encapsulated curcumin showed compromised toxicity comparing to the free curcumin. The result agreed with some literature where nanoparticle-encapsulated curcumin had marginally higher IC50 values comparing to the free curcumin.

5.2 Future Work

The final step in this study was conducting the animal experiment. Animal studies would be able to provide us information of nanoparticle-encapsulated curcumin in a system involving other biological effects such as the EPR effect. There were a few studies using nanoparticle-encapsulated curcumin in pharmacokinetic experiments.[11-15] Despite the slow release they achieved from *in vitro* release experiments, the elimination of drug *in vivo* was usually in several hours, which was much faster comparing to the *in vitro* release results.[16] The pharmacokinetic experiment was usually used to compare

nanoparticle-encapsulated curcumin and free curcumin. Several studies reported nanoparticle-encapsulated curcumin had a slower release *in vivo* comparing to the bare drug.[16, 17] The future work of this thesis could be comparing nanoparticle-encapsulated curcumin prepared by microfluidics and the bulk sample in *in vivo* studies.

Moreover, another *in vivo* experiment for future work could be the efficacy experiment, which was used to test drugs on tumour models in the mouse.[18] The samples with various sizes and loading efficiencies prepared on the microfluidic chip would be suitable to test for the EPR effect.

Before we move away to the animal *in vivo* studies, we need to solve the challenge of colloidal instability. Due to the weak anticancer effect of curcumin, therapeutic dose was usually much higher than the dose for conventional anticancer drug such as paclitaxel. However, at such a high concentration, nanoparticles would not be stable and may precipitate from the solution. Future work would need to investigate the reason of colloidal instability and solve this problem by changing to another block copolymer with either semicrystalline or glassy core or choosing new “on-chip” conditions.

5.3 Reference

1. Wang, C. W.; Sinton, D.; Moffitt, M. G., Flow-directed block copolymer micelle morphologies via microfluidic self-assembly. *J Am Chem Soc* **2011,** *133* (46), 18853-64.

2. Bains, A.; Cao, Y.; Moffitt, M. G., Multiscale Control of Hierarchical Structure in Crystalline Block Copolymer Nanoparticles Using Microfluidics. *Macromol Rapid Commun* **2015,** *36* (22), 2000-5.

3. Xu, Z. Q.; Yan, B.; Riordon, J.; Zhao, Y.; Sinton, D.; Moffitt, M. G., Microfluidic Synthesis of Photoresponsive Spool-Like Block Copolymer Nanoparticles: Flow-Directed Formation and Light-Triggered Dissociation. *Chemistry of Materials* **2015,** *27* (23), 8094-8104.

4. Yang, Y. Q.; Zhao, B.; Li, Z. D.; Lin, W. J.; Zhang, C. Y.; Guo, X. D.; Wang, J. F.; Zhang, L. J., pH-sensitive micelles self-assembled from multi-arm star triblock co-polymers poly(epsilon-caprolactone)-b-poly(2-(diethylamino)ethyl methacrylate)-b-poly(poly(ethylene glycol) methyl ether methacrylate) for controlled anticancer drug delivery. *Acta Biomaterialia* **2013,** *9* (8), 7679-7690.

5. Wang, H. R.; He, J. L.; Zhang, M. Z.; Ni, P. H., Amphiphilic poly(epsilon-caprolactone)-acetal-poly(ethylene glycol)-acetal-poly(epsilon-caprolactone) triblock copolymers: Synthesis, characterization and ph-sensitive drug delivery. *Journal of Controlled Release* **2013,** *172* (1), E60-E60.

6. Shalaby, K. S.; Soliman, M. E.; Bonacucina, G.; Cespi, M.; Palmieri, G. F.; Sammour, O. A.; El Shamy, A. A.; Illum, L.; Casettari, L., Nanoparticles Based on Linear and Star-Shaped Poly(Ethylene Glycol)-Poly(epsilon-Caprolactone) Copolymers for the Delivery of Antitubulin Drug. *Pharmaceutical Research* **2016,** *33* (8), 2010-2024.

7. Payyappilly, S. S.; Dhara, S.; Chattopadhyay, S., The heat-chill method for preparation of self-assembled amphiphilic poly(epsilon-caprolactone)-poly(ethylene glycol) block copolymer based micellar nanoparticles for drug delivery. *Soft Matter* **2014,** *10* (13), 2150-2159.

8. He, X. D.; Li, L.; Su, H.; Zhou, D. L.; Song, H. M.; Wang, L.; Jiang, X. H., Poly(ethylene glycol)-block-poly(epsilon-caprolactone)-and phospholipid-based stealth

nanoparticles with enhanced therapeutic efficacy on murine breast cancer by improved intracellular drug delivery. *International Journal of Nanomedicine* **2015,** *10*, 1791-1804.

9. G Kwon[a,] M. N., M Yokoyama[c], T Okanoc, Y Sakuraic, K Katao[ka]b,, Block copolymer micelles for drug delivery: loading and release of doxorubicin. Journal of Controlled Release: 13 October 1997.

10. Bains, A.; Wulff, J. E.; Moffitt, M. G., Microfluidic synthesis of dye-loaded polycaprolactone-block-poly (ethylene oxide) nanoparticles: Insights into flow-directed loading and in vitro release for drug delivery. *Journal of Colloid and Interface Science* **2016,** *475*, 136-148.

11. Khalil, N. M.; do Nascimento, T. C.; Casa, D. M.; Dalmolin, L. F.; de Mattos, A. C.; Hoss, I.; Romano, M. A.; Mainardes, R. M., Pharmacokinetics of curcumin-loaded PLGA and PLGA-PEG blend nanoparticles after oral administration in rats. *Colloids Surf B Biointerfaces* **2013,** *101*, 353-60.

12. Ma, Z.; Shayeganpour, A.; Brocks, D. R.; Lavasanifar, A.; Samuel, J., High-performance liquid chromatography analysis of curcumin in rat plasma: application to pharmacokinetics of polymeric micellar formulation of curcumin. *Biomed Chromatogr* **2007,** *21* (5), 546-52.

13. Mohanty, C.; Sahoo, S. K., The in vitro stability and in vivo pharmacokinetics of curcumin prepared as an aqueous nanoparticulate formulation. *Biomaterials* **2010,** *31* (25), 6597-611.

14. Schiborr, C.; Eckert, G. P.; Rimbach, G.; Frank, J., A validated method for the quantification of curcumin in plasma and brain tissue by fast narrow-bore high-performance liquid chromatography with fluorescence detection. *Anal Bioanal Chem* **2010,** *397* (5), 1917-25.

15. Zou, P.; Helson, L.; Maitra, A.; Stern, S. T.; McNeil, S. E., Polymeric curcumin nanoparticle pharmacokinetics and metabolism in bile duct cannulated rats. *Mol Pharm* **2013,** *10* (5), 1977-87.

16. Gou, M.; Men, K.; Shi, H.; Xiang, M.; Zhang, J.; Song, J.; Long, J.; Wan, Y.; Luo, F.; Zhao, X.; Qian, Z., Curcumin-loaded biodegradable polymeric micelles for colon cancer therapy in vitro and in vivo. *Nanoscale* **2011,** *3* (4), 1558-67.

17. Ma, Z.; Haddadi, A.; Molavi, O.; Lavasanifar, A.; Lai, R.; Samuel, J., Micelles of poly(ethylene oxide)-b-poly(epsilon-caprolactone) as vehicles for the solubilization, stabilization, and controlled delivery of curcumin. *J Biomed Mater Res A* **2008,** *86* (2), 300-10.

18. Yang, X.; Li, Z.; Wang, N.; Li, L.; Song, L.; He, T.; Sun, L.; Wang, Z.; Wu, Q.; Luo, N.; Yi, C.; Gong, C., Curcumin-encapsulated polymeric micelles suppress the development of colon cancer in vitro and in vivo. *Sci Rep* **2015,** *5*, 10322.

Appendix

Appendix A. Supporting Information for Chapter 2

Table S2-1 Actual Gas and Flow rate, Hydrodynamic Diameter and Loading Efficiency of PCL-*b*-PEO nanoparticle (cwc + 10 wt % Run 1)

Run 1				
Water content /wt %	Drug ratio	Flow rate / µL min^{-1}	Act. Flow rate / µL min^{-1}	DLS /nm
cwc + 10	0.25	0	0	48.9
		50	53	246
		100	100	193
		200	188	81.3
	0.5	0	0	37.2
		50	47	96.6
		100	100	85.0
		200	195	54.6
	0.75	0	0	62.9
		50	49	73.3
		100	102	60.0
		200	208	55.1
Water content /wt %	Drug ratio	Flow rate / µL min^{-1}	Act. Flow rate / µL min^{-1}	Loading Efficiency
cwc+10	0.25	0	0	46.0%
		50	53	20.3%
		100	100	26.7%
		200	188	40.7%
	0.50	0	0	26.5%
		50	47	30.8%
		100	100	49.9%
		200	195	59.1%
	0.75	0	0	11.5%
		50	49	41.6%
		100	102	63.2%
		200	208	61.9%

Table S2-2 Actual Gas and Flow rate, Hydrodynamic Diameter and Loading Efficiency of PCL-*b*-PEO nanoparticle (cwc + 10 wt % Run 2)

Run 2				
Water Content /wt %	Drug ratio	Flow rate / µL min^{-1}	Act. Flow rate / µL min^{-1}	DLS /nm
cwc + 10	0.25	0	0	45.7
		50	43	377
		100	87	298
		200	201	91.2
	0.5	0	0	55.0
		50	50	92.2
		100	89	79.1
		200	227	52.4
	0.75	0	0	46.3
		50	47	68.4
		100	83	59.2
		200	200	53.5
Water content /wt %	Drug ratio	Flow rate / µL min^{-1}	Act. Flow rate / µL min^{-1}	Loading Efficiency
cwc + 10	0.25	0	0	32.0%
		50	43	29.6%
		100	87	46.0%
		200	201	46.0%
	0.50	0	0	24.1%
		50	50	35.9%
		100	89	52.0%
		200	227	56.9%
	0.75	0	0	10.8%
		50	47	54.4%
		100	83	56.3%
		200	200	54.3%

Table S2-3 Actual Gas and Flow rate, Hydrodynamic Diameter and Loading Efficiency of PCL-*b*-PEO nanoparticle (cwc + 10 wt % Run 3)

Run 3				
Water content /wt %	Drug ratio	Flow rate / µL min^{-1}	Act. Flow rate / µL min^{-1}	DLS /nm
cwc+10	0.25	0	0	52.4
		50	52	362
		100	103	301
		200	181	56.7
	0.5	0	0	67.1
		50	47	53.5
		100	97	46.2
		200	169	57.6
	0.75	0	0	57.3
		50	48	59.5
		100	103	52.9
		200	177	57.1
Water content /wt %	Drug ratio	Flow rate / µL min^{-1}	Act. Flow rate / µL min^{-1}	Loading Efficiency
cwc+10	0.25	0	0	40.0%
		50	52	30.5%
		100	103	35.7%
		200	181	48.4%
	0.50	0	0	29.0%
		50	47	40.9%
		100	97	35.4%
		200	169	54.3%
	0.75	0	0	11.7%
		50	48	43.6%
		100	103	44.6%
		200	177	48.3%

Table S2-4 Actual Gas and Flow rate, Hydrodynamic Diameter and Loading Efficiency of PCL-*b*-PEO nanoparticle (cwc + 5 wt % Run 1)

Run 1				
Water content /wt %	Drug ratio	Flow rate / µL min^{-1}	Act. Flow rate / µL min^{-1}	DLS /nm
cwc + 5	0.25	50	53	765
		100	107	473
		200	210	151
	0.5	50	55	88.0
		100	108	126
		200	212	90.6
	0.75	50	48	92.8
		100	107	68.6
		200	209	96.0
Water content /wt %	Drug ratio	Flow rate / µL min^{-1}	Act. Flow rate / µL min^{-1}	Loading Efficiency
cwc + 5	0.25	50	53	11.3%
		100	107	18.5%
		200	210	42.5%
	0.5	50	55	21.6%
		100	108	20.5%
		200	212	28.7%
	0.75	50	48	30.1%
		100	107	14.1%
		200	209	10.3%

Table S2-5 Actual Gas and Flow rate, Hydrodynamic Diameter and Loading Efficiency of PCL-*b*-PEO nanoparticle (cwc + 5 wt % Run 2)

Run 2				
Water content /wt %	Drug ratio	Flow rate / µL min^{-1}	Act. Flow rate / µL min^{-1}	DLS /nm
cwc + 5	0.25	50	44	1235
		100	103	544
		200	175	234
	0.5	50	49	124
		100	105	94.1
		200	224	94.7
	0.75	50	50	104
		100	110	90.3
		200	210	284
Water content /wt %	Drug ratio	Flow rate / µL min^{-1}	Act. Flow rate / µL min^{-1}	Loading Efficiency
cwc + 5	0.25	50	44	19.9%
		100	103	27.8%
		200	175	38.8%
	0.5	50	49	17.6%
		100	105	37.4%
		200	224	38.6%
	0.75	50	50	11.2%
		100	110	9.7%
		200	210	7.9%

Table S2-6 Actual Gas and Flow rate, Hydrodynamic Diameter and Loading Efficiency of PCL-*b*-PEO nanoparticle (cwc + 5 wt % Run 3)

Run 3				
Water content /wt %	Drug ratio	Flow rate / µL min^{-1}	Act. Flow rate / µL min^{-1}	DLS /nm
cwc + 5	0.25	50	41	826
		100	106	582
		200	197	345
	0.5	50	49	411
		100	106	161
		200	203	100
	0.75	50	48	113
		100	95	90.3
		200	202	92.6
Water content /wt %	Drug ratio	Flow rate / µL min^{-1}	Act. Flow rate / µL min^{-1}	Loading Efficiency
cwc + 5	0.25	50	41	7.7%
		100	106	17.7%
		200	197	25.5%
	0.5	50	49	16.6%
		100	106	28.9%
		200	203	21.5%
	0.75	50	48	19.7%
		100	95	22.7%
		200	202	9.5%

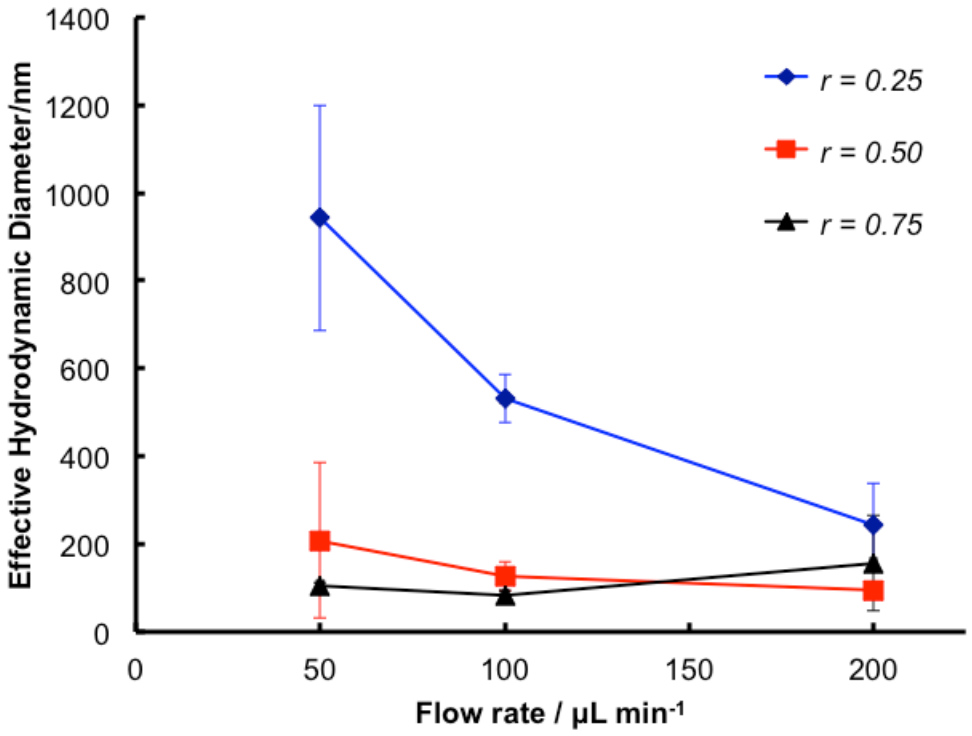

Figure S2-0-1 Hydrodynamic diameter of nanoparticles prepared on chip at cwc + 5 wt %

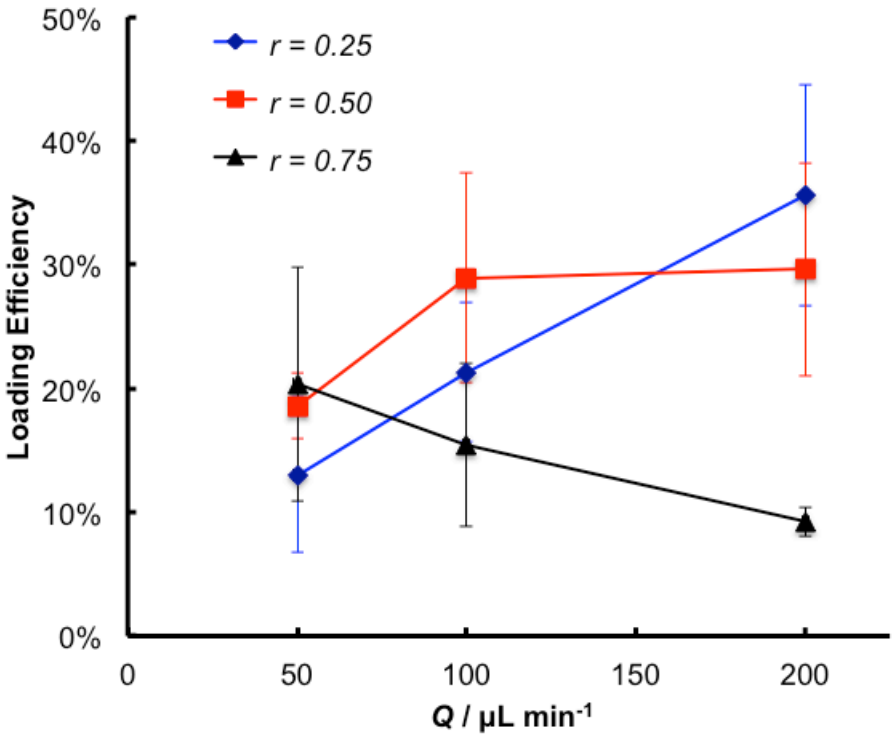

Figure S2-0-2 Loading efficiency of nanoparticles prepared on chip at cwc + 5 wt %

Appendix B. Supporting Information for Chapter 4

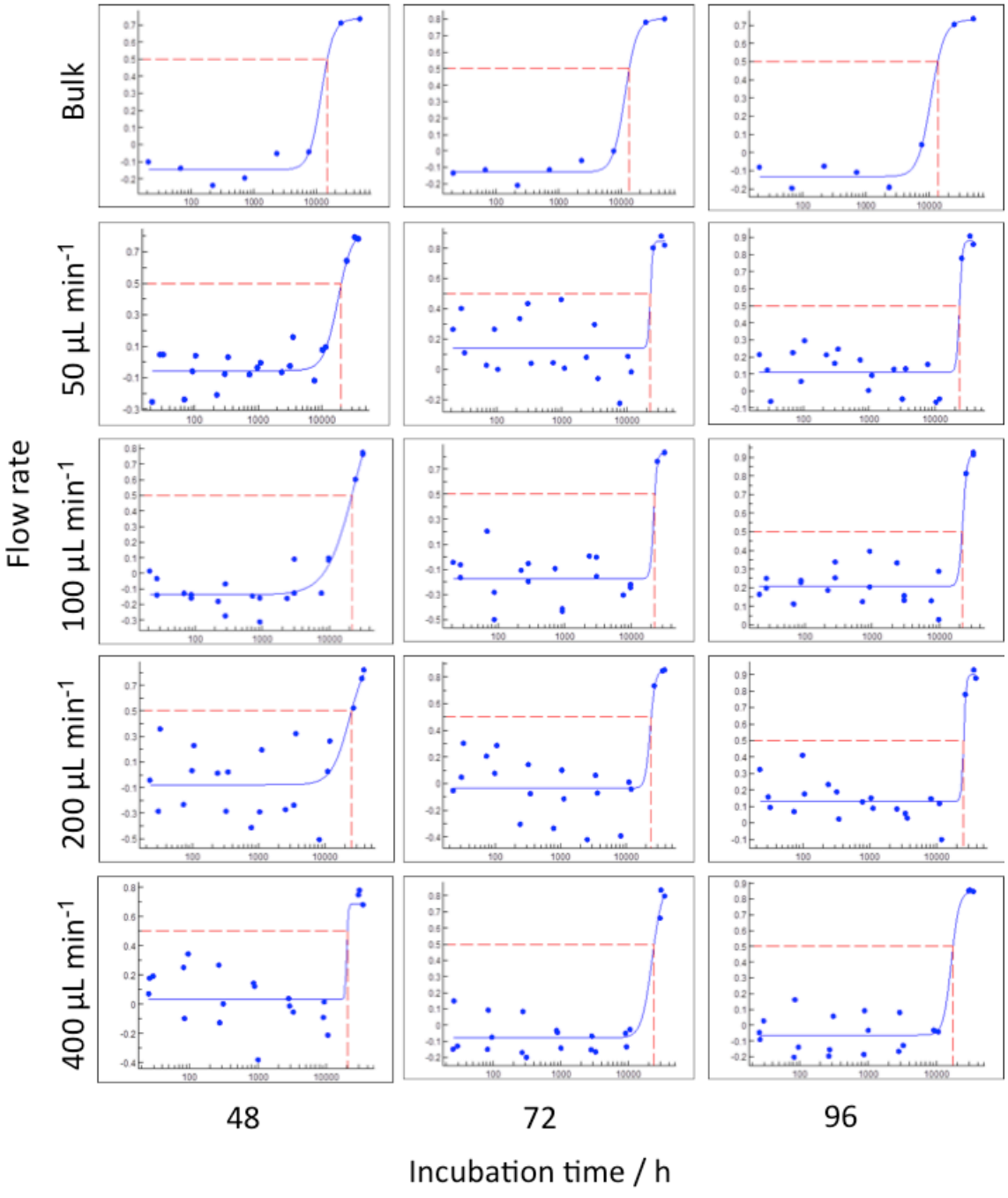

Figure S4-1 MDA-MB-231 cancer cell growth inhibition rate of nanoparticle formulations